Supplement of Earth Syst. Dynam., 12, 545–579, 2021
https://doi.org/10.5194/esd-12-545-2021-supplement

Supplement of

Comparison of CMIP6 historical climate simulations and future projected warming to an empirical model of global climate

Laura A. McBride et al.

Correspondence to: Laura A. McBride (mcbridel@umd.edu)

Supplement

Section 2.1 states "The effect of this update results in our model being able to fit the historical climate record with higher values of climate feedback, especially for strong aerosol cooling (see Fig. S1 and supplement for more information)". Figure S1 illustrates the impact of updating Eq. (2) in our model to be comparable to the formulation in Bony et al. (2006) and Schwartz (2012). This figure displays the change in GMST anomaly in 2100 relative to pre-industrial (ΔT_{2100}) as a function of λ_{Σ} and AER RF_{2011} for the two formulations of Eq. (2). Figure S1a uses the previous version of the EM-GC, where Q_{OCEAN} was subtracted outside of the climate feedback multiplicative term, and Fig. 1b uses the new version of the EM-GC where Q_{OCEAN} is subtracted within the climate feedback multiplicative term.

In the EM-GC framework, we calculate our value of Q_{OCEAN} by finding the κ needed to multiply the temperature difference between the atmosphere and the ocean to fit the observed OHC record. The model iterates over the ocean module, specifically the value of $\Delta T_{OCEAN,HUMAN}$ in Eq. (4), until the EM-GC converges on an estimate of κ for a single OHC record and value of AER RF_{2011}. Figure S1 illustrates that the effect of changing Eq. (2) in the EM-GC impacts our estimates of the rise in ΔT_{2100} at high values of AER RF_{2011}. Strong aerosol cooling results in the ocean taking up more heat from the atmosphere than in the previous version of the EM-GC. The larger value of Q_{OCEAN} results in a higher value of climate feedback needed to fit the historical climate record, because both AER RF_{2011} and Q_{OCEAN} are acting to cool the climate system. The higher values of climate feedback increase our maximum value of ΔT_{2100}. This change brings some of the projections of ΔT_{2100} from the EM-GC closer to values of ΔT_{2100} from the CMIP6 multi-model ensemble.

Section 2.1 states "Altering the training period of our model has a slight effect on our results (see Fig. S2, S3, and the supplement for information on various training periods)." Figure S2 shows the end of century projected warming as a function of λ_{Σ} and AER RF_{2011}, for four different training periods: 1850-1989 (Fig. S2a), 1850-1999 (Fig. S2b), 1850-2009 (Fig. S2c) and 1850-2019 (Fig. S2d), which is the normal training period used in our analysis. Values of ΔT_{2100} are shown only for combinations of λ_{Σ} and AER RF_{2011} that lead to good fits ($\chi^2 \leq 2$) to the climate record. We project relatively similar results for end of century warming for the training periods that end in 2019 and 2009. Our results using the training period from 1850-1999 are similar to observations and other reduced complexity models (Nicholls et al., 2020). The training period that ends in 1989 (Fig. S2a) yields a different "shape" of model parameter space for which good fits to the climate record can be obtained, compared to the other training periods. The different shape for this shorter training period is due to two factors. First, the formulation of the ocean component of our model for the training period that stops in 1989 uses 35 years of the observed OHC record. We are able to calculate good fits to the

OHC record over this shorter time period that diverge from the OHC record after 1989. Also, for this shorter time period, aerosol radiative forcing of climate cools in a manner that nearly mirrors the warming due to rising GHGs, resulting in a wider range of model parameters that lead to a “good fit” of the climate record, compared to model simulations constrained by data that extend closer to present-day. The highest values of ΔT_{2100} in Fig. S2a are associated with the largest values of λ_{Σ}, which in our model corresponds to excessively high values of κ that we can rule out, based on OHC data collected during 1990 to 2019.

Figure S3 shows the observed (HadCRUT5) and modeled ΔT anomaly from 1945-2060 for the four different training periods described above. Each panel contains three projections of future ΔT for SSP4-3.4: projection using the value of climate feedback that provides the best fit to the historical climate record for a value of AER RF_{2011} = −0.9 W m^{-2}, the lowest value of climate feedback that provides a good fit to the observed ΔT record for a value of AER RF_{2011} = −0.1 W m^{-2}, and the highest value of climate feedback that provides a good fit to the historical climate record (the associated value of AER RF_{2011} varies depending on the training period). As more years are added to the training period, the range of projection for future temperature decreases (Fig. S3a vs S3d). All of the best fit projections (solid line) and highest value of climate feedback (upper dashed line) closely follow the mid-point of the data, regardless of the training period. Given the nature of this test (i.e., predicting GMST out to 2019 for a series of trainings that stop in either 1989, 1999, or 2009), Figure S3 supports the quantitative accuracy of our approach for simulating and projecting future ΔT.

Section 2.2.1 states “We use the uncertainty time series from HadCRUT4 for all GMST records (see the supplement, Figs. S4 and S5, and Table S1 for more information)”. Figure S4 shows values of ΔT based on the seven individual GMST records (GISTEMP, BEG, HadCRUT4, CW14, HadCRUT5, NOAAGT, and JMA) with their corresponding 1σ and 2σ uncertainties. A horizontal line at zero denotes the time period of the baseline for each ΔT record. The multi-record mean, excluding the data set that is plotted, is also shown. Since the multi-record mean and individual ΔT record are plotted on the same baseline, these two quantities closely match over this time period. Panels (a), (b), (e), and (f) illustrate that the uncertainties for these GMST records are not large enough to encompass the multi-record mean over 1850-2019. The multi-record mean in panel (a) is below the GISTEMP 1σ uncertainty range between 1880 and 1900, and again between 1980 to 2019. In panel (b), the multi-record mean is above the BEG 1σ range from 1850 until 1865, 1880 to 1895, and below the 1σ uncertainty range from 2000 to 2019. The multi-record mean in panel (e) is below the HadCRUT5 1σ uncertainty range from 1990 until 2019. In panel (f), the multi-record mean is above the NOAAGT 1σ uncertainty range from 1920 until 1955. The JMA GMST record does not provide an uncertainty estimate. We therefore use the HadCRUT4 combined uncertainty (measurement, sampling, bias, and coverage uncertainties (Morice et al., 2012)) estimate for JMA in panel (g). The multi-record mean of ΔT for all data sets other than JMA lies at the edge of the 1σ uncertainty range from 1891 until 2000. After 2000, the multi-record mean falls above both the 1σ and 2σ HadCRUT4 uncertainty range. The HadCRUT4 uncertainty time series shown in panel (c) is the only uncertainty estimate large enough to cover the spread in the various GMST records.

Figure S5 shows ΔT based on all seven GMST records and the multi-record mean relative to three baseline periods. The 1σ and 2σ uncertainties from HadCRUT4 are plotted about the multi-record mean. Panels (a) and (d) show the GMST records relative to 1891-1920, which are the first 30 years all of the data sets have in common. Between 1850-1970, all of the data sets fall within the 1σ HadCRUT4 uncertainty. After 1970, the GMST records start to deviate and some fall outside of the 1σ uncertainty but within the 2σ uncertainty, and JMA falls outside of the 2σ uncertainty. Panels (b) and (e) show the GMST records relative to the HadCRUT baseline period of 1961-1990. We see similar behavior as in panels (a) and (d), where the GMST records largely fall within the HadCRUT4 1σ uncertainty until about 1970. Panels (c) and (f) show the GMST records forced to match HadCRUT5 from 2010-2019, which is baselined to 1961-1990. In these two panels, we see a large spread between the GMST records from the beginning of the time period until 2005.

Table S1 shows the percentage of ΔT data points that lie within the 1σ or 2σ HadCRUT4 uncertainty about the multi-record mean for all seven data records since 1940. Year 1940 is used to be consistent with the definition of our χ^2_{RECENT} parameter. Depending on the choice of baseline period, the number of data points within the uncertainty range varies. For a baseline of 1891-1920, 80% of the data points for all seven records are within the 1σ uncertainty and 95% of the data points are within the 2σ. For a baseline of 1961-1990, 88% and 93% of data points are within the 1σ and 2σ HadCRUT4 uncertainties, respectively. If the ΔT records are forced to match the average value of the HadCRUT5 data set over the last decade, 72% of the data points are within the 1σ uncertainty and 88% are within the 2σ uncertainty. This analysis shows that depending on which baseline is used, the percentage of points within the 1σ or 2σ uncertainty ranges varies. Overall, these comparisons support the utility of the HadCRUT4 uncertainty for the GMST, since the 1σ and 2σ uncertainty ranges capture a percentage of points approximately correct for a pure Gaussian distribution. Therefore, we have adopted the HadCRUT4 uncertainties in GMST for all of the analyses in the main paper. The uncertainties published by other data centers tend to be smaller than the HadCRUT4 uncertainties. Since only the HadCRUT4 uncertainties span the range of values for ΔT from the seven data records in a somewhat realistic fashion, we have decided to use these uncertainties uniformly throughout the analysis.

Section 2.2.1 also says "We then adjust each data set to the HadCRUT5 pre-industrial baseline as described in the supplement". The mean of the HadCRUT5 GMST record from 1850-1900 is −0.3589°C. We add 0.3589°C to each value of the HadCRUT5 record to adjust the data set onto the pre-industrial baseline. We use this same offset for all of the other data sets. We add 0.3589°C to each value of ΔT from the six data sets to match the HadCRUT5 1850-1900 baseline.

Section 2.2.3 states "Figure S6 shows the ozone RF time series used in this analysis and the supplement provides more information about the creation of the time series for the RF due to O_3^{TROP}". Figure S6 displays the time series of tropospheric ozone RF used in our analysis for the various SSPs. Tropospheric ozone is an important GHG that rivals nitrous oxide as the third most important anthropogenic GHG. We include the RF due to tropospheric ozone (O_3^{TROP}) in our model for completion, even though the SSP database does not provide RF estimates for the various SSPs. We use values from the RCP scenarios provided by the Potsdam Institute for Climate Impact Research (Meinshausen et al., 2011). The values of the RF due to O_3^{TROP} for SSP1-1.9 and SSP1-2.6 are from the RCP2.6 pathway. The RCP4.5 time series of O_3^{TROP} is used for SSP2-4.5, the RCP6.0 time series is used for SSP4-6.0, and the RCP8.5 time series is used for SSP5-8.5. We create linear combinations of RCP2.6 and RCP8.5 to generate two new time series of the RF due to O_3^{TROP} for SSP4-3.4 and SSP3-7.0. There is a large gap between the time series of the RF due to O_3^{TROP} for RCP6.0 (shown as SSP4-6.0) and RCP8.5 (shown as SSP5-8.5) in Fig. S6. We created a time series that would split the difference between the two RCPs to represent the RF due to O_3^{TROP} for SSP3-7.0. The SSP4-3.4 time series of the RF due to O_3^{TROP} that was created lies in between the RCP2.6 (shown as SSP1-2.6) and RCP4.5 (shown as SSP2-4.5) time series in Fig. S6.

Section 2.2.8 states "Figure S9 shows the five OHC records as well as the multi-measurement average". Figure S9 displays the five OHC content data sets, as well as the multi-measurement average, plotted as a function of time and normalized to year 1986. This figure illustrates how the shapes of the different OHC records compare. Each of the time series represents the amount of heat stored in the top 700 m of the world's oceans for that specific data set. Carton et al. (2018) is the shortest data set, and only spans 36 years (1982-2017). The second shortest record is Balmaseda et al. (2013a), which spans 52 years (1958.5-2009.5). Ishii et al. (2017) is the record in the middle with a range of 63 years (1955-2017). Both Cheng et al. (2017) and Levitus et al. (2012) have records that span 65 years (1955-2019). The length of the data set and the shape of the curve affect the estimate of ocean heat export (OHE), because we calculate OHE by taking a linear fit to the full OHC time series. Balmaseda et al. (2013a) has the lowest estimate of OHE because the slope of the curve is relatively shallow, due to the fact that it slightly rises, then decreases at the start of the record. Carton et al. (2018) has the highest estimate of OHE because the slope of the curve is the steepest of the five records.

Section 2.2.8 also says "For these five OHC data sets, uncertainty estimates are not always provided. Furthermore, some studies that do provide uncertainties give estimates that seem unreasonably small (see Fig S10 and the supplement)" and "Figure S10 and the supplement provide more detail on the creation of this time dependent uncertainty estimate for OHC". Figure S10 shows the multi-measurement average as well as the five OHC data records as a function of time, the uncertainty for each corresponding data set, and the combined uncertainty used in this analysis. Panel (a) shows the multi-measurement OHC average with the standard deviation of the mean plotted around the average time series. The standard deviation is large at the beginning of the time series, due to the spread in the estimates of OHC between the different records (illustrated in Fig. S9). The standard deviation decreases as the various OHC records converge near a similar estimate. The standard deviation is zero in 1986 because we normalized all of the time series to zero in this year to create the multi-measurement average. Because of this normalization, the standard deviation of the mean is not a realistic measure of uncertainty for the five OHC time series.

Panels (b), (c), (d), (e), and (f) display the uncertainty estimates for the five OHC data records. We use the standard deviation of the mean of five ensemble members of the European Centre for Medium-Range Weather Forecasts Ocean ReAnalysis System 4 (ORSA) (Balmaseda et al., 2013b) for the Balmaseda et al. (2013a) record. The standard deviation is plotted in panel (b) as the dotted blue line. The standard deviation is small at the beginning of the record, because the five ensemble members started at similar values of OHC in 1958 and diverged over time. The combined uncertainty of the standard deviation of the average of the five OHC records and the Cheng et al. (2017) estimate is plotted as a dashed blue line. Panel (c) shows the Levitus et al. (2012) time series for the top 700 m updated to the end of 2019. The Levitus time series utilizes the standard error over the whole ocean for their uncertainty estimate and is plotted as the dotted light blue line. The standard error is a very small uncertainty estimate compared to the other OHC data records, which is unreasonable considering the large variations in OHC between the different records. We use the standard deviation of eight reanalysis experiments to represent the uncertainty associated with the Carton et al. (2018) OHC record and is plotted as a dotted orange line in panel (e). The standard deviation of the eight reanalysis experiments is rather small, which also is unrealistic. Panel (f) displays the Cheng et al. (2017) OHC record updated through the end of 2019 with the 1σ uncertainty. This uncertainty does not vary much throughout the data record, making it more realistic as an estimate for such an uncertain quantity as OHC. We created the combined uncertainty estimate of the standard deviation of the average of the five OHC records and the Cheng et al. (2017) 1σ uncertainty to have the largest uncertainty possible due to the fact that OHC varies between the different records. The EM-GC cannot achieve $\chi^2_{OCEAN} \leq 2$ for Balmaseda et al. (2013a), Levitus et al (2012), and Carton et al. (2018) using their own respective estimates of uncertainty. Creating one uncertainty estimate to be used for all of the OHC records provides consistency and allows the EM-GC to achieve good fits between the observed and modeled OHC.

Section 2.3 states "Figure S12 illustrates the REG method used to determine AAWR from the CMIP6 GCMs". Figure S12 shows the change in ΔT from 1975-2014 from the CMIP6 GCMs and the contribution of SAOD from 1975-2014. There was about a 6 month lag between the response of ΔT and enhancements of SAOD following the eruption of Mount Pinatubo in June 1991 (Douglass and Knox, 2005; Thompson et al., 2009); a 6 month delay for the response of ΔT to SAOD is commonly used in regression analyses of the actual temperature record (Foster and Rahmstorf, 2011; Lean and Rind, 2008). The time needed for ΔT to respond to a change in the aerosol loading in the stratosphere due to a volcanic eruption in each GCM can exhibit a significant difference compared to this empirically determined response time. Therefore, a lag was determined for each GCM by calculating the value of the monthly delay that resulted in the largest regression coefficient for SAOD (versus ΔT). Due to the difference in model physics between the various GCMs, the value of the delay between the volcanic forcing and surface temperature response ranged from 0 to 11 months. The effect of SAOD on ΔT for the 50 GCMs is shown in Fig. S12d. Figure S12b shows the residual in ΔT after removing the influence of SOAD, and the median value of AAWR from the CMIP6 multi-model ensemble is plotted as a linear line. Figure S12c shows the human component of global warming, $\Delta T_{ATM,HUMAN}$, from the EM-GC. A linear fit and quadratic fit are shown to illustrate that $\Delta T_{ATM,HUMAN}$ is almost nearly linear from 1975-2014, supporting the approximation of $\Delta T_{ATM,HUMAN}$ as a linear function from 1975-2014 for the REG calculation.

Section 2.3 also states "Figure S13 and the supplement compare values of AAWR found using the REG method applied to EM-GC output with values of AAWR found using Eq. (9), as support for the validity of using the REG method to determine AAWR from CMIP6 output". We applied the REG method to the EM-GC simulations to check the validity of the REG method. We regressed the modeled ΔT time series from the EM-GC for an AER $RF_{2011} = -0.9$ W m^{-2} simulation with SAOD and applied a 6 month lag. A linear function is used to represent the anthropogenic effect on temperature from 1975-2014. Fig. S13 shows the results of using the REG method on output of the EM-GC.

The value of AAWR from the EM-GC determined using the REG method is 0.188°C $decade^{-1}$, compared to 0.167°C $decade^{-1}$ using Eq. (9) (Fig. S13c and Fig. 1). There is a 0.021°C $decade^{-1}$ difference between the two methods. This difference arises because the REG method, when applied to the EM-GC modeled ΔT time series, includes the contribution of AMOC in the value of AAWR (Fig. S13c). Figure 1 of our paper illustrates that AMOC contributes about 0.025°C decade^{-1} to the rise in ΔT. If we include AMOC as a regressor variable to the REG method, we obtain a value of AAWR of 0.161°C decade^{-1} from the output of the EM-GC (Fig. S13g).

The close agreement of values of AAWR from the REG method once we account for AMOC and Eq. (9) supports the validity of the REG method to determine AAWR from CMIP6 output. We do not explicitly use AMOC as a regressor variable when applying the REG method to CMIP6 GCMs for two reasons. The first reason is that GCMs have been shown to underestimate key aspects of the Atlantic multidecadal oscillation and are unable to simulate the many oceanic and atmospheric footprints of AMOC (Kavvada et al., 2013). The second reason is that CMIP6 GCM historical runs do not use prescribed SSTs. If the CMIP6 GCMs are representing AMOC, it is a random signal that is averaged out when we analyze the 50 GCMs in order to calculate AAWR.

Section 2.3 also says "Analysis of AAWR for these 50 GCMs of LIN versus REG (see Fig. S14)…". Figure S14 shows the similarity between the values of AAWR determined using the LIN and REG methods. The ratio between the values of AAWR determined utilizing LIN and REG is 1.009, indicating there is only about a 0.9% difference in the values of AAWR using the two methods. Figure S14 also shows the values of AAWR that are below the maximum value of AAWR determined by the EM-GC utilizing the HadCRUT5 temperature record (blue) and the values that are above the maximum (red). Less than half of the GCMs result in values of AAWR less than the maximum value from the EM-GC and more than half of the GCMs result in values of AAWR greater than the maximum value from the EM-GC utilizing the HadCRUT5 GMST record.

Section 2.4 states "For the estimate of climate sensitivity from the CMIP6 multi-model ensemble, we use the method described by Gregory et al. (2004) (See the supplement and Fig. S15 for more information)". To use the Gregory method, near surface air temperature output from the Abrupt 4×CO_2 and piControl simulations, as well as net downward radiative flux output from the Abrupt 4×CO_2 simulation is used to calculate ECS. The near surface air temperature and net downward radiative flux was converted from monthly gridded output to annual global averages. We calculate the temperature change for the Abrupt 4×CO_2 simulation by subtracting the piControl near surface air temperature (Chen et al., 2019) (Fig. S15). This computed temperature anomaly is then regressed against the net downward radiative flux, with the x-intercept yielding the response of ΔT to a quadrupling of CO_2. This response is then divided by two (Jones et al., 2019) to arrive at the effective climate sensitivity (Fig. S15).

Section 2.5 states "See Fig. S16 for unweighted ECS values and Section 3.2 states "See Fig S16 for results without aerosol weighting". Figure S16 displays the values of ECS using the EM-GC and the CMIP6 multi-model ensemble. The EM-GC box contains the 25^{th}, 50^{th}, and 75^{th} percentiles, the whiskers denote the 5^{th} and 95^{th} percentiles, and the stars represent the minimum and maximum values of ECS. The box labeled CMIP6 is unchanged from Fig. 7. The values of ECS are not treated with the aerosol weighting described in Sect. 2.5. This figure shows that most of the estimates of ECS found using the EM-GC are concentrated towards small values of ECS, due to the fact that the majority of the EM-GC model runs with good fits to the climate record (χ^2_{ATM}, χ^2_{RECENT}, and χ^2_{OCEAN}) have weak aerosol cooling and low values of λ_{Σ} (Fig. 5b). We use the aerosol weighting method to assign the same weights for the IPCC 2013 "likely" range limits of AER RF_{2011} of −0.4 and −1.5 W m^{-2} at the one sigma values of a Gaussian, and the −0.1 and −1.9 W m^{-2} are at the two sigma values of a Gaussian. Using the aerosol weighting method adjusts our estimates of ECS so that the calculated percentiles occur at higher values.

Section 3.2 in the Fig. 8 caption says, "See supplement for the confidence intervals plotted for each study". All of the studies except Dessler et al. (2018), Rugenstein et al. (2020), IPCC 2013, and Zelinka et al. (2020) have the 5 to 95% confidence intervals shown. The 66% confidence intervals are shown for IPCC 2013, and the minimum and maximum are shown for Dessler et al. (2020), Rugenstein et al. (2020) and Zelinka et al. (2020).

The Fig. 8 caption in Sect. 3.2 also refers to the supplement for information about which studies are estimating effective climate sensitivity or equilibrium climate sensitivity. We designate each study based on information found in their manuscripts if their analysis uses the Gregory et al. (2004) method or infers climate feedback from the historical climate record will persist until equilibrium. The use of either of these two factors results in our designation of effective climate sensitivity (Gregory et al., 2004; Sherwood et al., 2020; Tokarska et al., 2020a; Zelinka et al., 2020). Based on our examination of IPCC 2013, it seems their estimate is a combination of effective climate sensitivity and equilibrium climate sensitivity.

Section 3.3.4 states "see Fig. S21 and the supplement" and "see the supplement for more information". Figure S21 shows the rise in ΔT from pre-industrial for SSP5-8.5 versus the cumulative emissions of CO_2, in Gt C, since 1870. The colored lines denote the probability of reaching at least that temperature by the end of century. The large spread in projections of future ΔT is driven by the uncertainty in AER RF. The computed probabilities are based on the aerosol weighting method, so the uncertainty in AER RF is considered when determining the likelihood of achieving the Paris Agreement target of 1.5°C and upper limit of 2.0°C for the cumulative carbon emissions.

We use the uncertainty suggested by coupled atmospheric / carbon cycle models in how atmospheric CO_2 will respond to the prescribed carbon emissions. Examination of Fig. 2 and Table 3 from Friedlingstein et al. (2014) and Fig. 9b from Murphy et al. (2014) led to our determination that the uncertainty in estimates of atmospheric CO_2 from emissions driven runs of CMIP5 coupled atmospheric / carbon cycle models is about 10% (1σ). We include this 10% uncertainty in our determination of the carbon budgets for each probability of achieving the Paris Agreement target and upper limit shown in Table 2.

Section 3.3.6 states "Figure S23 is identical to Fig. 14, except for the use of no delay between the RF perturbations and the response of climate feedback.". Figure S23 shows the effect of time variant λ^{-1}, assuming an instantaneous response between λ^{-1} and a change in radiative forcing for a simulation using a value of AER $RF_{2011} = -0.9$ W m^{-2}. The instantaneous response causes the modeled ΔT to deviate more from the observed temperature than results found using the 32.5-year delay in the response (Fig. S23g, h versus Fig. 14g, h). The deviation between the modeled and observed ΔT does not allow for a large change in λ^{-1} over time to still achieve the $\chi^2_{ATM} \leq 2$ and $\chi^2_{RECENT} \leq 2$ constraints. The deviation between modeled and observed ΔT in Fig. S23d resembles the behavior of some CMIP6 GCMs (see Fig. 9 and Tokarska et al. (2020b)).

Section 3.3.6 also states "In Figs. 14 and S23 we also analyze a RF scenario termed SSP2-4.5′ that serves as a doubled CO_2 scenario (dotted lines)". In the SSP2-4.5′ simulation, only CO_2 is allowed to change after the end of 2019. All other GHGs and aerosols are kept constant at their December 2019 values. This simulation allows us to examine the effect of time variant λ^{-1} on changes in ΔT due only to the future rise in CO_2. In the SSP2-4.5 scenario, CH_4, tropospheric O_3, and ODSs decrease after 2019 leading to a future decline in RF, whereas N_2O and tropospheric aerosols result in a future increase in RF. When all of these RF are kept constant in the SSP2-4.5′ scenario for the AER $RF_{2011} = -0.9$ W m^{-2} scaling assumption, the terms result in a near balance out to 2100. For the weaker aerosol cooling scenario (AER $RF_{2011} = -0.4$ W m^{-2}), the value of RF due to tropospheric aerosols is not large enough to completely offset the other GHGs that are held constant. Consequently, the SSP2-4.5′ simulation (dotted line) results in slightly larger total RF and associated warming than the SSP2-4.5 scenario (solid line) shown in Fig. S24. For the stronger aerosol cooling scenario (AER $RF_{2011} = -1.5$ W m^{-2}), the value of RF due to tropospheric aerosols is larger than the RF due to the other GHGs that are held constant, resulting in the SSP2-4.5′ having a slightly lower total RF and associated warming than the SSP2-4.5 scenario (Fig. S25).

The effect of the uncertainty in AER RF_{2011} on ECS found using time dependent climate feedback ($ECS_{\lambda(t)}$ in Main) is based on results shown in Figs. 14b, 24b, and 25c. If we apply the χ^2_{RECENT} constraint equally to the −0.4, −0.9, and −1.5 W m^{-2} simulations, our new estimate of $ECS_{\lambda(t)}$ is 3.52°C (range of 2.71 to 5.53°C)

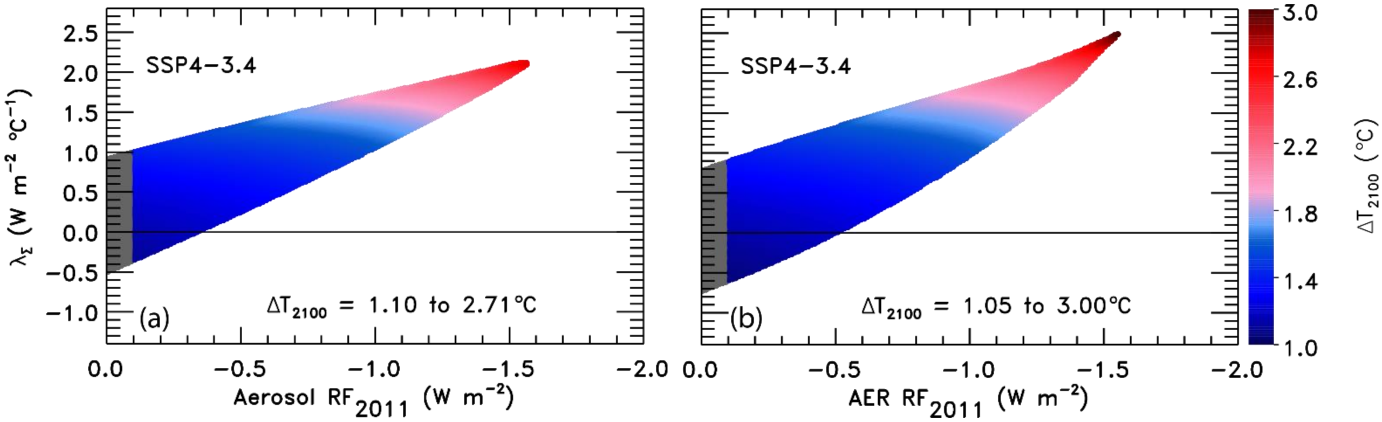

Figure S1. GMST anomaly in 2100 relative to pre-industrial (ΔT_{2100}) as a function of climate feedback parameter and AER RF_{2011} for two versions of the EM-GC trained with the HadCRUT4 ΔT record. (a) The change in ΔT_{2100} for SSP4-3.4 using the original formulation of Eq. (2) where Q_{OCEAN} is subtracted outside of the feedback multiplicative term. (b) The change in ΔT_{2100} for SSP4-3.4 using the updated formulation of Eq. (2) where Q_{OCEAN} is subtracted within the feedback multiplicative term similar to Bony et al. (2006) and Schwartz (2012). The EM-GC is able to fit higher values of λ_Σ at strong aerosol cooling (around −1.5 W m^{-2}) for the new Eq. (2) compared to the original formulation in Canty et al. (2013) and Hope et al. (2017). The maximum value of future warming has increased due to the higher λ_Σ values.

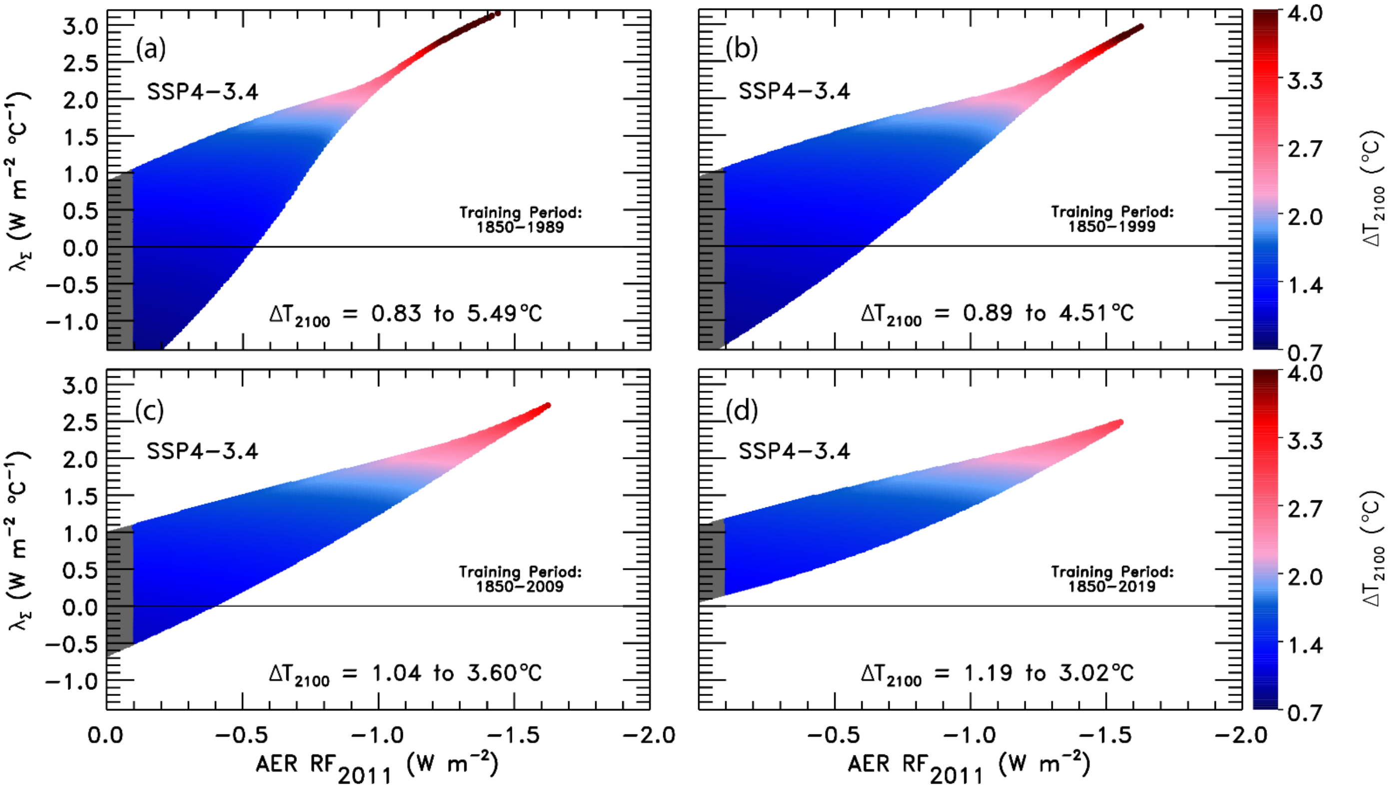

Figure S2. ΔT_{2100} as a function of climate feedback parameter and tropospheric aerosol radiative forcing in 2011 using the EM-GC trained with the HadCRUT5 ΔT record for SSP4-3.4. (a) Training period of 1850-1989. The region outside of the AER RF_{2011} range provided by IPCC 2013 is shaded (grey). Colors denote the GMST change in year 2100 relative to pre-industrial. The color bar is the same across all four panels for comparison. (b) Training period of 1850-1999. (c) Training period of 1850-2009. (d) Training period of 1850-2019, which is the normal training period used in our analysis.

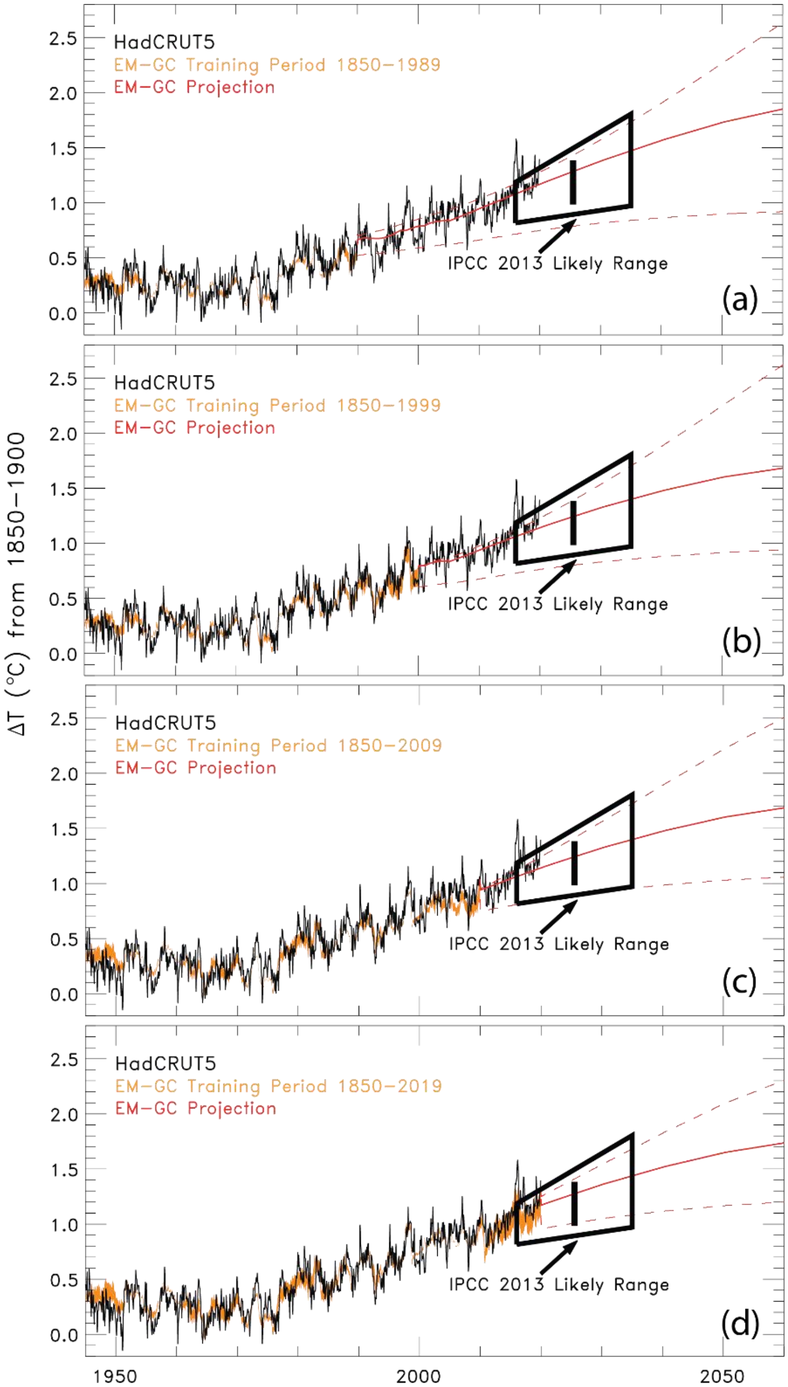

Figure S3. Observed and modeled GMST anomaly relative to 1850-1900 from 1945-2060 for four training periods. (a) Observations from HadCRUT5 (black), the EM-GC ΔT simulation for a training period of 1850-1989 (orange) of HadCRUT5, and the EM-GC projections for SSP4-3.4 out to 2060. Three EM-GC projections are shown in red: The best estimate of climate feedback for AER RF_{2011} = −0.9 W m^{-2}, the lowest value of climate feedback that satisfies the χ^2 constraints for AER RF_{2011} = −0.1 W m^{-2}, and the highest value of climate feedback that satisfies the χ^2 constraints (the value of AER RF_{2011} varies for each training period). The IPCC 2013 likely range of warming is denoted as the black trapezoid. (b) Training period of 1850-1999. (c) Training period of 1850-2009. (d) Training period of 1850-2019.

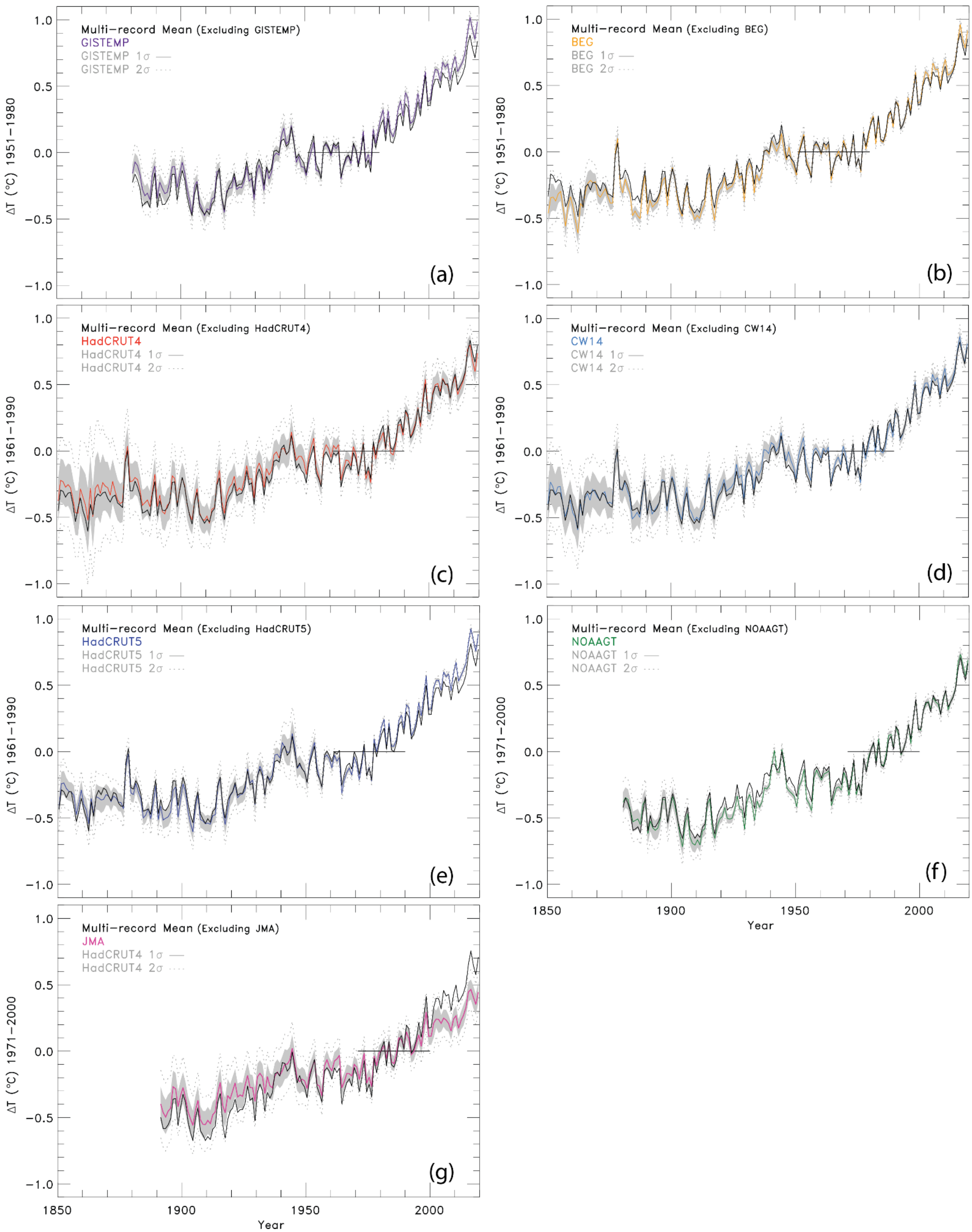

Figure S4. Annual GMST (ΔT) anomaly for seven data records relative to their individual baseline and the multi-record mean. The multi-record mean does not include the data set that is being shown. The 1σ and 2σ uncertainties for each GMST record are shown, and the horizontal line for ΔT=0 spans the baseline used for the specific panel. (a) GISTEMP. (b) BEG. (c) HadCRUT4. (d) CW14. (e) HadCRUT5. (f) NOAAGT. (g) JMA. Since the JMA data provider does not provide an uncertainty time series, the HadCRUT4 uncertainty is used.

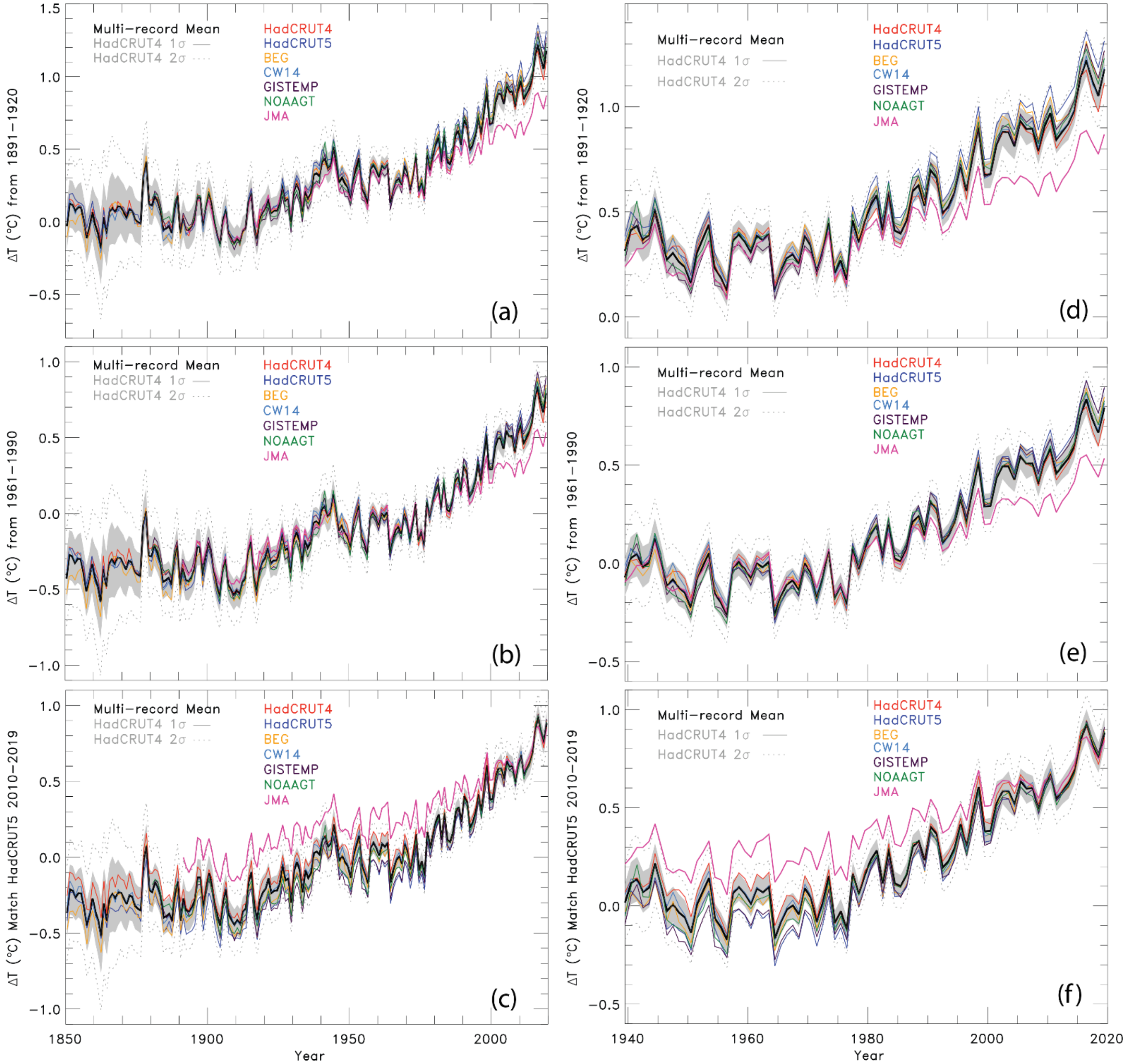

Figure S5. Annual GMST (ΔT) anomaly relative to several baseline periods for seven data records. The 1σ (shaded grey) and 2σ (dotted grey) HadCRUT4 uncertainties are plotted about the multi-model record mean (black). (a) Baseline of 1891-1920 plotted from 1850-2019. (b) Same as (a) using a baseline of 1961-1990. (c) Same as (a) except all of the ΔT records are forced to match the average ΔT anomaly over 2010-2019 given by HadCRUT5 that is relative to 1961-1990. (d) – (f) Same as (a) – (c) except plotted from 1940-2019.

Table S1. Percentage of annual values between 1940-2019 of the GMST record within the 1 sigma or 2 sigma HadCRUT4 uncertainties about the multi-record mean for each baseline period.

Baseline: 1891-1920	1σ			2σ		
	N_{WITHIN}	N_{TOTAL}	%	N_{WITHIN}	N_{TOTAL}	%
HadCRUT4	77	80	96	80	80	100
HadCRUT5	42	80	53	80	80	100
CW14	80	80	100	80	80	100
BEG	71	80	89	80	80	100
GISTEMP	73	80	91	80	80	100
NOAAGT	76	80	95	80	80	100
JMA	29	80	36	54	80	68
AVERAGE			**80%**			**95%**
Baseline: 1961-1990						
HadCRUT4	80	80	100	80	80	100
HadCRUT5	68	80	85	80	80	100
CW14	80	80	100	80	80	100
BEG	80	80	100	80	80	100
GISTEMP	75	80	94	80	80	100
NOAAGT	80	80	100	80	80	100
JMA	27	80	34	48	80	60
AVERAGE			**88%**			**93%**
Match 2010-2019						
HadCRUT4	68	80	86	80	80	100
HadCRUT5	47	80	59	76	80	95
CW14	78	80	98	80	80	100
BEG	77	80	96	80	80	100
GISTEMP	47	80	59	79	80	99
NOAAGT	73	80	61	80	80	100
JMA	11	80	14	18	80	23
AVERAGE			**72%**			**88%**

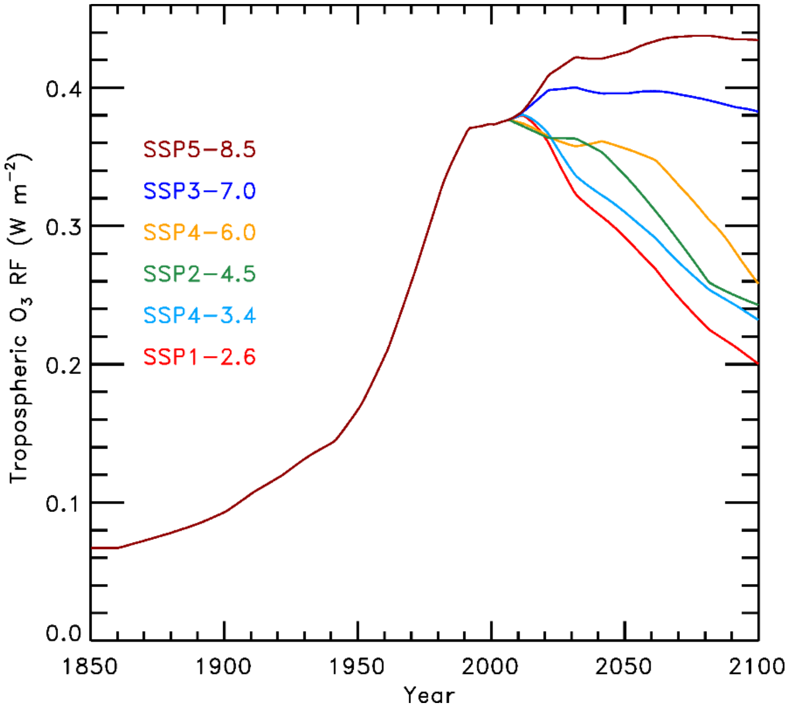

Figure S6. Radiative forcing of tropospheric ozone for the various SSPs analyzed in our study. The time series labeled SSP1-2.6, SSP2-4.5, SSP4-6.0, and SSP5-8.5 are from the corresponding RCP scenarios. We created the time series from SSP4-3.4 and SSP3-7.0 using linear combinations of the SSP1-2.6 and SSP5-8.5 time series.

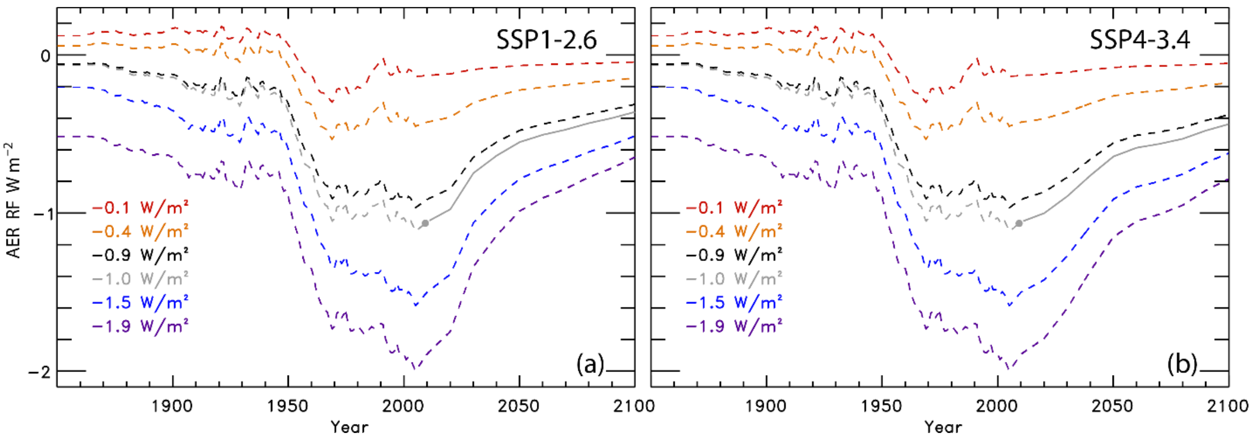

Figure S7. Radiative forcing time series due to tropospheric aerosols. (a) The RF time series due to tropospheric aerosols for SSP1-2.6. The solid grey circle denotes the value of AER RF_{2011} given by the SSP database. The solid grey lined labeled the −1.0 W m^{-2} time series is the AER RF time series given by the SSP database for SSP1-2.6. We appended a historical AER RF time series from the RCP scenarios and created five additional AER RF time series as described in Sect. 2.2.4. (b) Anthropogenic aerosol radiative forcing time series for SSP4-3.4.

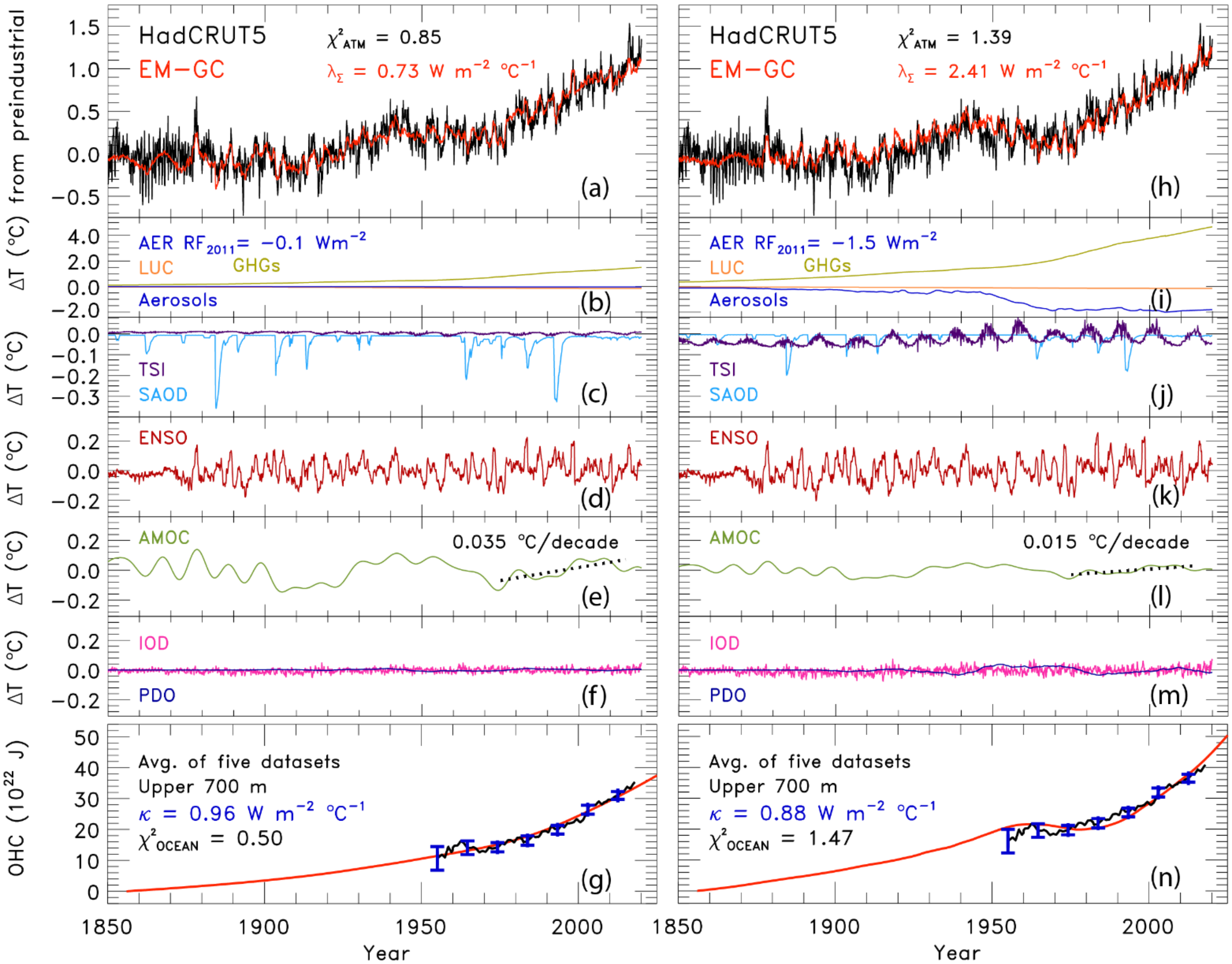

Figure S8. Measured (HadCRUT5) and modeled GMST anomaly (ΔT) relative to a pre-industrial (1850-1900) baseline for an AER RF_{2011} = −0.1 W m^{-2} and −1.5 W m^{-2}. (a) Observed (black) and modeled (red) ΔT from 1850-2019. This panel also displays the values of λ_Σ and χ^2_{ATM} (see text) for this best-fit simulation. (b) Contributions from total human activity. This panel also denotes the numerical value of the attributable anthropogenic warming rate from 1975-2014 (black dashed) as well as the 2σ uncertainty in the slope. (c) Solar irradiance (light blue) and major volcanoes (purple). (d) Influences from ENSO on ΔT. (e) Contributions from AMOC to ΔT and to observed warming from 1975-2014. (f) Influences from PDO (blue) and IOD (pink) on ΔT. (g) Measured (black) and modeled (red) ocean heat content (OHC) as a function of time for the average of five data sets (see text), the value of χ^2_{OCEAN} for this run, as well as the ocean heat uptake efficiency, κ, needed to provide the best-fit to the OHC record. The error bars (blue) denote the uncertainty in OHC used in this analysis (see Sect. 2.2.8). (h)-(n) Same as (a)-(g), except for AER RF_{2011} = −1.5 W m^{-2}.

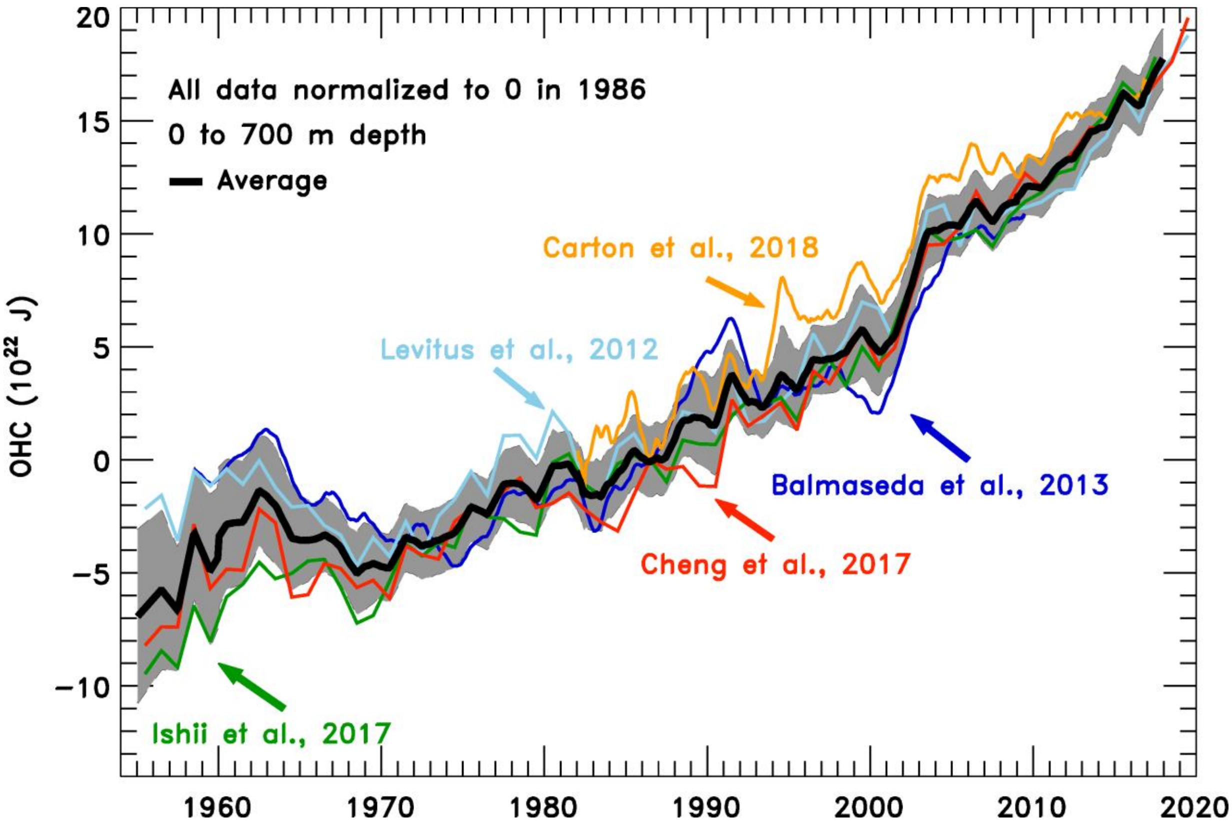

Figure S9. Ocean heat content time series. The five ocean heat content data records used in this analysis, normalized to the year 1986 because this year is in the middle of the average time series. The grey shaded region is the combined uncertainty estimate used in this analysis, centered around the average of the five data sets. The average of the ocean heat content records (1955 – 2017) is computed when there are three or more data sets available for a given year.

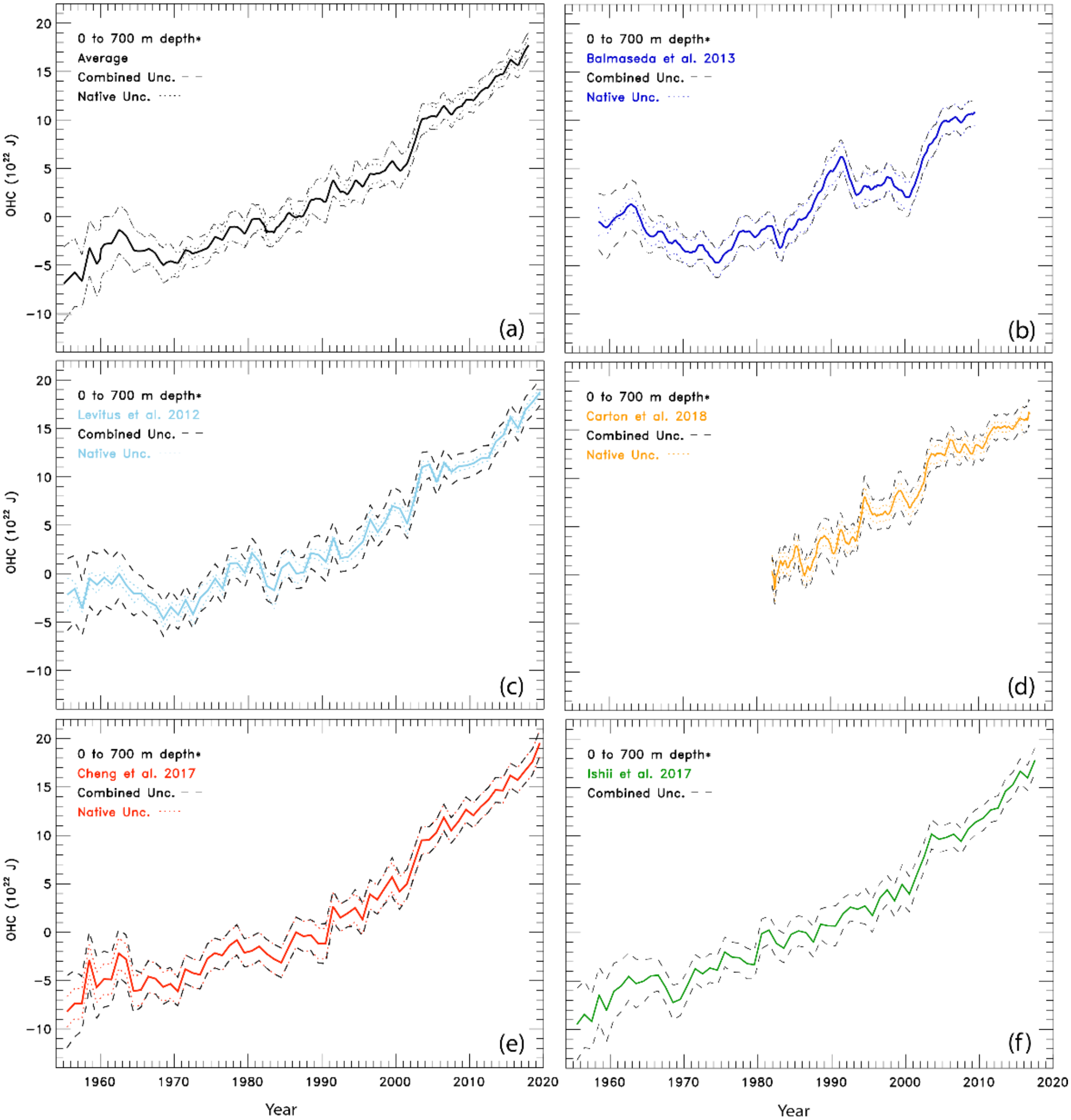

Figure S10. The ocean heat content records and uncertainty estimates analyzed in this study. (a) The average OHC record along with the standard deviation of the mean represented by the dotted black line, and the combined uncertainty of the 1σ standard deviation of the average of the five OHC records and the Cheng et al. (2017) estimates shown as the dashed black line. (b) Balmaseda OHC record with the standard deviation of the five ORSA ensemble members as the dotted line, and the combined uncertainty as the dashed line. (c) Levitus OHC record with the standard error as the native uncertainty, and the combined uncertainty. (d) Carton OHC record with the standard deviation of the mean of multiple ensemble members, and the combined uncertainty. (e) Cheng OHC record with the 1σ native uncertainty and the combined uncertainty. (f) Ishii OHC record with the combined uncertainty as the dashed line.

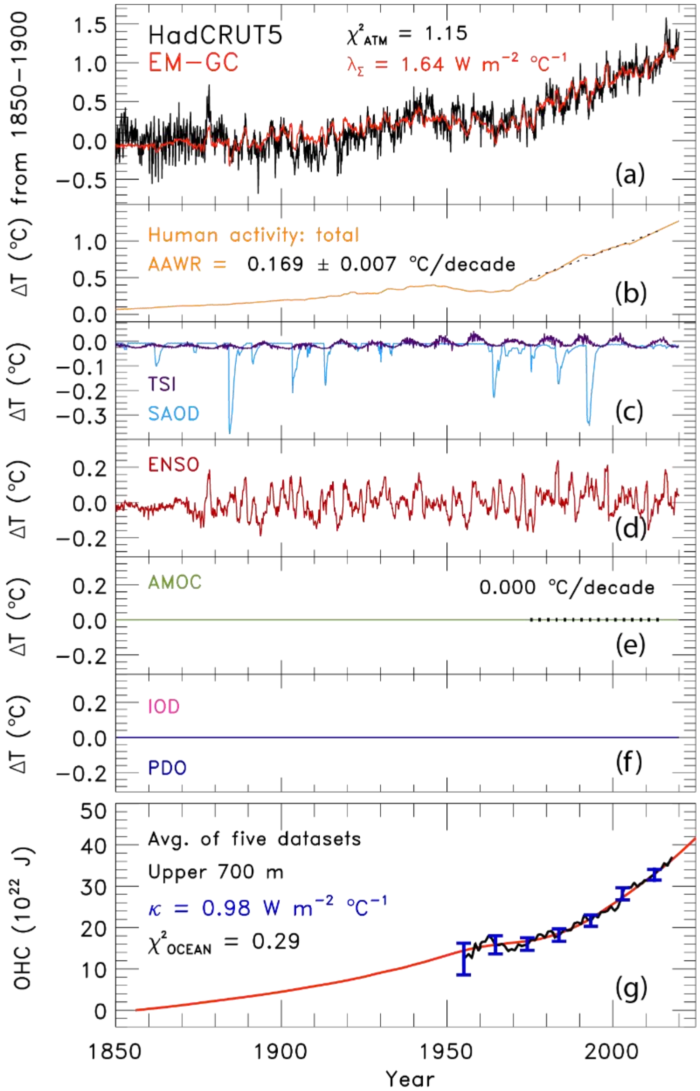

Figure S11. Measured (HadCRUT5) and modeled GMST anomaly (ΔT) relative to a pre-industrial (1850-1900) baseline without AMOC, PDO, and IOD. (a) Observed (black) and modeled (red) ΔT from 1850-2019. This panel also displays the values of λ_{Σ} and χ^2_{ATM} (see text) for this best-fit simulation. (b) Contributions from total human activity. This panel also denotes the numerical value of the attributable anthropogenic warming rate from 1975-2014 (black dashed) as well as the 2σ uncertainty in the slope. The estimates of AAWR show similar results if AMOC is or is not included (see Fig. 1b). (c) Solar irradiance (light blue) and major volcanoes (purple). (d) Influences from ENSO on ΔT. (e-f) Contributions from AMOC, PDO, and IOD to ΔT are set to zero (g) Measured (black) and modeled (red) ocean heat content (OHC) as a function of time for the average of five data sets (see text), the value of χ^2_{OCEAN} for this run, as well as the ocean heat uptake efficiency, κ, needed to provide the best-fit to the OHC record. The error bars (blue) denote the uncertainty in OHC used in this analysis (see Sect. 2.2.8).

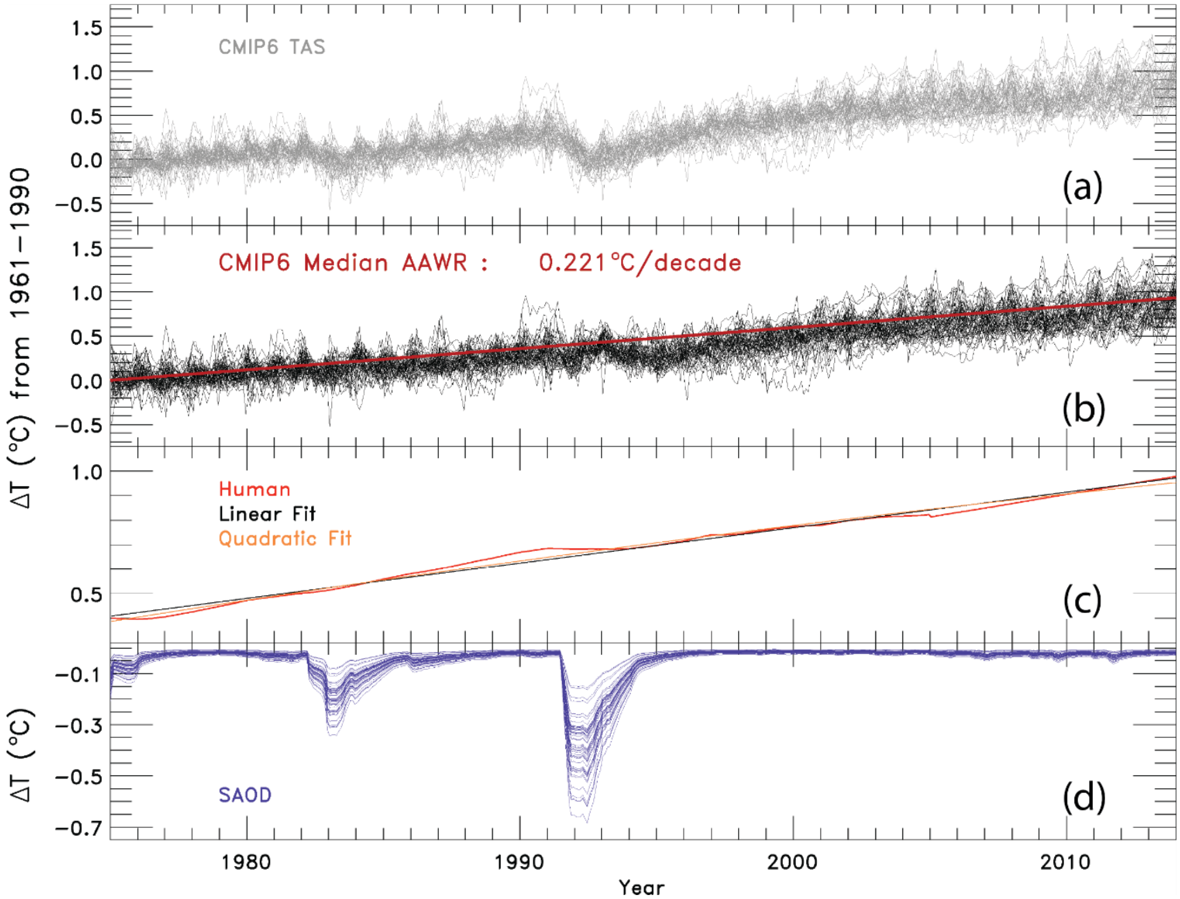

Figure S12. The change in GMST (ΔT) relative to 1961-1990 from the CMIP6 GCMs and the contribution from SAOD from 1975-2014. (a) ΔT from the 50 CMIP6 GCMs. (b) The residual in the change of GMST from the 50 CMIP6 GCMs after subtracting the contribution of SAOD determined by the updated REG method. The median value of AAWR is written on this panel and plotted in red. (c) The human component of global warming, $\Delta T_{ATM,HUMAN}$, from the EM-GC. A linear fit (black) and quadratic fit (red) are plotted on top to show that $\Delta T_{ATM,HUMAN}$ is almost exactly linear. (d) The contribution of SAOD in the 50 CMIP6 GCMs using a lag month calculated for each model.

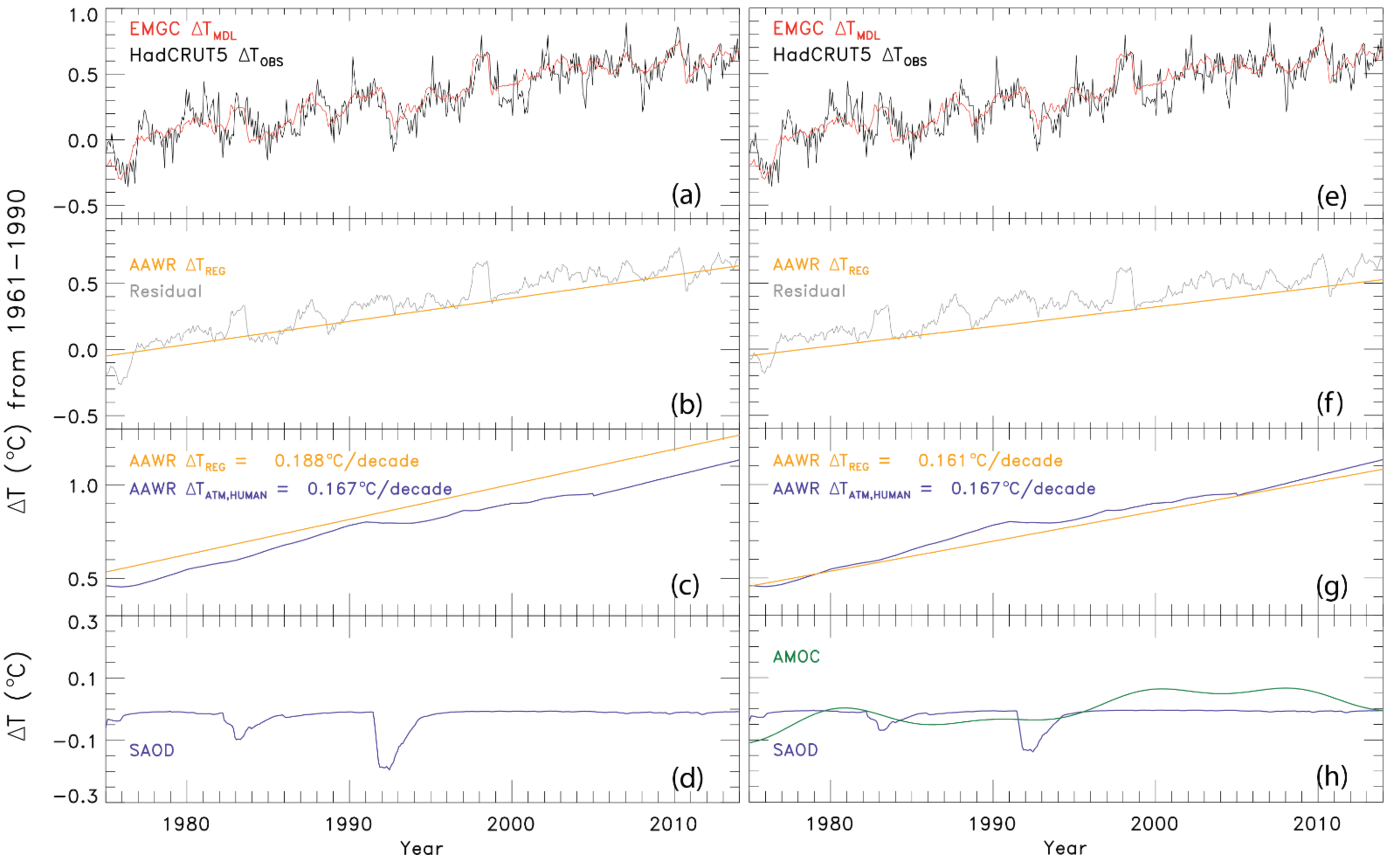

Figure S13. The change in GMST (ΔT) relative to 1961-1990 from observations and modeled output. (a) ΔT from HadCRUT5 and EM-GC simulation. (b) The residual in ΔT from the EM-GC simulation after subtracting the contribution of SAOD determined by the REG method (grey) and ΔT due to humans from the REG method (orange). (c) ΔT due to humans from the REG method (orange) and from the EM-GC (blue). The values of AAWR determined using the REG method and Eq. (9) are shown. (d) The contribution of SAOD to ΔT. (e) Same as (a). (f) Same as (b) but also subtracting the contribution of AMOC determined by the REG method. (g) Same as (c) but using AMOC as a regressor. (h) Same as (d) also showing the contribution of AMOC to ΔT found using the REG method.

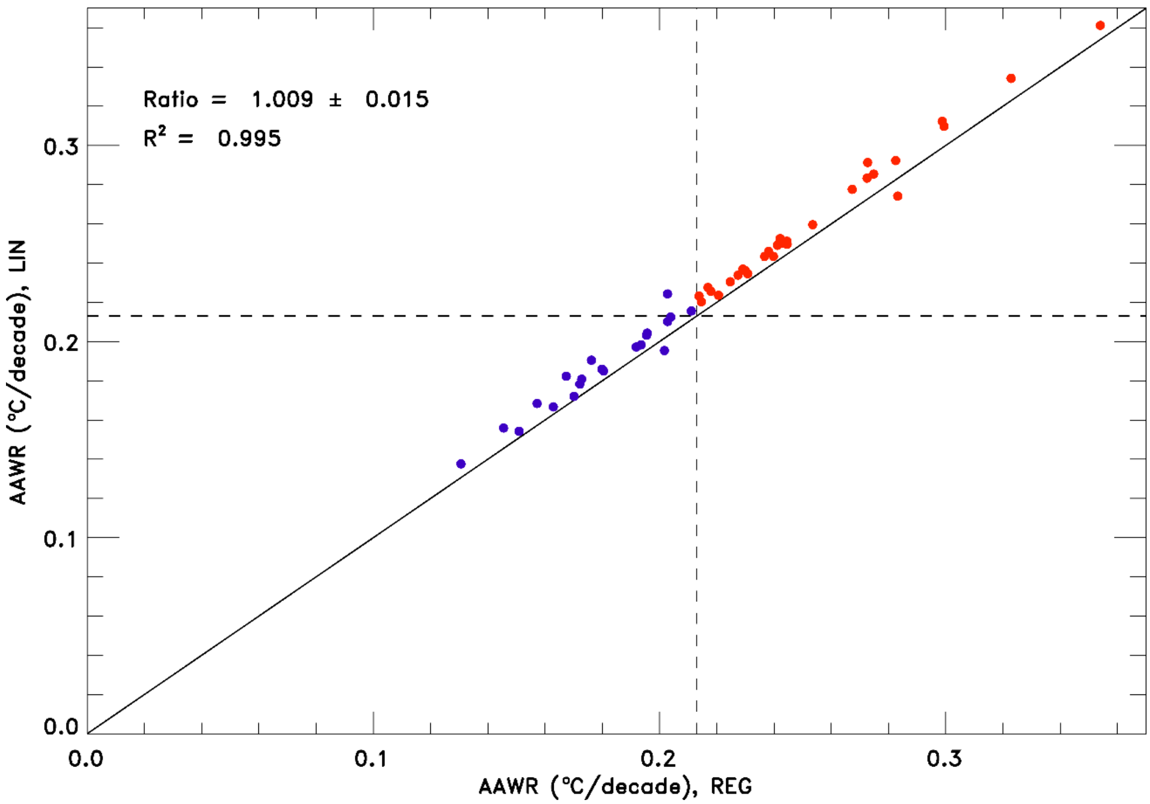

Figure S14. Values of AAWR for 50 CMIP6 GCMs using the LIN and REG methods. The solid black line is the 1:1 line and the vertical and horizontal dashed lines are the maximum value of AAWR determined using the EM-GC and the HadCRUT temperature record. The CMIP6 GCMs that have values of AAWR less than the maximum value from the EM-GC are blue, and the CMIP6 GCMs that have values of AAWR greater than the maximum value from the EM-GC are red. The slope, 1σ standard deviation, and R^2 of the values of AAWR from the CMIP6 GCMs are shown.

Table S2. Values of AAWR calculated using the EM-GC as a function of start and end year. The value of AAWR from 1975-2014 used in the main manuscript is shown in red. Each model run uses the best estimate of AER RF_{2011} (−0.9 W m^{-2}), the average of five OHC records, and the HadCRUT5 GMST record. The impact on varying the start and end year on AAWR is slight, except when a short record is used (i.e., 1984-2004, a 21-year span). A two-decade time span is not long enough to calculate an accurate estimate of AAWR. The value of AAWR is more sensitive to the choice of OHC or temperature record used than the chosen time span.

		Start Year					
	AAWR (°C decade^{-1})	**1970**	**1973**	**1975**	**1979**	**1982**	**1984**
End Year	**2004**	0.181 ± 0.007	0.180 ± 0.009	0.180 ± 0.010	0.169 ± 0.011	0.159 ± 0.013	0.149 ± 0.012
	2006	0.177 ± 0.008	0.175 ± 0.009	0.174 ± 0.010	0.163 ± 0.011	0.153 ± 0.012	0.143 ± 0.011
	2008	0.173 ± 0.007	0.171 ± 0.008	0.169 ± 0.009	0.159 ± 0.010	0.150 ± 0.010	0.141 ± 0.009
	2010	0.172 ± 0.007	0.169 ± 0.008	0.167 ± 0.008	0.158 ± 0.008	0.150 ± 0.009	0.143 ± 0.008
	2012	0.171 ± 0.006	0.168 ± 0.007	0.167 ± 0.008	0.158 ± 0.008	0.152 ± 0.008	0.145 ± 0.007
	2014	0.171 ± 0.005	0.168 ± 0.006	0.167 ± 0.007	0.160 ± 0.007	0.154 ± 0.007	0.149 ± 0.007
	2016	0.171 ± 0.005	0.169 ± 0.006	0.168 ± 0.006	0.161 ± 0.006	0.157 ± 0.007	0.153 ± 0.007
	2018	0.171 ± 0.005	0.170 ± 0.005	0.169 ± 0.006	0.163 ± 0.006	0.159 ± 0.006	0.156 ± 0.006

Table S3. Average values of AAWR calculated from the CMIP6 multi-model results using the regression method as a function of start and end year. The uncertainty corresponds to the 1σ standard deviation of AAWR found from the 50 GCMs. The value of AAWR from 1975-2014 used in the main manuscript is shown in red. The values of AAWR from the CMIP6 multi-model ensemble is more sensitive to the choice of start and end year than the EM-GC due to the small number of models. We use the same start and end year, 1975-2014, for the determination of AAWR for both the EM-GC and the CMIP6 multi-model ensemble for consistency.

		Start Year					
	AAWR (°C decade^{-1})	**1970**	**1973**	**1975**	**1979**	**1982**	**1984**
End Year	**2004**	0.185	0.196	0.200	0.208	0.224	0.230
	2006	0.192	0.203	0.207	0.216	0.232	0.238
	2008	0.196	0.207	0.211	0.220	0.234	0.241
	2010	0.200	0.209	0.214	0.222	0.236	0.241
	2012	0.204	0.213	0.218	0.226	0.239	0.244
	2014	0.208	0.217	0.222	0.230	0.242	0.247

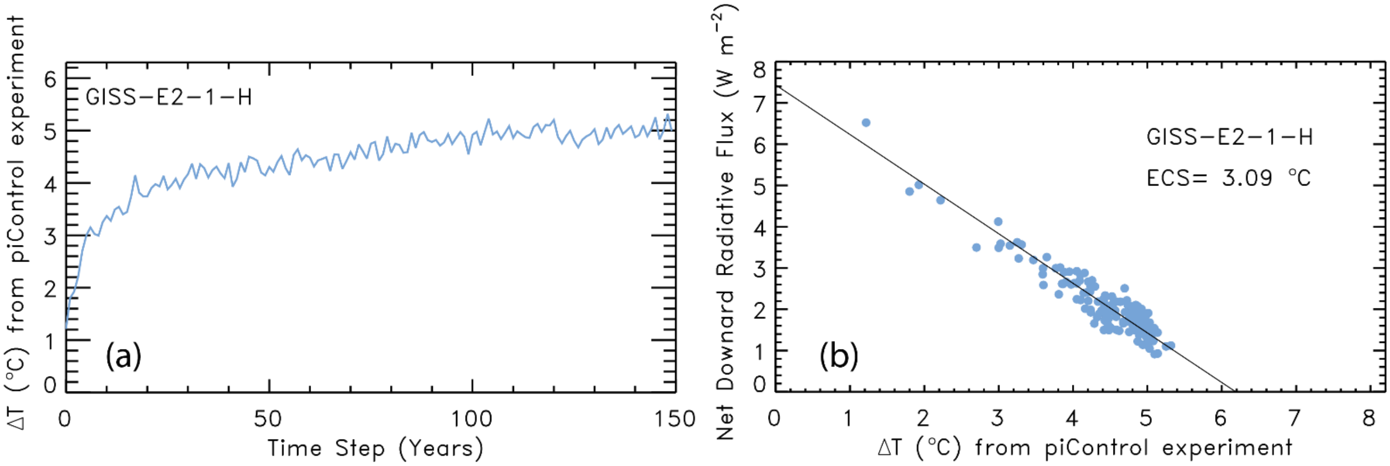

Figure S15. Steps for the calculation of ECS using the Gregory et al. (2004) method, using GISS-E2-1-H (Kelley et al., 2020) as an example. (a) The change in Abrupt 4×CO_2 GMST (variable: tas) from the piControl experiment for 150 years. (b) Abrupt 4×CO_2 net downward radiative flux (variable: rtmt) versus the Abrupt 4×CO_2 GMST change from the piControl experiment for 150 years. The x-intercept of the orthogonal linear least squares fit of the GCM output shown in panel (b), divided by two yields the effective climate sensitivity, which in this case is 3.09°C.

Table S4. Values of AAWR from 1975-2014 for the 50 CMIP6 multi-model Historical simulations available at time of the analysis (April 2020) for both the REG and LIN methods. The asterisk symbol (*) indicates there is only one run used to compute the value of AAWR for that GCM. No asterisk indicates the AAWR value shown in the table is the average of the values of AAWR for all runs of that model. The average ratio of LIN to REG for all 50 models is 1.009 ± 0.015, shown at the bottom of the table and in Fig. S14. The correlation coefficient (r^2) of 0.995 is also shown. We conclude our determination of AAWR from the CMIP6 multi-model ensemble is accurate to ±1%, which is much smaller than the difference between the CMIP6 multi-model ensemble values of AAWR and those found using the EM-GC framework.

Model	AAWR, REG (°C decade^{-1})	AAWR, LIN (°C decade^{-1})	Model	AAWR, REG (°C decade^{-1})	AAWR, LIN (°C decade^{-1})
ACCESS-CM2	0.211	0.216	GFDL-CM4*	0.243	0.250
ACCESS-ESM1-5	0.238	0.246	GFDL-ESM4	0.203	0.224
AWI-CM-1-1-MR	0.215	0.220	GISS-E2-1-G	0.194	0.198
BCC-CSM2-MR	0.217	0.228	GISS-E2-1-G-CC	0.204	0.213
BCC-ESM1	0.241	0.249	GISS-E2-1-H	0.237	0.244
CAMS-CSM1-0	0.131	0.138	HadGEM3-GC31-LL	0.283	0.292
CanESM5	0.354	0.361	HadGEM3-GC31-MM	0.227	0.234
CanESM5-CanOE	0.323	0.334	INM-CM4-8*	0.173	0.181
CAS-ESM2-0	0.196	0.204	INM-CM5-0	0.146	0.156
CESM2	0.240	0.243	IPSL-CM6A-LR	0.230	0.236
CESM2-FV2	0.221	0.224	KACE-1-0-G	0.254	0.260
CESM2-WACCM	0.273	0.291	MCM-UA-1-0	0.225	0.231
CESM2-WACCM-FV2	0.231	0.235	MIROC6	0.157	0.168
CIESM	0.245	0.251	MIROC-ES2L	0.163	0.167
CNRM-CM6-1	0.202	0.196	MPI-ESM1-2-HAM	0.180	0.186
CNRM-CM6-1-HR*	0.172	0.178	MPI-ESM1-2-HR	0.195	0.203
CNRM-ESM2-1	0.170	0.172	MPI-ESM1-2-LR	0.192	0.197
E3SM-1-0	0.267	0.278	MRI-ESM2-0	0.203	0.210
E3SM-1-1*	0.283	0.285	NESM3	0.242	0.253
E3SM-1-1-ECA*	0.275	0.274	NorCPM1	0.180	0.185
EC-Earth3*	0.299	0.310	NorESM2-LM	0.167	0.182
EC-Earth3-Veg*	0.214	0.223	NorESM2-MM*	0.151	0.154
FGOALS-f3-L	0.218	0.226	SAM0-UNICON*	0.245	0.250
FGOALS-g3	0.176	0.191	TaiESM1*	0.273	0.283
FIO-ESM-2-0	0.229	0.237	UKESM1-0-LL	0.299	0.312
Ratio = 1.009 ± 0.015			R^2 = 0.995		

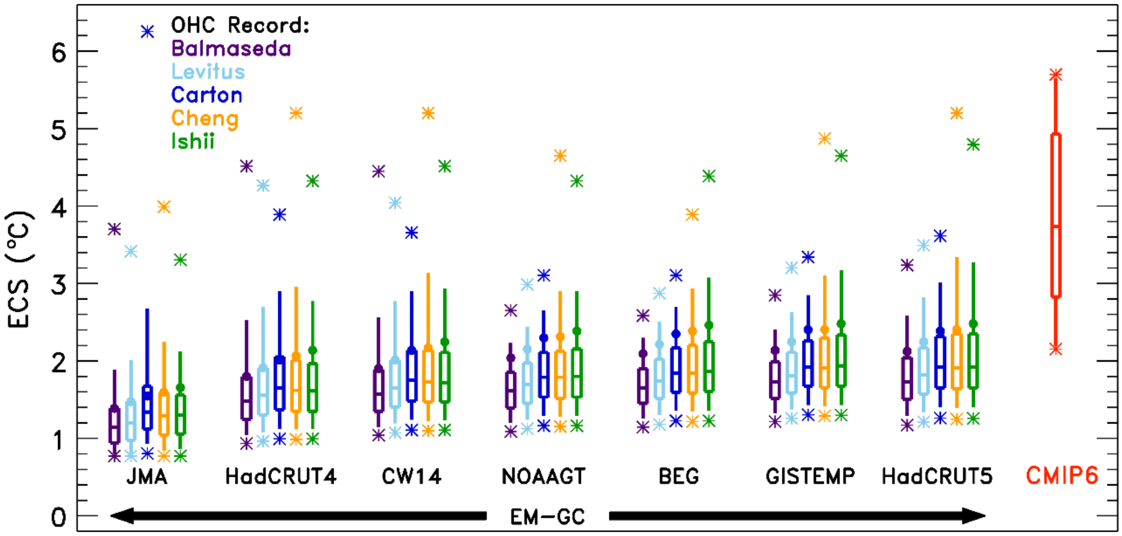

Figure S16. Values of ECS found using the EM-GC and the CMIP6 multi-model ensemble without the aerosol weighting method. Values of ECS utilizing the EM-GC are calculated using seven temperature data sets and five ocean heat content records (as indicated). The box represents the 25th, 50th, and 75th percentiles of the values of ECS and the whiskers denote the 5th and 95th percentiles for the different OHC records and each temperature record without using the aerosol weighting method (unweighted). The stars indicate the minimum and maximum values of ECS. The circles are the values of ECS associated with the best estimate of AER RF_{2011} of −0.9 W m^{-2}. The box labeled CMIP6 is the 25th, 50th, and 75th percentiles of the values of ECS from the CMIP6 multi-model ensemble, the whiskers indicate the 5th and 95th percentiles, and the stars represent the minimum and maximum values of ECS from the CMIP multi-model ensemble.

Table S5. Effective climate sensitivity (ECS) from 28 CMIP6 GCMs. We can only calculate ECS for GCMs that provide Abrupt 4×CO_2 near surface air temperature (output variable: tas), net downward radiative flux (output variable: rtmt), and piControl near surface air temperature (output variable: tas) to the CMIP6 archive at time of the analysis (April 2020). All estimates are for one model run except for CanESM5, which is the average of two runs.

Model	ECS (K)
ACCESS-CM2	4.93
ACCESS-ESM1-5	3.63
BCC-CSM2-MR	3.16
BCC-ESM1	3.74
CanESM5	5.70
CESM2	5.32
CESM2-FV2	5.06
CESM2-WACCM	4.73
CESM2-WACCM-FV2	4.56
E3SM-1-0	5.28
EC-Earth3-Veg	4.34
GFDL-CM4	3.78
GFDL-ESM4	2.61
GISS-E2-1-G	2.71
GISS-E2-2-G	2.25
GISS-E2-1-H	3.09
HadGEM3-GC31-LL	5.65
INM-CM4-8	2.32
INM-CM5-0	2.39
IPSL-CM6A-LR	4.97
MCM-UA-1-0	3.68
MIROC6	2.84
MIROC-ES2L	2.83
NorESM2-LM	2.19
NorESM2-MM	2.15
SAM0-UNICON	3.53
TaiESM1	4.33
UKESM1-0-LL	5.40

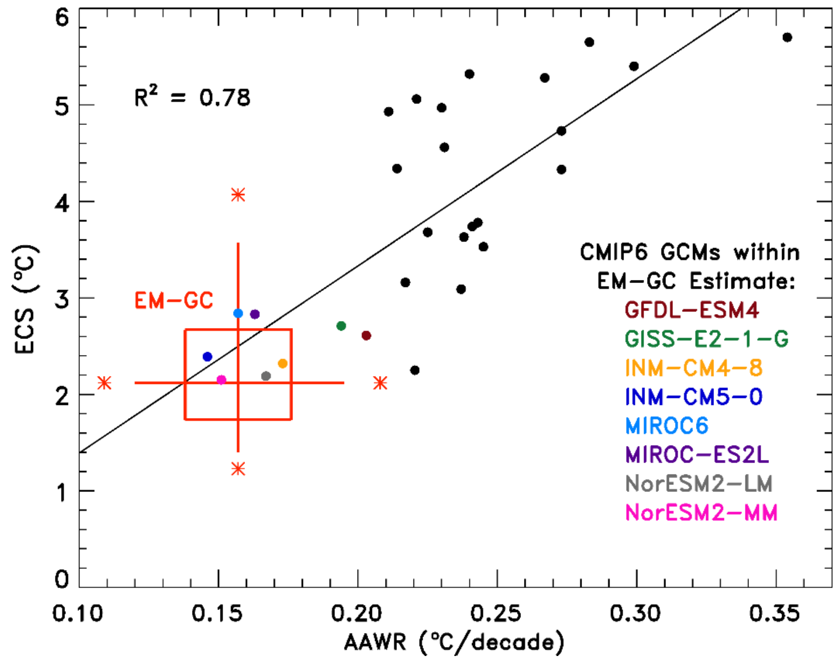

Figure S17. Values of ECS versus AAWR for the CMIP6 multi-model ensemble. The EM-GC estimates of AAWR and ECS based on training to the HadCRUT5 GMST record are plotted as a box and whisker. The box shows the average 25th, 50th, and 75th percentiles for the five OHC records shown for HadCRUT5 in Fig. 6 and Fig. 7. The whiskers represent the average 5th and 95th percentiles. The stars denote the average minimum and maximum values of AAWR or ECS. The eight CMIP6 GCMs that obtain values of AAWR and ECS that are both within the minimum and maximum estimates provided by the EM-GC are identified on the figure. Values of AAWR explain about 78% of the variance in ECS among the CMIP6 GCMs.

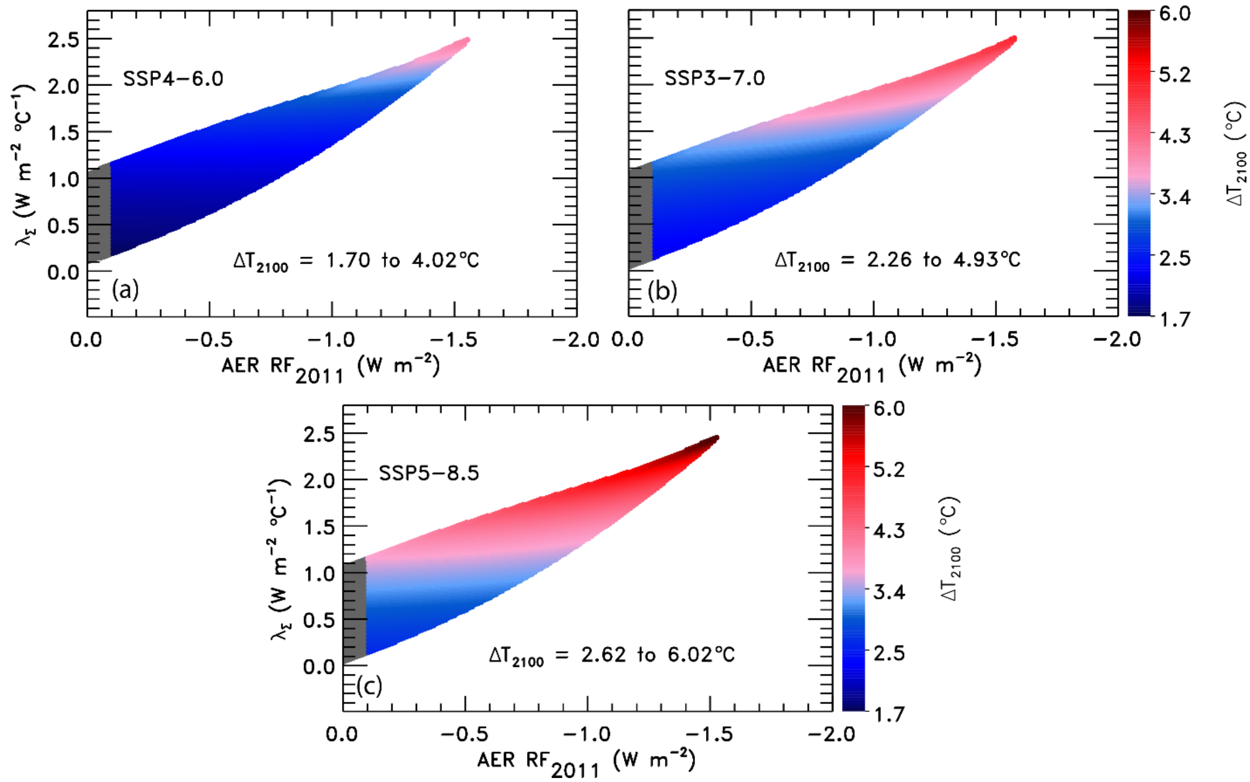

Figure S18. GMST anomaly in 2100 from pre-industrial (ΔT_{2100}) as a function of climate feedback parameter and AER RF_{2011} found using the EM-GC trained with ΔT from HadCRUT5. (a) ΔT_{2100} for SSP4-6.0. The region outside of the tropospheric aerosol radiative forcing rage provided by IPCC 2013 (Myhre et al., 2013) is shaded grey. Colors denote the change in ΔT_{2100}. (b) ΔT_{2100} for SSP3-7.0. (c) ΔT_{2100} for SSP5-8.5.

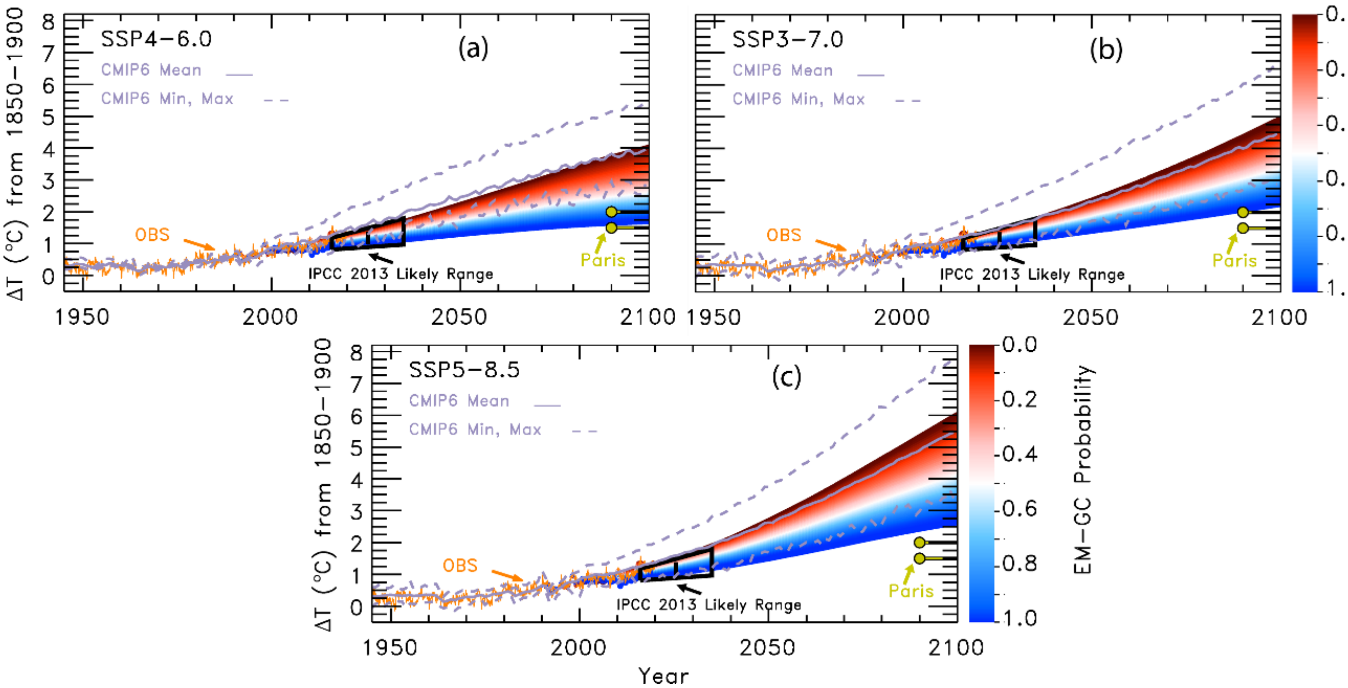

Figure S19. Probabilistic forecasts of future projections of ΔT using the EM-GC trained with ΔT from HadCRUT5 for the SSP4-6.0, SSP3-7.0, and SSP5-8.5 scenarios. (a) Future projections of ΔT for SSP4-6.0. Observations (orange) are from HadCRUT5. The IPCC 2013 likely range of warming (black) is from Figure 11.25b of chapter 11 of the IPCC 2013 report. The Paris Agreement target and upper limit (yellow) are shown for comparison to projections of ΔT using the EM-GC. The CMIP6 minimum, multi-model mean, and maximum values of the rise in ΔT are shown to compare to projections from the EM-GC. Colors denote the probability of reaching at least that temperature by the end of the century and are computed using the aerosol weighting method (see Sect. 2.5). (b) Future projections of ΔT for SSP3-7.0. (c) Future projections of ΔT for SSP5-8.5.

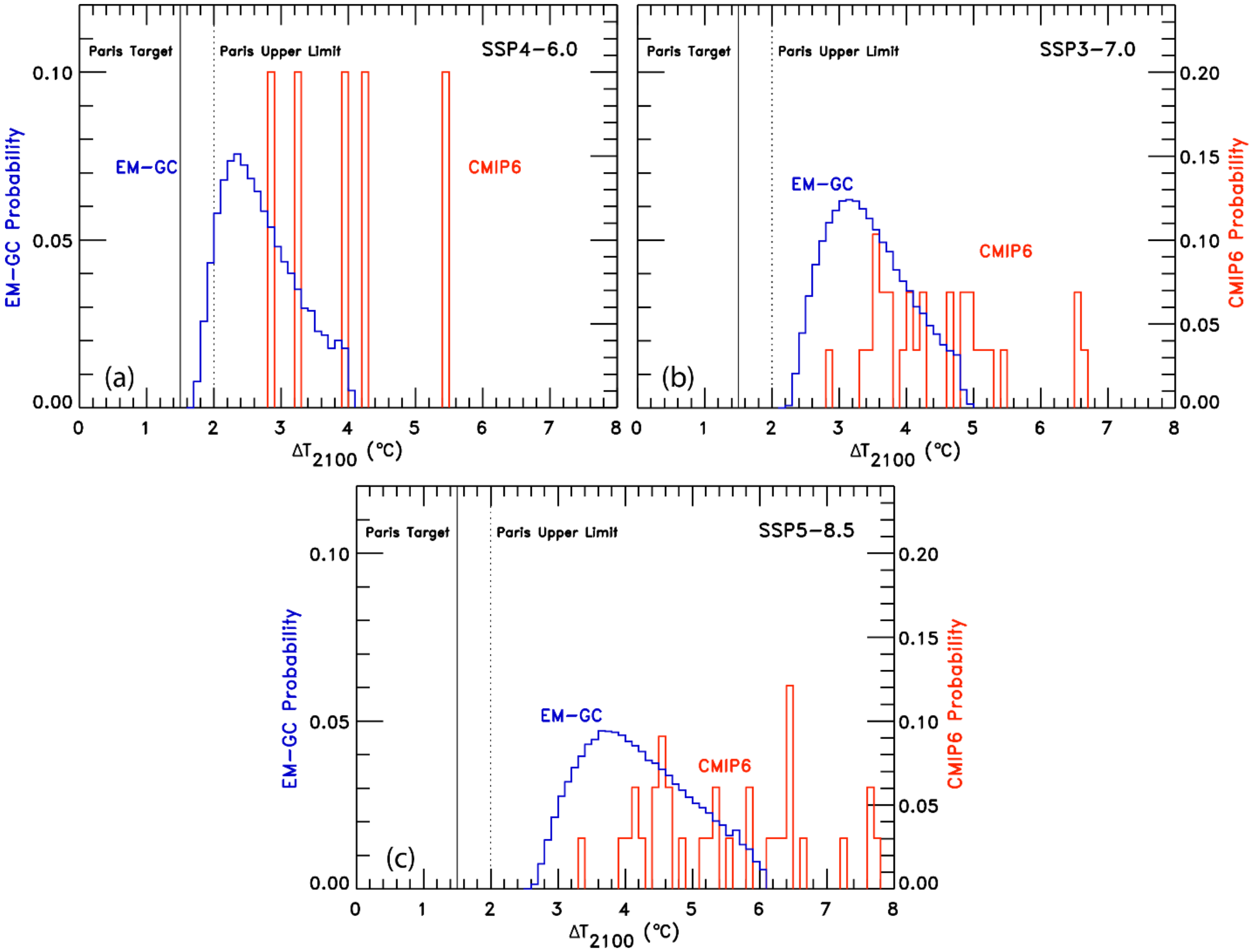

Figure S20. Probability density functions (PDF) for the increase in ΔT_{2100} using the EM-GC and the CMIP6 multi-model ensemble. (a) PDF for EM-GC (blue) results trained with ΔT from HadCRUT5 and CMIP6 multi-model results (red) for SSP4-6.0. The left-hand y-axis is for EM-GC probabilities and the righthand y-axis is for GCM probabilities. (b) PDF for SSP3-7.0. (c) PDF for SSP5-8.5.

Table S6. Probabilities of achieving the Paris Agreement target and upper limit for the various SSP scenarios based on the EM-GC using the HadCRUT4 or HadCRUT5 GMST data set and the CMIP6 multi-model ensemble. The probabilities using the EM-GC are computed using the aerosol weighting method. The probabilities using the CMIP6 GCMs are computed by calculating how many of the models for that scenario are below the temperature limits compared to the total number of models.

	Probability of Staying at or Below 1.5°C			**Probability of Staying at or Below 2.0°C**		
	HadCRUT4	**HadCRUT5**	**CMIP6**	**HadCRUT4**	**HadCRUT5**	**CMIP6**
SSP1-1.9	84%	81%	50%	99%	98%	80%
SSP1-2.6	64%	53%	18%	90%	86%	47%
SSP4-3.4	35%	19%	0%	74%	64%	17%
SSP2-4.5	9%	0%	0%	52%	33%	3%
SSP4-6.0	0%	0%	0%	26%	8%	0%
SSP3-7.0	0%	0%	0%	1%	0%	0%
SSP5-8.5	0%	0%	0%	0%	0%	0%

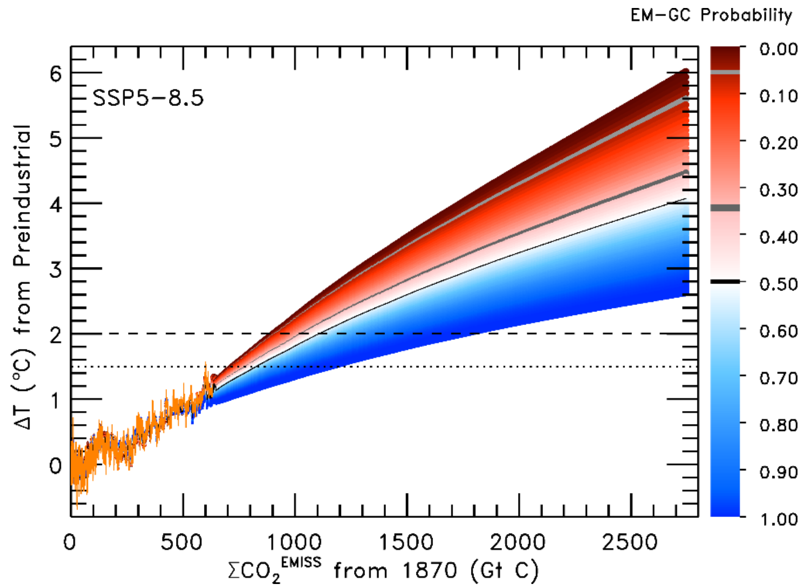

Figure S21. Transient climate response to cumulative CO_2 emissions for SSP5-8.5 using the EM-GC trained with the HadCRUT5 ΔT record. Simulations of the rise in ΔT versus cumulative CO_2 emissions in units of Gt C. The orange line is observations of ΔT from HadCRUT5 plotted against cumulative carbon emissions from the Global Carbon Budget project (Friedlingstein et al., 2019). The dotted and dashed lines denote the Paris Agreement target and upper limit, respectively. The EM-GC projections represent the probability that the future value of ΔT will rise to the indicated level, considering only acceptable fits to the climate record. The probabilities were determined using the aerosol weighting method. The light grey, dark grey, and black curves denote the 95, 66, and 50% probabilities of either the Paris target (intersection of dotted horizontal lines) or upper limit (intersection of dashed lines with curves) being achieved.

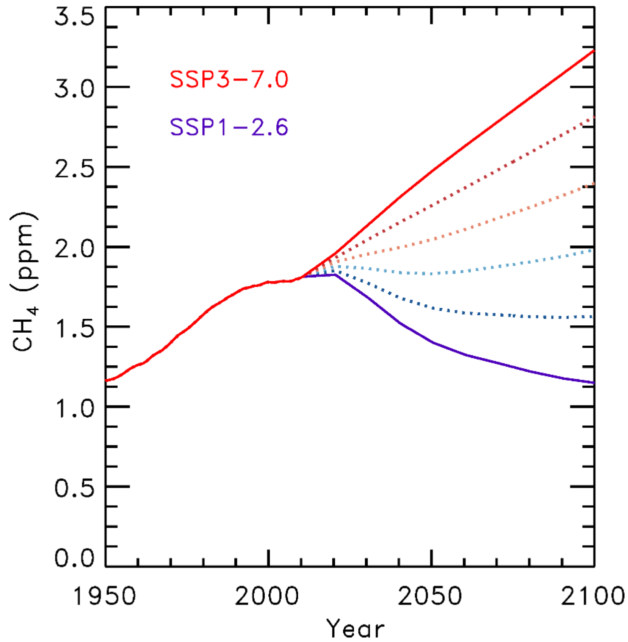

515 **Figure S22.** Blended methane mixing ratios. The dotted lines are linear combinations of the time series of methane abundances using SSP1-2.6 and SSP3-7.0 to span the range of values of future methane. The solid lines are the SSP1-2.6 and SSP3-7.0 methane mixing ratio time series.

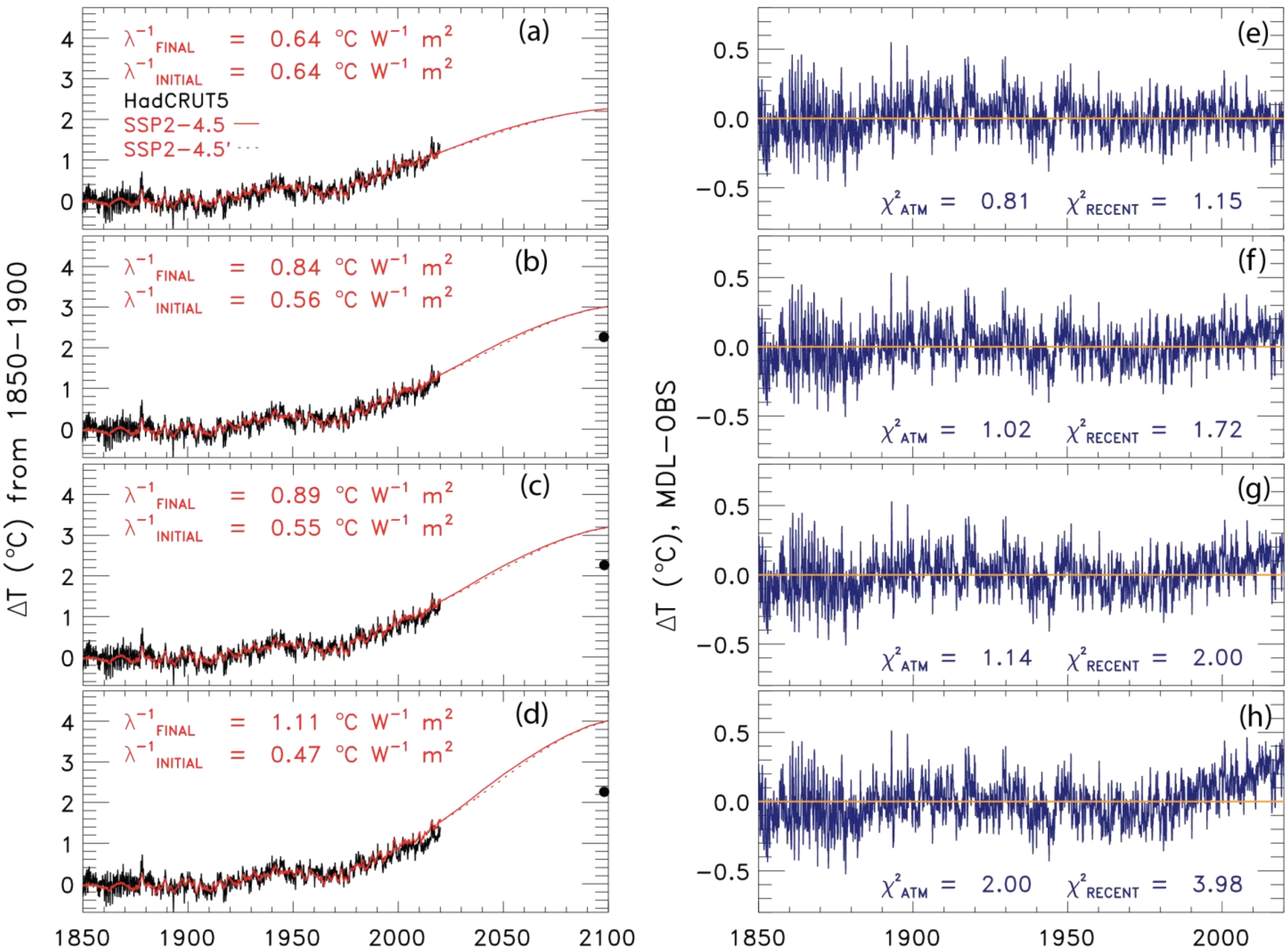

Figure S23. Change in GMST (ΔT) from 1850-2019 for observations from HadCRUT5 (black) and 1850-2100 for modeled (red) using SSP2-4.5 and a value of AER RF_{2011} = −0.9 W m^{-2} and the residual between modeled and observations using an instantaneous time variant λ^{-1}. The solid line denotes a simulation for the original SSP2-4.5 scenario and the dashed line indicates the SSP2-4.5′ simulation (see Sect. 3.3.6). (a) ΔT assuming a constant value of λ^{-1}. (b) ΔT allowing λ^{-1} to increase by 50%. (c) ΔT allowing λ^{-1} to vary while the value of χ^2_{RECENT} is kept below 2. (d) ΔT allowing λ^{-1} to vary while the value of χ^2_{ATM} is kept below 2. (e) Residual between modeled and observed ΔT from 1850-2019 for constant λ^{-1}. (f) Same as (e) but for increasing λ^{-1} by 50%. (g) Same as (f) but for varying λ^{-1} while the value of χ^2_{RECENT} is kept below 2. (h) same as (g) but for varying λ^{-1} while the value of χ^2_{ATM} is kept below 2.

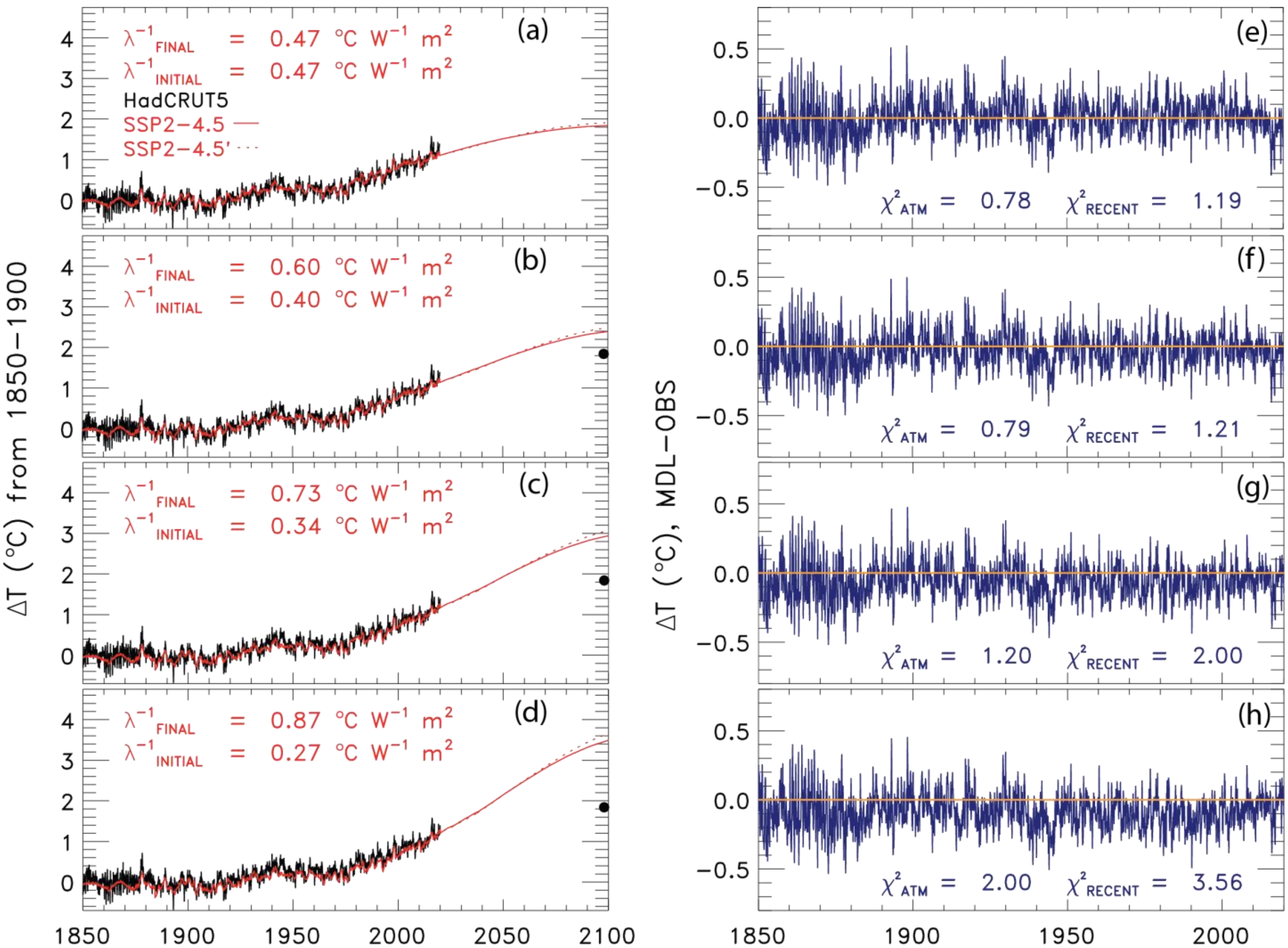

Figure S24. Change in GMST (ΔT) from 1850-2019 for observations from HadCRUT5 (black) and 1850-2100 for modeled (red) using SSP2-4.5 and a value of AER RF_{2011} = −0.4 W m^{-2} and the residual between modeled and observations incorporating a 32.5-year delay between λ^{-1} and a change in RF. The solid line denotes a simulation for the original SSP2-4.5 scenario and the dashed line indicates the SSP2-4.5′ simulation (see Sect. 3.3.6). (a) ΔT assuming a constant value of λ^{-1}. (b) ΔT allowing λ^{-1} to increase by 50%. (c) ΔT allowing λ^{-1} to vary while the value of χ^2_{RECENT} is kept below 2. (d) ΔT allowing λ^{-1} to vary while the value of χ^2_{ATM} is kept below 2. (e) Residual between modeled and observed ΔT from 1850-2019 for constant λ^{-1}. (f) Same as (e) but for increasing λ^{-1} by 50%. (g) Same as (f) but for varying λ^{-1} while the value of χ^2_{RECENT} is kept below 2. (h) same as (g) but for varying λ^{-1} while the value of χ^2_{ATM} is kept below 2.

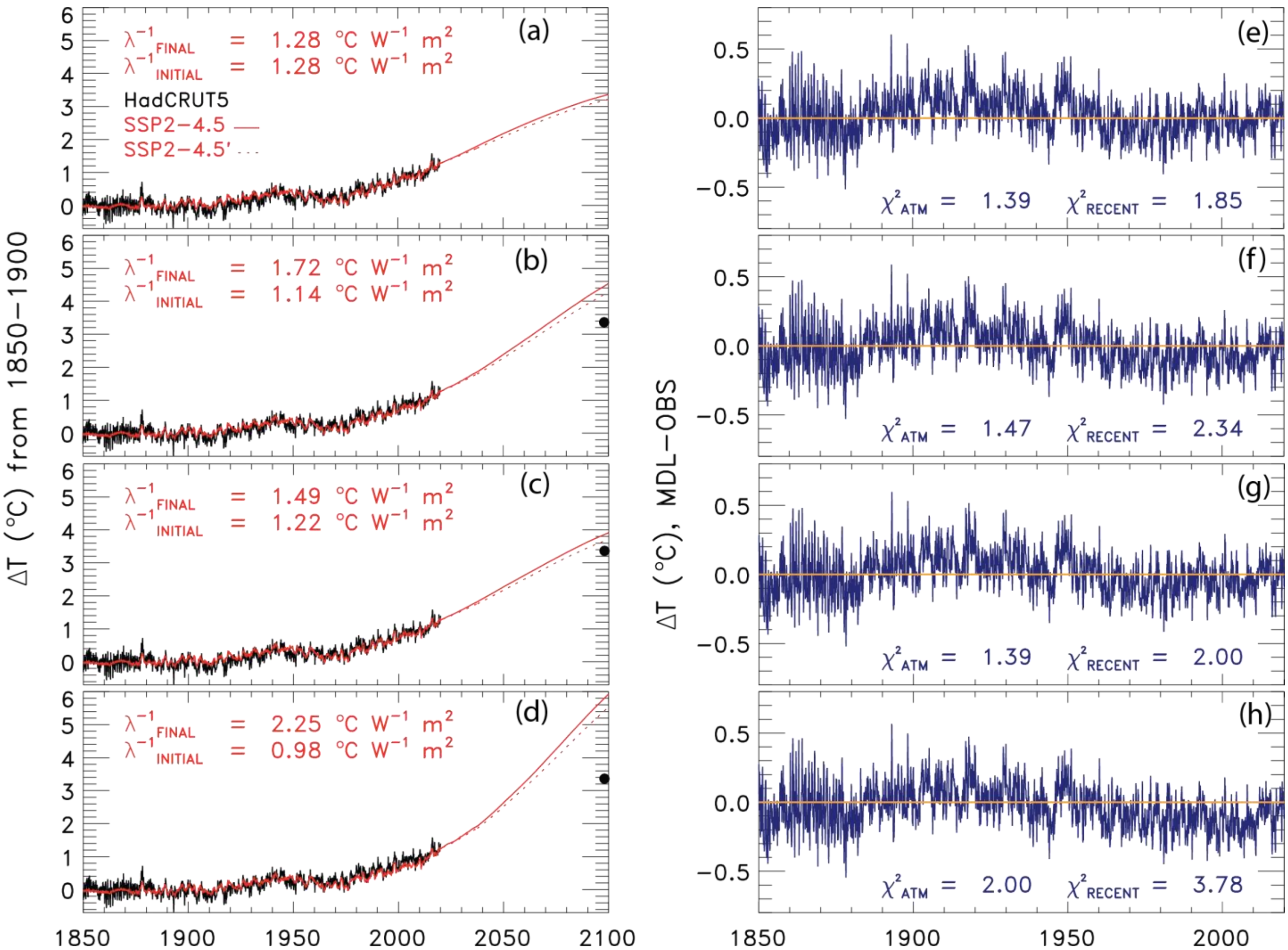

Figure S25. Change in GMST (ΔT) from 1850-2019 for observations from HadCRUT5 (black) and 1850-2100 for modeled (red) using SSP2-4.5 and a value of AER RF_{2011} = −1.5 W m^{-2} and the residual between modeled and observations incorporating a 32.5-year delay between λ^{-1} and a change in RF. The solid line denotes a simulation for the original SSP2-4.5 scenario and the dashed line indicates the SSP2-4.5′ simulation (see Sect. 3.3.6). (a) ΔT assuming a constant value of λ^{-1}. (b) ΔT allowing λ^{-1} to increase by 50%. (c) ΔT allowing λ^{-1} to vary while the value of χ^2_{RECENT} is kept below 2. (d) ΔT allowing λ^{-1} to vary while the value of χ^2_{ATM} is kept below 2. (e) Residual between modeled and observed ΔT from 1850-2019 for constant λ^{-1}. (f) Same as (e) but for increasing λ^{-1} by 50%. (g) Same as (f) but for varying λ^{-1} while the value of χ^2_{RECENT} is kept below 2. (h) same as (g) but for varying λ^{-1} while the value of χ^2_{ATM} is kept below 2.

Table S7. Details of the CMIP6 GCMs used in this study.

Institution	Model	Model Output
AS-RCEC	TaiESM1	No reference provided
AWI	AWI-CM-1-1-MR	(Semmler et al., 2018a, 2018b, 2018c, 2019a, 2019b)
BCC	BCC-CSM2-MR	(Wu et al., 2018a, 2018b, 2018c; Xin et al., 2019a, 2019b, 2019c, 2019d)
	BCC-ESM1	(Zhang et al., 2018a, 2018b, 2019)
CAMS	CAMS-CSM1-0	(Rong, 2019a, 2019b, 2019c, 2019d, 2019e, 2019f)
CAS	CAS-ESM2-0	(Chai, 2019)
	FGOALS-f3-L	(YU, 2019a, 2019b, 2019c, 2019d, 2019e)
	FGOALS-g3	(Li, 2019a, 2019b, 2019c, 2019d, 2019e)
CCCma	CanESM5	(Swart et al., 2019f, 2019g, 2019h, 2019i, 2019j, 2019k, 2019l, 2019m, 2019n, 2019o)
	CanESM5-CanOE	(Swart et al., 2019a, 2019b, 2019c, 2019d, 2019e)
CNRM-CERFACS	CNRM-CM6-1	(Voldoire, 2018, 2019c, 2019d, 2019e, 2019f)
	CNRM-CM6-1-HR	(Voldoire, 2019a, 2019b, 2020a, 2020b)
	CNRM-ESM2-1	(Seferian, 2018; Voldoire, 2019g, 2019h, 2019i, 2019j, 2019k, 2019l)
CSIRO	ACCESS-ESM1-5	(Ziehn et al., 2019a, 2019b, 2019c, 2019d, 2019e, 2019f, 2019g)
CSIRO-ARCCSS	ACCESS-CM2	(Dix et al., 2019a, 2019b, 2019c, 2019d, 2019e, 2019f, 2019g)
E3SM-Project	E3SM-1-0	(Bader et al., 2018, 2019a, 2019b)
	E3SM-1-1-ECA	(Bader et al., 2020)
E3SM-Project RUBISCO	E3SM-1-1	(Bader et al., 2019c)
EC-Earth-Consortium	EC-Earth3	(EC-Earth Consortium (EC-Earth), 2019i, 2019j, 2019k, 2019l, 2019m)
	EC-Earth3-Veg	(EC-Earth Consortium (EC-Earth), 2019a, 2019b, 2019c, 2019d, 2019e, 2019f, 2019g, 2019h)

FIO-QLNM	FIO-ESM-2-0	(Song et al., 2019a, 2019b, 2019c, 2019d)
HAMMOZ-Consortium	MPI-ESM1-2-HAM	(Neubauer et al., 2019)
INM	INM-CM4-8	(Volodin et al., 2019a, 2019b, 2019c, 2019d, 2019e, 2019f, 2019g)
	INM-CM5-0	(Volodin et al., 2019m, 2019h, 2019n, 2019i, 2019j, 2019k, 2019l)
IPSL	IPSL-CM6A-LR	(Boucher et al., 2018a, 2018b, 2018c, 2019a, 2019b, 2019c, 2019d, 2019e, 2019f, 2019g)
MIROC	MIROC6	(Shiogama et al., 2019a, 2019b, 2019c, 2019d, 2019e, 2019f, 2019g; Tatebe and Watanabe, 2018a, 2018b, 2018c)
	MIROC-ES2L	(Hajima et al., 2019; Tachiiri et al., 2019a, 2019b, 2019c, 2019d, 2019e)
MOHC	HadGEM3-GC31-MM	(Ridley et al., 2019c)
MOHC NERC	HadGEM3-GC31-LL	(Good, 2019, 2020a, 2020b; Ridley et al., 2018, 2019a, 2019b)
MOHC, NERC, NIMS-KMA, NIWA	UKESM1-0-LL	(Byun, 2020; Good et al., 2019a, 2019b, 2019c, 2019d, 2019e, 2019f; Tang et al., 2019a, 2019b, 2019c)
MPI-M AWI	MPI-ESM1-2-LR	(Wieners et al., 2019a, 2019b, 2019c, 2019d, 2019e)
MPI-M DWD DKRZ	MPI-ESM1-2-HR	(Jungclaus et al., 2019; Schupfner et al., 2019a, 2019b, 2019c, 2019d; Steger et al., 2019)
MRI	MRI-ESM2-0	(Yukimoto et al., 2019a, 2019b, 2019c, 2019d, 2019e, 2019f, 2019g, 2019h)
NASA-GISS	GISS-E2-1-G	(NASA Goddard Institute for Space Studies (NASA/GISS), 2018a, 2018b, 2018c, 2020a, 2020b, 2020c, 2020d)
	GISS-E2-1-G-CC	No reference provided
	GISS-E2-2-G	(NASA Goddard Institute for Space Studies (NASA/GISS), 2019a)
	GISS-E2-1-H	(NASA Goddard Institute for Space Studies (NASA/GISS), 2018d, 2019b, 2019c)
NCAR	CESM2-WACCM-FV2	(Danabasoglu, 2019d, 2019e, 2020a)

	CESM2	(Danabasoglu, 2019c, 2019d, 2019e, 2019f, 2019g, 2019h; Danabasoglu et al., 2019)
	CESM2-FV2	(Danabasoglu, 2019b, 2019c, 2020b)
	CESM2-WACCM	(Danabasoglu, 2019f, 2019g, 2019h, 2019a, 2019i, 2019j, 2019k)
	NorCPM1	(Bethke et al., 2019a, 2019b, 2019c)
NCC	NorESM2-LM	(Seland et al., 2019a, 2019b, 2019c, 2019d, 2019e, 2019f, 2019g)
	NorESM2-MM	(Bentsen et al., 2019a, 2019b, 2019c, 2019d, 2019e, 2019f, 2019g)
NIMS-KMA	KACE-1-0-G	(Byun et al., 2019a, 2019b, 2019c, 2019d, 2019e)
NOAA-GFDL	GFDL-CM4	(Guo et al., 2018a, 2018b, 2018c, 2018d, 2018e)
	GFDL-ESM4	(John et al., 2018a, 2018b, 2018c, 2018d, 2018e; Krasting et al., 2018a, 2018b, 2018c)
NUIST	NESM3	(Cao, 2019a, 2019b, 2019c; Cao and Wang, 2019)
SNU	SAM0-UNICON	(Park and Shin, 2019a, 2019b, 2019c)
THU	CIESM	(Huang, 2019a, 2019b, 2020a, 2020b)
UA	MCM-UA-1-0	(Stouffer, 2019a, 2019b, 2019c, 2019d, 2019e, 2019f, 2019g)

References

Bader, D. C., Leung, R., Taylor, M. and McCoy, R. B.: E3SM-Project E3SM1.0 model output prepared for CMIP6 CMIP piControl, Earth System Grid Federation, , doi:https://doi.org/10.22033/ESGF/CMIP6.4499, 2018.

Bader, D. C., Leung, R., Taylor, M. and McCoy, R. B.: E3SM-Project E3SM1.0 model output prepared for CMIP6 CMIP abrupt-4xCO2, Earth System Grid Federation, , doi:https://doi.org/10.22033/ESGF/CMIP6.4491, 2019a.

Bader, D. C., Leung, R., Taylor, M. and McCoy, R. B.: E3SM-Project E3SM1.0 model output prepared for CMIP6 CMIP historical, Earth System Grid Federation, , doi:https://doi.org/10.22033/ESGF/CMIP6.4497, 2019b.

Bader, D. C., Leung, R., Taylor, M. and McCoy, R. B.: E3SM-Project E3SM1.1 model output prepared for CMIP6 CMIP historical, Earth System Grid Federation, , doi:https://doi.org/10.22033/ESGF/CMIP6.11485, 2019c.

Bader, D. C., Leung, R., Taylor, M. and McCoy, R. B.: E3SM-Project E3SM1.1ECA model output prepared for CMIP6 CMIP historical, Earth System Grid Federation, , doi:https://doi.org/10.22033/ESGF/CMIP6.11486, 2020.

Balmaseda, M. A., Trenberth, K. E. and Källén, E.: Distinctive climate signals in reanalysis of global ocean heat content, Geophys. Res. Lett., 40(9), 1754–1759, doi:10.1002/grl.50382, 2013a.

Balmaseda, M. A., Mogensen, K. and Weaver, A. T.: Evaluation of the ECMWF ocean reanalysis system ORAS4, Q. J. R. Meteorol. Soc., 139(674), 1132–1161, doi:10.1002/qj.2063, 2013b.

Bentsen, M., Oliviè, D. J. L., Seland, Ø., Toniazzo, T., Gjermundsen, A., Graff, L. S., Debernard, J. B., Gupta, A. K., He, Y., Kirkevåg, A., Schwinger, J., Tjiputra, J., Aas, K. S., Bethke, I., Fan, Y., Griesfeller, J., Grini, A., Guo, C., Ilicak, M., Karset, I. H. H., Landgren, O. A., Liakka, J., Moseid, K. O., Nummelin, A., Spensberger, C., Tang, H., Zhang, Z., Heinze, C., Iversen, T. and Schulz, M.: NCC NorESM2-MM model output prepared for CMIP6 CMIP abrupt-4xCO2, Earth System Grid Federation, , doi:https://doi.org/10.22033/ESGF/CMIP6.7840, 2019a.

Bentsen, M., Oliviè, D. J. L., Seland, Ø., Toniazzo, T., Gjermundsen, A., Graff, L. S., Debernard, J. B., Gupta, A. K., He, Y., Kirkevåg, A., Schwinger, J., Tjiputra, J., Aas, K. S., Bethke, I., Fan, Y., Griesfeller, J., Grini, A., Guo, C., Ilicak, M., Karset, I. H. H., Landgren, O. A., Liakka, J., Moseid, K. O., Nummelin, A., Spensberger, C., Tang, H., Zhang, Z., Heinze, C., Iversen, T. and Schulz, M.: NCC NorESM2-MM model output prepared for CMIP6 CMIP historical, Earth System Grid Federation, , doi:https://doi.org/10.22033/ESGF/CMIP6.8040, 2019b.

Bentsen, M., Oliviè, D. J. L., Seland, Ø., Toniazzo, T., Gjermundsen, A., Graff, L. S., Debernard, J. B., Gupta, A. K., He, Y., Kirkevåg, A., Schwinger, J., Tjiputra, J., Aas, K. S., Bethke, I., Fan, Y., Griesfeller, J., Grini, A., Guo, C., Ilicak, M., Karset, I. H. H., Landgren, O. A., Liakka, J., Moseid, K. O., Nummelin, A., Spensberger, C., Tang, H., Zhang, Z., Heinze, C., Iversen, T. and Schulz, M.: NCC NorESM2-MM model output prepared for CMIP6 CMIP piControl, Earth System Grid Federation, , doi:https://doi.org/10.22033/ESGF/CMIP6.8221, 2019c.

Bentsen, M., Oliviè, D. J. L., Seland, Ø., Toniazzo, T., Gjermundsen, A., Graff, L. S., Debernard, J. B., Gupta, A. K., He, Y., Kirkevåg, A., Schwinger, J., Tjiputra, J., Aas, K. S., Bethke, I., Fan, Y., Griesfeller, J., Grini, A., Guo, C., Ilicak, M., Karset, I. H. H., Landgren, O. A., Liakka, J., Moseid, K. O., Nummelin, A., Spensberger, C., Tang, H., Zhang, Z., Heinze, C., Iversen, T. and Schulz, M.: NCC NorESM2-MM model output prepared for CMIP6 ScenarioMIP ssp126, Earth System Grid Federation, , doi:https://doi.org/10.22033/ESGF/CMIP6.8250, 2019d.

Bentsen, M., Oliviè, D. J. L., Seland, Ø., Toniazzo, T., Gjermundsen, A., Graff, L. S., Debernard, J. B., Gupta, A. K., He, Y., Kirkevåg, A., Schwinger, J., Tjiputra, J., Aas, K. S., Bethke, I., Fan, Y., Griesfeller, J., Grini, A., Guo, C., Ilicak, M., Karset, I. H. H., Landgren, O. A., Liakka, J., Moseid, K. O., Nummelin, A., Spensberger, C., Tang, H., Zhang, Z., Heinze, C., Iversen, T. and Schulz, M.: NCC NorESM2-MM model output prepared for CMIP6 ScenarioMIP ssp245, Earth System Grid Federation, , doi:https://doi.org/10.22033/ESGF/CMIP6.8255, 2019e.

Bentsen, M., Oliviè, D. J. L., Seland, Ø., Toniazzo, T., Gjermundsen, A., Graff, L. S., Debernard, J. B., Gupta, A. K., He, Y., Kirkevåg, A., Schwinger, J., Tjiputra, J., Aas, K. S., Bethke, I., Fan, Y., Griesfeller, J., Grini, A., Guo, C., Ilicak, M., Karset, I. H. H., Landgren, O. A., Liakka, J., Moseid, K. O., Nummelin, A., Spensberger, C., Tang, H., Zhang, Z., Heinze, C., Iversen, T. and Schulz, M.: NCC NorESM2-MM model output prepared for CMIP6 ScenarioMIP ssp370, Earth System Grid Federation, , doi:https://doi.org/10.22033/ESGF/CMIP6.8270, 2019f.

Bentsen, M., Oliviè, D. J. L., Seland, Ø., Toniazzo, T., Gjermundsen, A., Graff, L. S., Debernard, J. B., Gupta, A. K., He, Y., Kirkevåg, A., Schwinger, J., Tjiputra, J., Aas, K. S., Bethke, I., Fan, Y., Griesfeller, J., Grini, A., Guo, C., Ilicak, M., Karset, I. H. H., Landgren, O. A., Liakka, J., Moseid, K. O., Nummelin, A., Spensberger, C., Tang, H., Zhang, Z., Heinze, C., Iversen, T. and Schulz, M.: NCC NorESM2-MM model output prepared for CMIP6 ScenarioMIP ssp585, Earth System Grid Federation, , doi:https://doi.org/10.22033/ESGF/CMIP6.8321, 2019g.

Bethke, I., Wang, Y., Counillon, F., Kimmritz, M., Fransner, F., Samuelsen, A., Langehaug, H. R., Chiu, P.-G., Bentsen, M., Guo, C., Tjiputra, J., Kirkevåg, A., Oliviè, D. J. L., Seland, Ø., Fan, Y., Lawrence, P., Eldevik, T. and Keenlyside, N.: NCC NorCPM1 model output prepared for CMIP6 CMIP abrupt-4xCO2, Earth System Grid Federation, , doi:https://doi.org/10.22033/ESGF/CMIP6.10862, 2019a.

Bethke, I., Wang, Y., Counillon, F., Kimmritz, M., Fransner, F., Samuelsen, A., Langehaug, H. R., Chiu, P., Bentsen, M., Guo, C., Tjiputra, J., Kirkevåg, A., Oliviè, D. J. L., Seland, Ø., Fan, Y., Lawrence, P., Eldevik, T. and Keenlyside, N.: NCC NorCPM1 model output prepared for CMIP6 CMIP historical, Earth System Grid Federation, , doi:https://doi.org/10.22033/ESGF/CMIP6.10894, 2019b.

Bethke, I., Wang, Y., Counillon, F., Kimmritz, M., Fransner, F., Samuelsen, A., Langehaug, H. R., Chiu, P.-G., Bentsen, M., Guo, C., Tjiputra, J., Kirkevåg, A., Oliviè, D. J. L., Seland, Ø., Fan, Y., Lawrence, P., Eldevik, T. and Keenlyside, N.: NCC NorCPM1 model output prepared for CMIP6 CMIP piControl, Earth System Grid Federation, , doi:https://doi.org/10.22033/ESGF/CMIP6.10896, 2019c.

Bony, S., Colman, R., Kattsov, V. M., Allan, R. P., Bretherton, C. S., Dufresne, J. L., Hall, A., Hallegatte, S., Holland, M. M., Ingram, W., Randall, D. A., Soden, B. J., Tselioudis, G. and Webb, M. J.: How well do we understand and evaluate climate change feedback processes?, J. Clim., 19(15), 3445–3482, doi:10.1175/JCLI3819.1, 2006.

Boucher, O., Denvil, S., Caubel, A. and Foujols, M. A.: IPSL IPSL-CM6A-LR model output prepared for CMIP6 CMIP abrupt-4xCO2, Earth System Grid Federation, , doi:https://doi.org/10.22033/ESGF/CMIP6.5109, 2018a.

Boucher, O., Denvil, S., Caubel, A. and Foujols, M. A.: IPSL IPSL-CM6A-LR model output prepared for CMIP6 CMIP historical, Earth System Grid Federation, , doi:https://doi.org/10.22033/ESGF/CMIP6.5195, 2018b.

Boucher, O., Denvil, S., Caubel, A. and Foujols, M. A.: IPSL IPSL-CM6A-LR model output prepared for CMIP6 CMIP piControl, Earth System Grid Federation, , doi:https://doi.org/10.22033/ESGF/CMIP6.5251, 2018c.

Boucher, O., Denvil, S., Caubel, A. and Foujols, M. A.: IPSL IPSL-CM6a-LR model output prepared for CMIP6 ScenarioMIP ssp119, Earth System Grid Federation, , doi:https://doi.org/10.22033/ESGF/CMIP6.5261, 2019a.

Boucher, O., Denvil, S., Caubel, A. and Foujols, M. A.: IPSL IPSL-CM6A-LR model output prepared for CMIP6 ScenarioMIP ssp126, Earth System Grid Federation, , doi:https://doi.org/10.22033/ESGF/CMIP6.5262, 2019b.

Boucher, O., Denvil, S., Caubel, A. and Foujols, M. A.: IPSL IPSL-CM6A-LR model output prepared for CMIP6 ScenarioMIP ssp370, Earth System Grid Federation, , doi:https://doi.org/10.22033/ESGF/CMIP6.5265, 2019c.

Boucher, O., Denvil, S., Caubel, A. and Foujols, M. A.: IPSL IPSL-CM6A-LR model output prepared for CMIP6 ScenarioMIP ssp434, Earth System Grid Federation, , doi:https://doi.org/10.22033/ESGF/CMIP6.5267, 2019d.

Boucher, O., Denvil, S., Caubel, A. and Foujols, M. A.: IPSL IPSL-CM6A-LR model output prepared for CMIP6 ScenarioMIP ssp460, Earth System Grid Federation, , doi:https://doi.org/10.22033/ESGF/CMIP6.5268, 2019e.

Boucher, O., Denvil, S., Caubel, A. and Foujols, M. A.: IPSL IPSL-CM6A-LR model output prepared for CMIP6 ScenarioMIP ssp585, Earth System Grid Federation, , doi:https://doi.org/10.22033/ESGF/CMIP6.5271, 2019f.

Boucher, O., Denvil, S., Caubel, A. and Foujols, M. A.: PSL IPSL-CM6A-LR model output prepared for CMIP6 ScenarioMIP ssp245, Earth System Grid Federation, , doi:https://doi.org/10.22033/ESGF/CMIP6.5264, 2019g.

Byun, Y.-H.: NIMS-KMA UKESM1.0-LL model output prepared for CMIP6 CMIP historical, Earth System Grid Federation, , doi:https://doi.org/10.22033/ESGF/CMIP6.8379, 2020.

Byun, Y.-H., Lim, Y.-J., Sung, H. M., Kim, J., Sun, M. and Kim, B.-H.: NIMS-KMA KACE1.0-G model output prepared for CMIP6 CMIP historical, Earth System Grid Federation, , doi:https://doi.org/10.22033/ESGF/CMIP6.8378, 2019a.

Byun, Y.-H., Lim, Y.-J., Shim, S., Sung, H. M., Sun, M., Kim, J., Kim, B.-H., Lee, J.-H. and Moon, H.: NIMS-KMA KACE1.0-G model output prepared for CMIP6 ScenarioMIP ssp126, Earth System Grid Federation, , doi:https://doi.org/10.22033/ESGF/CMIP6.8432, 2019b.

Byun, Y.-H., Lim, Y.-J., Shim, S., Sung, H. M., Sun, M., Kim, J., Kim, B.-H., Lee, J.-H. and Moon, H.: NIMS-KMA KACE1.0-G model output prepared for CMIP6 ScenarioMIP ssp245, Earth System Grid Federation, , doi:https://doi.org/10.22033/ESGF/CMIP6.8435, 2019c.

Byun, Y.-H., Lim, Y.-J., Shim, S., Sung, H. M., Sun, M., Kim, J., Kim, B.-H., Lee, J.-H. and Moon, H.: NIMS-KMA KACE1.0-G model output prepared for CMIP6 ScenarioMIP ssp370, Earth System Grid Federation, , doi:https://doi.org/10.22033/ESGF/CMIP6.8437, 2019d.

Byun, Y.-H., Lim, Y.-J., Shim, S., Sung, H. M., Sun, M., Kim, J., Kim, B.-H., Lee, J.-H. and Moon, H.: NIMS-KMA KACE1.0-G model output prepared for CMIP6 ScenarioMIP ssp585, Earth System Grid Federation, , doi:https://doi.org/10.22033/ESGF/CMIP6.8456, 2019e.

Canty, T., Mascioli, N. R., Smarte, M. D. and Salawitch, R. J.: An empirical model of global climate – Part 1: A critical evaluation of volcanic cooling, Atmos. Chem. Phys., 13(8), 3997–4031, doi:10.5194/acp-13-3997-2013, 2013.

Cao, J.: NUIST NESMv3 model output prepared for CMIP6 ScenarioMIP ssp126, Earth System Grid Federation, , doi:https://doi.org/10.22033/ESGF/CMIP6.8780, 2019a.

Cao, J.: NUIST NESMv3 model output prepared for CMIP6 ScenarioMIP ssp245, Earth System Grid Federation, , doi:https://doi.org/10.22033/ESGF/CMIP6.8781, 2019b.

Cao, J.: NUIST NESMv3 model output prepared for CMIP6 ScenarioMIP ssp585, Earth System Grid Federation, , doi:https://doi.org/10.22033/ESGF/CMIP6.8790, 2019c.

Cao, J. and Wang, B.: NUIST NESMv3 model output prepared for CMIP6 CMIP historical, , doi:https://doi.org/10.22033/ESGF/CMIP6.8769, 2019.

Carton, J. A., Chepurin, G. A. and Chen, L.: SODA3: A New Ocean Climate Reanalysis, J. Clim., 31(17), 6967–6983, doi:10.1175/jcli-d-18-0149.1, 2018.

Chai, Z.: CAS CAS-ESM1.0 model output prepared for CMIP6 CMIP historical, Earth System Grid Federation, , doi:https://doi.org/10.22033/ESGF/CMIP6.3353, 2019.

Chen, X., Guo, Z., Zhou, T., Li, J., Rong, X., Xin, Y., Chen, H. and Su, J.: Climate Sensitivity and Feedbacks of a New Coupled Model CAMS-CSM to Idealized CO2 Forcing: A Comparison with CMIP5 Models, J. Meteorol. Res., 33(1), 31–45, doi:10.1007/s13351-019-8074-5, 2019.

Cheng, L., Trenberth, K. E., Fasullo, J., Boyer, T., Abraham, J. and Zhu, J.: Improved estimates of ocean heat content from 1960 to 2015, Sci. Adv., 3(3), 1–11, doi:10.1126/sciadv.1601545, 2017.

Danabasoglu, G.: NCAR CESM-WACCM model output prepared for CMIP6 ScenarioMIP ssp126, Earth System Grid Federation, , doi:https://doi.org/10.22033/ESGF/CMIP6.10100, 2019a.

Danabasoglu, G.: NCAR CESM2-FV2 model output prepared for CMIP6 CMIP historical, Earth System Grid Federation, , doi:https://doi.org/10.22033/ESGF/CMIP6.11297, 2019b.

Danabasoglu, G.: NCAR CESM2-FV2 model output prepared for CMIP6 CMIP piControl, Earth System Grid Federation, , doi:https://doi.org/10.22033/ESGF/CMIP6.11301, 2019c.

Danabasoglu, G.: NCAR CESM2-WACCM-FV2 model output prepared for CMIP6 CMIP historical, Earth System Grid Federation, , doi:https://doi.org/10.22033/ESGF/CMIP6.11298, 2019d.

Danabasoglu, G.: NCAR CESM2-WACCM-FV2 model output prepared for CMIP6 CMIP piControl, Earth System Grid Federation, , doi:https://doi.org/10.22033/ESGF/CMIP6.11302, 2019e.

Danabasoglu, G.: NCAR CESM2-WACCM model output prepared for CMIP6 CMIP abrupt-4xCO2, Earth System Grid Federation, , doi:https://doi.org/10.22033/ESGF/CMIP6.10039, 2019f.

Danabasoglu, G.: NCAR CESM2-WACCM model output prepared for CMIP6 CMIP historical, Earth System Grid Federation, , doi:https://doi.org/10.22033/ESGF/CMIP6.10071, 2019g.

Danabasoglu, G.: NCAR CESM2-WACCM model output prepared for CMIP6 CMIP piControl, Earth System Grid Federation, , doi:https://doi.org/10.22033/ESGF/CMIP6.10094, 2019h.

Danabasoglu, G.: NCAR CESM2-WACCM model output prepared for CMIP6 ScenarioMIP ssp245, Earth System Grid Federation, , doi:https://doi.org/10.22033/ESGF/CMIP6.10101, 2019i.

Danabasoglu, G.: NCAR CESM2-WACCM model output prepared for CMIP6 ScenarioMIP ssp370, Earth System Grid Federation, , doi:https://doi.org/10.22033/ESGF/CMIP6.10102, 2019j.

Danabasoglu, G.: NCAR CESM2-WACCM model output prepared for CMIP6 ScenarioMIP ssp585, Earth System Grid Federation, , doi:https://doi.org/10.22033/ESGF/CMIP6.10115, 2019k.

Danabasoglu, G.: NCAR CESM2 model output prepared for CMIP6 CMIP abrupt-4xCO2, Earth System Grid Federation, , doi:https://doi.org/10.22033/ESGF/CMIP6.7519, 2019l.

Danabasoglu, G.: NCAR CESM2 model output prepared for CMIP6 CMIP historical, Earth System Grid Federation,

, doi:https://doi.org/10.22033/ESGF/CMIP6.7627, 2019m.

Danabasoglu, G.: NCAR CESM2 model output prepared for CMIP6 ScenarioMIP ssp126, Earth System Grid Federation, , doi:https://doi.org/10.22033/ESGF/CMIP6.7746, 2019n.

Danabasoglu, G.: NCAR CESM2 model output prepared for CMIP6 ScenarioMIP ssp245, Earth System Grid Federation, , doi:https://doi.org/10.22033/ESGF/CMIP6.7748, 2019o.

Danabasoglu, G.: NCAR CESM2 model output prepared for CMIP6 ScenarioMIP ssp370, Earth System Grid Federation, , doi:https://doi.org/10.22033/ESGF/CMIP6.7753, 2019p.

Danabasoglu, G.: NCAR CESM2 model output prepared for CMIP6 ScenarioMIP ssp585, Earth System Grid Federation, , doi:https://doi.org/10.22033/ESGF/CMIP6.7768, 2019q.

Danabasoglu, G.: CAR CESM2-WACCM-FV2 model output prepared for CMIP6 CMIP abrupt-4xCO2, Earth System Grid Federation, , doi:https://doi.org/10.22033/ESGF/CMIP6.11286, 2020a.

Danabasoglu, G.: NCAR CESM2-FV2 model output prepared for CMIP6 CMIP abrupt-4xCO2, Earth System Grid Federation, , doi:https://doi.org/10.22033/ESGF/CMIP6.11285, 2020b.

Danabasoglu, G., Lawrence, D., Lindsay, K., Lipscomb, W. and Strand, G.: NCAR CESM2 model output prepared for CMIP6 CMIP piControl, Earth System Grid Federation, , doi:https://doi.org/10.22033/ESGF/CMIP6.7733, 2019.

Dix, M., Bi, D., Dobrohotoff, P., Fiedler, R., Harman, I., Law, R., Mackallah, C., Marsland, S., O'Farrell, S., Rashid, H., Srbinovsky, J., Sullivan, A., Trenham, C., Vohralik, P., Watterson, I., Williams, G., Woodhouse, M., Bodman, R., Dias, F. B., Domingues, C., Hannah, N., Heerdegen, A., Savita, A., Wales, S., Allen, C., Druken, K., Evans, B., Richards, C., Ridzwan, S. M., Roberts, D., Smillie, J., Snow, K., Ward, M. and Yang, R.: CSIRO-ARCCSS ACCESS-CM2 model output prepared for CMIP6 CMIP abrupt-4xCO2, Earth System Grid Federation, , doi:https://doi.org/10.22033/ESGF/CMIP6.4237, 2019a.

Dix, M., Bi, D., Dobrohotoff, P., Fiedler, R., Harman, I., Law, R., Mackallah, C., Marsland, S., O'Farrell, S., Rashid, H., Srbinovsky, J., Sullivan, A., Trenham, C., Vohralik, P., Watterson, I., Williams, G., Woodhouse, M., Bodham, R., Dias, F. B., Domingues, C. M., Hannah, N., Heerdegen, A., Savita, A., Wales, S., Allen, C., Druken, K., Evans, B., Richards, C., Ridzwan, S. M., Robers, D., Smillie, J., Snow, K., Ward, M. and Yang, R.: CSIRO-ARCCSS ACCESS-CM2 model output prepared for CMIP6 CMIP historical, Earth System Grid Federation, , doi:https://doi.org/10.22033/ESGF/CMIP6.4271, 2019b.

Dix, M., Bi, D., Dobrohotoff, P., Fiedler, R., Harman, I., Law, R., Mackallah, C., Marsland, S., O'Farrell, S., Rashid, H., Srbinovsky, J., Sullivan, A., Trenham, C., Vohralik, P., Watterson, I., Williams, G., Woodhouse, M., Bodman, R., Dias, F. B., Domingues, C., Hannah, N., Heerdegen, A., Savita, A., Wales, S., Allen, C., Druken, K., Evans, B., Richards, C., Ridzwan, S. M., Roberts, D., Smillie, J., Snow, K., Ward, M. and Yang, R.: CSIRO-ARCCSS ACCESS-CM2 model output prepared for CMIP6 CMIP piControl, Earth System Grid Federation, , doi:https://doi.org/10.22033/ESGF/CMIP6.4311, 2019c.

Dix, M., Bi, D., Dobrohotoff, P., Fiedler, R., Harman, I., Law, R., Mackallah, C., Marsland, S., O'Farrell, S., Rashid, H., Srbinovsky, J., Sullivan, A., Trenham, C., Vohralik, P., Watterson, I., Williams, G., Woodhouse, M., Bodman, R., Dias, F. B., Domingues, C. M., Hannah, N., Heerdegen, A., Savita, A., Wales, S., Allen, C., Druken, K., Evans, B., Richards, C., Ridzwan, S. M., Roberts, D., Smillie, J., Snow, K., Ward, M. and Yang, R.: CSIRO-ARCCSS ACCESS-CM2 model output prepared for CMIP6 ScenarioMIP ssp126, Earth System Grid Federation, , doi:https://doi.org/10.22033/ESGF/CMIP6.4319, 2019d.

Dix, M., Bi, D., Dobrohotoff, P., Fiedler, R., Harman, I., Law, R., Mackallah, C., Marsland, S., O'Farrell, S., Rashid, H., Srbinovsky, J., Sullivan, A., Trenham, C., Vohralik, P., Watterson, I., Williams, G., Woodhouse, M., Bodman, R., Dias, F. B., Domingues, C., Hannah, N., Heerdegen, A., Savita, A., Wales, S., Allen, C., Druken, K., Evans, B., Richards, C., Ridzwan, S. M., Roberts, D., Smillie, J., Snow, K., Ward, M. and Yang, R.: CSIRO-ARCCSS ACCESS-CM2 model output prepared for CMIP6 ScenarioMIP ssp245, Earth System Grid Federation, , doi:https://doi.org/10.22033/ESGF/CMIP6.4321, 2019e.

Dix, M., Bi, D., Dobrohotoff, P., Fiedler, R., Harman, I., Law, R., Mackallah, C., Marsland, S., O'Farrell, S., Rashid, H., Srbinovsky, J., Sullivan, A., Trenham, C., Vohralik, P., Watterson, I., Williams, G., Woodhouse, M., Bodman, R., Dias, F. B., Domingues, C., Hannah, N., Heerdegen, A., Savita, A., Wales, S., Allen, C., Druken, K., Evans, B., Richards, C., Ridzwan, S. M., Roberts, D., Smillie, J., Snow, K., Ward, M. and Yang, R.: CSIRO-ARCCSS ACCESS-CM2 model output prepared for CMIP6 ScenarioMIP ssp370, Earth System Grid Federation, , doi:https://doi.org/10.22033/ESGF/CMIP6.4323, 2019f.

Dix, M., Bi, D., Dobrohotoff, P., Fiedler, R., Harman, I., Law, R., Mackallah, C., Marsland, S., O'Farrell, S., Rashid, H., Srbinovsky, J., Sullivan, A., Trenham, C., Vohralik, P., Watterson, I., Williams, G., Woodhouse, M., Bodman, R., Dias, F. B., Domingues, C., Hannah, N., Heerdegen, A., Savita, A., Wales, S., Allen, C., Druken, K., Evans, B., Richards, C., Ridzwan, S. M., Roberts, D., Smillie, J., Snow, K., Ward, M. and Yang, R.: CSIRO-ARCCSS ACCESS-CM2 model output prepared for CMIP6 ScenarioMIP ssp585, Earth System Grid Federation, , doi:https://doi.org/10.22033/ESGF/CMIP6.4332, 2019g.

Douglass, D. H. and Knox, R. S.: Climate forcing by the volcanic eruption of Mount Pinatubo, Geophys. Res. Lett., 32(5), 1–5, doi:10.1029/2004GL022119, 2005.

EC-Earth Consortium (EC-Earth): EC-Earth-Consortium EC-Earth3-Veg model output prepared for CMIP6 CMIP, Earth System Grid Federation, , doi:https://doi.org/10.22033/ESGF/CMIP6.4706, 2019a.

EC-Earth Consortium (EC-Earth): EC-Earth-Consortium EC-Earth3-Veg model output prepared for CMIP6 CMIP abrupt-4xCO2, Earth System Grid Federation, , doi:https://doi.org/10.22033/ESGF/CMIP6.4524, 2019b.

EC-Earth Consortium (EC-Earth): EC-Earth-Consortium EC-Earth3-Veg model output prepared for CMIP6 CMIP piControl, Earth System Grid Federation, , doi:https://doi.org/10.22033/ESGF/CMIP6.4848, 2019c.

EC-Earth Consortium (EC-Earth): EC-Earth-Consortium EC-Earth3-Veg model output prepared for CMIP6 ScenarioMIP ssp119, Earth System Grid Federation, , doi:https://doi.org/10.22033/ESGF/CMIP6.4872, 2019d.

EC-Earth Consortium (EC-Earth): EC-Earth-Consortium EC-Earth3-Veg model output prepared for CMIP6 ScenarioMIP ssp126, Earth System Grid Federation, , doi:https://doi.org/10.22033/ESGF/CMIP6.4876, 2019e.

EC-Earth Consortium (EC-Earth): EC-Earth-Consortium EC-Earth3-Veg model output prepared for CMIP6 ScenarioMIP ssp245, Earth System Grid Federation, , doi:https://doi.org/10.22033/ESGF/CMIP6.4882, 2019f.

EC-Earth Consortium (EC-Earth): EC-Earth-Consortium EC-Earth3-Veg model output prepared for CMIP6 ScenarioMIP ssp370, Earth System Grid Federation, , doi:https://doi.org/10.22033/ESGF/CMIP6.4886, 2019g.

EC-Earth Consortium (EC-Earth): EC-Earth-Consortium EC-Earth3-Veg model output prepared for CMIP6 ScenarioMIP ssp585, Earth System Grid Federation, , doi:https://doi.org/10.22033/ESGF/CMIP6.4914, 2019h.

EC-Earth Consortium (EC-Earth): EC-Earth-Consortium EC-Earth3 model output prepared for CMIP6 CMIP abrupt-4xCO2, Earth System Grid Federation, , doi:https://doi.org/10.22033/ESGF/CMIP6.4518, 2019i.

EC-Earth Consortium (EC-Earth): EC-Earth-Consortium EC-Earth3 model output prepared for CMIP6 CMIP historical, Earth System Grid Federation, , doi:https://doi.org/10.22033/ESGF/CMIP6.4700, 2019j.

EC-Earth Consortium (EC-Earth): EC-Earth-Consortium EC-Earth3 model output prepared for CMIP6 CMIP piControl, Earth System Grid Federation, , doi:https://doi.org/10.22033/ESGF/CMIP6.4842, 2019k.

EC-Earth Consortium (EC-Earth): EC-Earth-Consortium EC-Earth3 model output prepared for CMIP6 ScenarioMIP ssp126, Earth System Grid Federation, , doi:https://doi.org/10.22033/ESGF/CMIP6.4874, 2019l.

EC-Earth Consortium (EC-Earth): EC-Earth-Consortium EC-Earth3 model output prepared for CMIP6 ScenarioMIP ssp370, Earth System Grid Federation, , doi:https://doi.org/10.22033/ESGF/CMIP6.4884, 2019m.

Foster, G. and Rahmstorf, S.: Global temperature evolution 1979–2010, Environ. Res. Lett., 6(4), 044022, doi:10.1088/1748-9326/6/4/044022, 2011.

Friedlingstein, P., Meinshausen, M., Arora, V. K., Jones, C. D., Anav, A., Liddicoat, S. K. and Knutti, R.: Uncertainties in CMIP5 climate projections due to carbon cycle feedbacks, J. Clim., 27(2), 511–526, doi:10.1175/JCLI-D-12-00579.1, 2014.

Friedlingstein, P., Jones, M. W., Sullivan, M. O., Andrew, R. M., Hauck, J., Peters, G. P., Peters, W., Pongratz, J., Sitch, S., Quéré, C. Le, Bakker, D. C. E., Canadell, J. G., Ciais, P., Jackson, R. B., Anthoni, P., Barbero, L., Bastos, A., Bastrikov, V., Becker, M., Bopp, L., Buitenhuis, E., Chandra, N., Chevallier, F., Chini, L. P., Currie, K., Feely, R. A., Gehlen, M., Gilfillan, D., Gkritzalis, T., Goll, D. S., Gruber, N., Gutekunst, S., Harris, I., Haverd, V., Houghton, R. A., Hurtt, G., Ilyina, T., Jain, A. K., Joetzjer, E., Kaplan, J. O., Kato, E., Goldewijk, K. K., Korsbakken, J. I., Landschützer, P., Lauvset, S. K., Lefevre, N., Lenton, A., Lienert, S., Lombardozzi, D., Marland, G., McGuire, P. C., Melton, J. R., Metzl, N., Munro, D. R., Nabel, J. E. M. S., Nakaoka, S., Neill, C., Omar, A. M., Ono, T., Peregon, A., Pierrot, D., Poulter, B., Rehder, G., Resplandy, L., Robertson, E., Rodenbeck, C., Seferian, R., Schwinger, J., Smith, N., Tans, P. P., Tian, H., Tilbrook, B., Tubiello, F. N., Van Der Werf, G. R., Wiltshire, A. J. and Zaehle, S.: Global Carbon Budget 2019, Earth Syst. Sci. Data, (11), 1783–1838, 2019.

Good, P.: MOHC HadGEM3-GC31-LL model output prepared for CMIP6 ScenarioMIP ssp245, Earth System Grid Federation, , doi:https://doi.org/10.22033/ESGF/CMIP6.10851, 2019.

Good, P.: MOHC HadGEM3-GC31-LL model output prepared for CMIP6 ScenarioMIP ssp126, Earth System Grid Federation, , doi:https://doi.org/10.22033/ESGF/CMIP6.10849, 2020a.

Good, P.: MOHC HadGEM3-GC31-LL model output prepared for CMIP6 ScenarioMIP ssp585, Earth System Grid Federation, , doi:https://doi.org/10.22033/ESGF/CMIP6.10901, 2020b.

Good, P., Sellar, A., Tang, Y., Rumbold, S., Ellis, R., Kelley, D. and Kuhlbrodt, T.: MOHC UKESM1.0-LL model output prepared for CMIP6 ScenarioMIP ssp119, Earth System Grid Federation, , doi:https://doi.org/10.22033/ESGF/CMIP6.6329, 2019a.

Good, P., Sellar, A., Tang, Y., Rumbold, S., Ellis, R., Kelley, D. and Kuhlbrodt, T.: MOHC UKESM1.0-LL model output prepared for CMIP6 ScenarioMIP ssp126, Earth System Grid Federation, , doi:https://doi.org/10.22033/ESGF/CMIP6.6333, 2019b.

Good, P., Sellar, A., Tang, Y., Rumbold, S., Ellis, R., Kelley, D. and Kuhlbrodt, T.: MOHC UKESM1.0-LL model output prepared for CMIP6 ScenarioMIP ssp245, Earth System Grid Federation, , doi:https://doi.org/10.22033/ESGF/CMIP6.6339, 2019c.

Good, P., Sellar, A., Tang, Y., Rumbold, S., Ellis, R., Kelley, D. and Kuhlbrodt, T.: MOHC UKESM1.0-LL model output prepared for CMIP6 ScenarioMIP ssp370, Earth System Grid Federation, , doi:https://doi.org/10.22033/ESGF/CMIP6.6347, 2019d.

Good, P., Sellar, A., Tang, Y., Rumbold, S., Ellis, R., Kelley, D. and Kuhlbrodt, T.: MOHC UKESM1.0-LL model output prepared for CMIP6 ScenarioMIP ssp434, Earth System Grid Federation, , doi:https://doi.org/10.22033/ESGF/CMIP6.6389, 2019e.

Good, P., Sellar, A., Tang, Y., Rumbold, S., Ellis, R., Kelley, D. and Kuhlbrodt, T.: MOHC UKESM1.0-LL model output prepared for CMIP6 ScenarioMIP ssp585, Earth System Grid Federation, , doi:https://doi.org/10.22033/ESGF/CMIP6.6405, 2019f.

Gregory, J. M., Ingram, W. J., Palmer, M. A., Jones, G. S., Stott, P. A., Thorpe, R. B., Lowe, J. A., Johns, T. C. and Williams, K. D.: A new method for diagnosing radiative forcing and climate sensitivity, Geophys. Res. Lett., 31(3), 2–5, doi:10.1029/2003GL018747, 2004.

Guo, H., John, J. G., Blanton, C., McHugh, C., Nikonov, S., Radhakrishnan, A., Zadeh, N. T., Balaji, V., Durachta, J., Dupuis, C., Menzel, R., Robinson, T., Underwood, S., Vahlenkamp, H., Dunne, K. A., Gauthier, P. P., Ginoux, P., Griffies, S. M., Hallberg, R., Harrison, M., Hurlin, W., Malyshev, S., Naik, V., Paulot, F., Paynter, D. J., Ploshay, J., Schwarzkopf, D. M., Seman, C. J., Shao, A., Silvers, L., Wyman, B., Zeng, Y., Adcroft, A., Dunne, J. P., Held, I. M., Krasting, J. P., Horowitz, L. W., Milly, P. C. ., Shevliakova, E., Winton, M. and Zhao, M.: NOAA-GFDL GFDL-CM4 model output prepared for CMIP6 CMIP abrupt-4xCO2, Earth System Grid Federation, , doi:https://doi.org/10.22033/ESGF/CMIP6.8486, 2018a.

Guo, H., John, J. G., Blanton, C., McHugh, C., Nikonov, S., Radhakrishnan, A., Zadeh, N. T., Balaji, V., Durachta, J., Dupuis, C., Menzel, R., Robinson, T., Underwood, S., Vahlenkamp, H., Dunne, K. A., Gauthier, P. P., Ginoux, P., Griffies, S. M., Hallberg, R. W., Harrison, M., Hurlin, W., Malyshev, S., Naik, V., Paulot, F., Paynter, D. J., Ploshay, J., Schwarzkopf, D. M., Seman, C. J., Shao, A., Silvers, L. G., Wyman, B., Zeng, Y., Adcroft, A. J., Dunne, J. P., Held, I. M., Krasting, J. P., Horowitz, L. W., Milly, P. C. ., Shevliakova, E., Winton, M. and Zhao, M.: NOAA-GFDL GFDL-CM4 model output prepared for CMIP6 CMIP historical, Earth System Grid Federation, , doi:https://doi.org/10.22033/ESGF/CMIP6.8594, 2018b.

Guo, H., John, J. G., Blanton, C., McHugh, C., Nikonov, S., Radhakrishnan, A., Zadeh, N. T., Balaji, V., Durachta, J., Dupuis, C., Menzel, R., Robinson, T., Underwood, S., Vahlenkamp, H., Dunne, K. A., Gauthier, P. P., Ginoux, P., Griffies, S. M., Hallberg, R., Harrison, M., Hurlin, W., Malyshev, S., Naik, V., Paulot, F., Paynter, D. J., Ploshay, J., Rand, K., Schwarzkopf, D. M., Seman, C. J., Shao, A., Silvers, L., Wyman, B., Zeng, Y., Adcroft, A., Dunne, J. P., Held, I. M., Krasting, J. P., Horowitz, L. W., Milly, C., Shevliakova, E., Winton, M., Zhao, M., Yan, X. and Zhang, R.: NOAA-GFDL GFDL-CM4 model output prepared for CMIP6 ScenarioMIP ssp245, Earth System Grid Federation, , doi:https://doi.org/10.22033/ESGF/CMIP6.9263, 2018c.

Guo, H., John, J. G., Blanton, C., McHugh, C., Nikonov, S., Radhakrishnan, A., Zadeh, N. T., Balaji, V., Durachta, J., Dupuis, C., Menzel, R., Robinson, T., Underwood, S., Vahlenkamp, H., Dunne, K. A., Gauthier, P. P., Ginoux, P., Griffies, S. M., Hallberg, R., Harrison, M., Hurlin, W., Malyshev, S., Naik, V., Paulot, F., Paynter, D. J., Ploshay, J., Rand, K., Schwarzkopf, D. M., Seman, C. J., Shao, A., Silvers, L., Wyman, B., Zeng, Y., Adcroft, A., Dunne, J. P., Held, I. M., Krasting, J. P., Horowitz, L. W., Milly, C., Shevliakova, E., Winton, M., Zhao, M., Yan, X. and Zhang, R.: NOAA-GFDL GFDL-CM4 model output prepared for CMIP6 ScenarioMIP ssp585, Earth System Grid Federation, , doi:https://doi.org/10.22033/ESGF/CMIP6.9268, 2018d.

Guo, H., John, J. G., Blanton, C., McHugh, C., Nikonov, S., Radhakrishnan, A., Zadeh, N. T., Balaji, V., Durachta, J., Dupuis, C., Menzel, R., Robinson, T., Underwood, S., Vahlenkamp, H., Dunne, K. A., Gauthier, P. P., Ginoux, P., Griffies, S. M., Hallberg, R., Harrison, M., Hurlin, W., Malyshev, S., Naik, V., Paulot, F., Paynter, D. J., Ploshay, J., Schwarzkopf, D. M., Seman, C. J., Shao, A., Silvers, L., Wyman, B., Zeng, Y., Adcroft, A., Dunne, J. P., Held, I. M., Krasting, J. P., Horowitz, L. W., Milly, P. C. ., Shevliakova, E., Winton, M. and Zhao, M.: NOAA-GFDL GFDL-CM4 piControl model output, Earth System Grid Federation, , doi:https://doi.org/10.22033/ESGF/CMIP6.8666, 2018e.

Hajima, T., Abe, M., Arakawa, O., Suzuki, T., Komuro, Y., Ogura, T., Ogochi, K., Watanabe, M., Yamamoto, A., Tatebe, H., Noguchi, M. A., Ohgaito, R., Ito, A., Yamazaki, D., Ito, A., Takata, K., Watanabe, S., Kawamiya, M. and Tachiiri, K.: MIROC MIROC-ES2L model output prepared for CMIP6 CMIP historical, Earth System Grid Federation, , doi:https://doi.org/10.22033/ESGF/CMIP6.5602, 2019.

Hope, A. P., Canty, T. P., Salawitch, R. J., Tribett, W. R. and Bennett, B. F.: Forecasting Global Warming, in Paris Climate Agreement: Beacon of Hope, pp. 51–114, Springer Climate., 2017.

Huang, W.: THU CIESM model output prepared for CMIP6 CMIP historical, Earth System Grid Federation, , doi:https://doi.org/10.22033/ESGF/CMIP6.7789, 2019a.

Huang, W.: THU CIESM model output prepared for CMIP6 ScenarioMIP ssp126, Earth System Grid Federation, , doi:https://doi.org/10.22033/ESGF/CMIP6.8857, 2019b.

Huang, W.: THU CIESM model output prepared for CMIP6 ScenarioMIP ssp245, Earth System Grid Federation, , doi:https://doi.org/10.22033/ESGF/CMIP6.8858, 2020a.

Huang, W.: THU CIESM model output prepared for CMIP6 ScenarioMIP ssp585, Earth System Grid Federation, , doi:https://doi.org/10.22033/ESGF/CMIP6.8863, 2020b.

Ishii, M., Fukuda, Y., Hirahara, S., Yasui, S., Suzuki, T. and Sato, K.: Accuracy of Global Upper Ocean Heat Content Estimation Expected from Present Observational Data Sets, Sci. Online Lett. Atmos., 13(0), 163–167, doi:10.2151/sola.2017-030, 2017.

John, J. G., Blanton, C., McHugh, C., Nikonov, S., Radhakrishnan, A., Rand, K., Vahlenkamp, H., Zadeh, N. T., Gauthier, P. P., Ginoux, P., Harrison, M., Horowitz, L. W., Malyshev, S., Naik, V., Paynter, D. J., Ploshay, J., Silvers, L. G., Stock, C., Winton, M., Zeng, Y. and Dunne, J. P.: NOAA-GFDL GFDL-ESM4 model output prepared for CMIP6 ScenarioMIP ssp119, Earth System Grid Federation, , doi:https://doi.org/10.22033/ESGF/CMIP6.8683, 2018a.

John, J. G., Blanton, C., McHugh, C., Nikonov, S., Radhakrishnan, A., Rand, K., Vahlenkamp, H., Zadeh, N. T., Gauthier, P. P., Ginoux, P., Harrison, M., Horowitz, L. W., Malyshev, S., Naik, V., Paynter, D. J., Ploshay, J., Silvers, L. G., Stock, C., Winton, M., Zeng, Y. and Dunne, J. P.: NOAA-GFDL GFDL-ESM4 model output prepared for CMIP6 ScenarioMIP ssp126, Earth System Grid Federation, , doi:https://doi.org/10.22033/ESGF/CMIP6.8684, 2018b.

John, J. G., Blanton, C., McHugh, C., Radhakrishnan, A., Rand, K., Vahlenkamp, H., Wilson, C., Zadeh, N. T., Gauthier, P. P., Dunne, J. P., Dussin, R., Horowitz, L. W., Lin, P., Malyshev, S., Naik, V., Ploshay, J., Silvers, L., Stock, C., Winton, M. and Zeng, Y.: NOAA-GFDL GFDL-ESM4 model output prepared for CMIP6 ScenarioMIP ssp245, Earth System Grid Federation, , doi:https://doi.org/10.22033/ESGF/CMIP6.8686, 2018c.

John, J. G., Blanton, C., McHugh, C., Nikonov, S., Radhakrishnan, A., Rand, K., Vahlenkamp, H., Zadeh, N. T., Gauthier, P. P., Ginoux, P., Harrison, M., Horowitz, L. W., Malyshev, S., Naik, V., Paynter, D. J., Ploshay, J., Silvers, L., Stock, C., Winton, M., Zeng, Y. and Dunne, J. P.: NOAA-GFDL GFDL-ESM4 model output prepared for CMIP6 ScenarioMIP ssp370, Earth System Grid Federation, , doi:https://doi.org/10.22033/ESGF/CMIP6.8691, 2018d.

John, J. G., Blanton, C., McHugh, C., Nikonov, S., Radhakrishnan, A., Rand, K., Vahlenkamp, H., Zadeh, N. T., Gauthier, P. P., Ginoux, P., Harrison, M., Horowitz, L. W., Malyshev, S., Naik, V., Paynter, D. J., Ploshay, J., Silvers, L., Stock, C., Winton, M., Zeng, Y. and Dunne, J. P.: NOAA-GFDL GFDL-ESM4 model output prepared for CMIP6 ScenarioMIP ssp585, Earth System Grid Federation, , doi:https://doi.org/10.22033/ESGF/CMIP6.8706, 2018e.

Jones, C., Sellar, A., Tang, Y. and Rumbold, S.: Results from the UKESM1 CMIP6 DECK and historical simulations, UKESM [online] Available from: https://ukesm.ac.uk/portfolio-item/ukesm1-cmip6-deck-and-historical/# (Accessed 9 October 2019), 2019.

Jungclaus, J. H., Bittner, M., Wieners, K.-H., Wachsmann, F., Schupfner, M., Legutke, S., Giorgetta, M., Reick, C., Gayler, V., Haak, H., de Vrese, P., Raddatz, T., Esch, M., Mauritsen, T., von Storch, J.-S., Behrens, J., Brovkin, V., Claussen, M., Crueger, T., Fast, I., Fiedler, S., Hagemann, S., Hohenegger, C., Jahns, T., Kloster, S., Kinne, S., Lasslop, G., Kornblueh, L., Marotzke, J., Matai, D., Meraner, K., Mikolajewicz, U., Modali, K., Muller, W., Nabel, J., Notz, D., Peters, K., Pincus, R., Pohlmann, H., Pongratz, J., Rast, S., Schmidt, H., Schnur, R., Schulzweida, U., Six, K., Stevens, B., Voigt, A. and Roeckner, E.: MPI-M MPI-ESM1.2-HR model output prepared for CMIP6 CMIP historical, Earth System Grid Federation, , doi:https://doi.org/10.22033/ESGF/CMIP6.6594, 2019.

Kavvada, A., Ruiz-Barradas, A. and Nigam, S.: AMO's structure and climate footprint in observations and IPCC AR5 climate simulations, Clim. Dyn., 41(5–6), 1345–1364, doi:10.1007/s00382-013-1712-1, 2013.

Kelley, M., Schmidt, G., Nazarenko, L., Bauer, S., Ruedy, R., Russell, G., Ackerman, A., Aleinov, I., Bauer, M., Bleck, R., Canuto, V., Cesana, G., Cheng, Y., Clune, T., Cook, B., Cruz, C., Del Genio, A., Elsaesser, G., Faluvegi, G., Kiang, N., Kim, D., Lacis, A., Leboissetier, A., LeGrande, A., Lo, K., Marshall, J., Matthews, E., McDermid, S., Mezuman, K., Miller, R., Murray, L., Oinas, V., Orbe, C., Pérez García-Pando, C., Perlwitz, J., Puma, M., Rind, D., Romanou, A., Shindell, D., Sun, S., Tausnev, N., Tsigaridis, K., Tselioudis, G., Weng, E., Wu, J. and Yao, M.: GISS-E2.1: Configurations and Climatology, J. Adv. Model. Earth Syst., 2018(Phase 6), doi:10.1029/2019MS002025, 2020.

Krasting, J. P., John, J. G., Blanton, C., McHugh, C., Nikonov, S., Radhakrishnan, A., Rand, K., Zadeh, N. T., Balaji, V., Durachta, J., Dupuis, C., Menzel, R., Robinson, T., Underwood, S., Vahlenkamp, H., Dunne, K. A., Gauthier, P. P., Ginoux, P., Griffies, S. M., Hallberg, R., Harrison, M., Hurlin, W., Malyshev, S., Naik, V., Paulot, F., Paynter, D. J., Ploshay, J., Schwarzkopf, D. M., Seman, C. J., Silvers, L., Wyman, B., Zeng, Y., Adcroft, A., Dunne, J. P., Guo, H., Held, I. M., Horowitz, L. W., Milly, P. C. ., Shevliakova, E., Stock, C., Winton, M. and Zhao, M.: NOAA-GFDL GFDL-ESM4 model output prepared for CMIP6 CMIP abrupt-4xCO2, Earth System Grid Federation, , doi:https://doi.org/10.22033/ESGF/CMIP6.8489, 2018a.

Krasting, J. P., John, J. G., Blanton, C., McHugh, C., Nikonov, S., Radhakrishnan, A., Rand, K., Zadeh, N. T., Balaji, V., Durachta, J., Dupuis, C., Menzel, R., Robinson, T., Underwood, S., Vahlenkamp, H., Dunne, K. A., Gauthier, P. P., Ginoux, P., Griffies, S. M., Hallberg, R. W., Harrison, M., Hurlin, W., Malyshev, S., Naik, V., Paulot, F., Paynter, D. J., Ploshay, J., Schwarzkopf, D. M., Seman, C. J., Silvers, L. G., Wyman, B., Zeng, Y., Adcroft, A. J., Dunne, J. P., Guo, H., Held, I. M., Horowitz, L. W., Milly, P. C. ., Shevliakova, E., Stock, C., Winton, M. and Zhao, M.: NOAA-GFDL GFDL-ESM4 model output prepared for CMIP6 CMIP historical, Earth System Grid Federation, , doi:https://doi.org/10.22033/ESGF/CMIP6.8597, 2018b.

Krasting, J. P., John, J. G., Blanton, C., McHugh, C., Nikonov, S., Radhakrishnan, A., Rand, K., Zadeh, N. T., Balaji, V., Durachta, J., Dupuis, C., Menzel, R., Robinson, T., Underwood, S., Vahlenkamp, H., Dunne, K. A., Gauthier, P. P., Ginoux, P., Griffies, S. M., Hallberg, R., Harrison, M., Hurlin, W., Malyshev, S., Naik, V., Paulot, F., Paynter, D. J., Ploshay, J., Schwarzkopf, D. M., Seman, C. J., Silvers, L., Wyman, B., Zeng, Y., Adcroft, A., Dunne, J. P., Guo, H., Held, I. M., Horowitz, L. W., Milly, P. C. ., Shevliakova, E., Stock, C., Winton, M. and Zhao, M.: NOAA-GFDL GFDL-ESM4 model output prepared for CMIP6 CMIP piControl, Earth System Grid Federation, , doi:https://doi.org/10.22033/ESGF/CMIP6.8669, 2018c.

Lean, J. L. and Rind, D. H.: How natural and anthropogenic influences alter global and regional surface temperatures: 1889 to 2006, Geophys. Res. Lett., 35(18), 1–6, doi:10.1029/2008GL034864, 2008.

Levitus, S., Antonov, J. I., Boyer, T. P., Baranova, O. K., Garcia, H. E., Locarnini, R. A., Mishonov, A. V., Reagan, J. R., Seidov, D., Yarosh, E. S. and Zweng, M. M.: World ocean heat content and thermosteric sea level change (0-2000m), 1955-2010, Geophys. Res. Lett., 39(10), 1–5, doi:10.1029/2012GL051106, 2012.

Li, L.: CAS FGOALS-g3 model output prepared for CMIP6 CMIP historical, Earth System Grid Federation, , doi:https://doi.org/10.22033/ESGF/CMIP6.3356, 2019a.

Li, L.: CAS FGOALS-g3 model output prepared for CMIP6 ScenarioMIP ssp126, Earth System Grid Federation, , doi:https://doi.org/10.22033/ESGF/CMIP6.3465, 2019b.

Li, L.: CAS FGOALS-g3 model output prepared for CMIP6 ScenarioMIP ssp245, Earth System Grid Federation, , doi:https://doi.org/10.22033/ESGF/CMIP6.3469, 2019c.

Li, L.: CAS FGOALS-g3 model output prepared for CMIP6 ScenarioMIP ssp370, Earth System Grid Federation, , doi:https://doi.org/10.22033/ESGF/CMIP6.3480, 2019d.

Li, L.: CAS FGOALS-g3 model output prepared for CMIP6 ScenarioMIP ssp585, Earth System Grid Federation, , doi:https://doi.org/10.22033/ESGF/CMIP6.3503, 2019e.

Meinshausen, M., Smith, S. J., Calvin, K., Daniel, J. S., Kainuma, M. L. T., Lamarque, J., Matsumoto, K., Montzka, S. A., Raper, S. C. B., Riahi, K., Thomson, A., Velders, G. J. M. and van Vuuren, D. P. P.: The RCP greenhouse gas concentrations and their extensions from 1765 to 2300, Clim. Change, 109(1), 213–241, doi:10.1007/s10584-011-0156-z, 2011.

Morice, C. P., Kennedy, J. J., Rayner, N. A. and Jones, P. D.: Quantifying uncertainties in global and regional temperature change using an ensemble of observational estimates: The HadCRUT4 data set, J. Geophys. Res. Atmos., 117(8), 1–22, doi:10.1029/2011JD017187, 2012.

Murphy, J. M., Booth, B. B. B., Boulton, C. A., Clark, R. T., Harris, G. R., Lowe, J. A. and Sexton, D. M. H.: Transient climate changes in a perturbed parameter ensemble of emissions-driven earth system model simulations, Clim. Dyn., 43(9–10), 2855–2885, doi:10.1007/s00382-014-2097-5, 2014.

Myhre, G., Shindell, D., Bréon, F.-M., Collins, W., Fuglestvedt, J., Huang, J., Koch, D., Lamarque, J.-F., Lee, D., Mendoza, B., Nakajima, T., Robock, A., Stephens, G., Takemura, T. and Zhang, H.: Anthropogenic and Natural Radiative Forcing, Clim. Chang. 2013 Phys. Sci. Basis. Contrib. Work. Gr. I to Fifth Assess. Rep. Intergov. Panel Clim. Chang., 659–740, doi:10.1017/ CBO9781107415324.018, 2013.

NASA Goddard Institute for Space Studies (NASA/GISS): NASA-GISS GISS-E2.1G model output prepared for CMIP6 CMIP abrupt-4xCO2, Earth System Grid Federation, , doi:https://doi.org/10.22033/ESGF/CMIP6.6976, 2018a.

NASA Goddard Institute for Space Studies (NASA/GISS): NASA-GISS GISS-E2.1G model output prepared for CMIP6 CMIP historical, Earth System Grid Federation, , doi:https://doi.org/10.22033/ESGF/CMIP6.7127, 2018b.

NASA Goddard Institute for Space Studies (NASA/GISS): NASA-GISS GISS-E2.1G model output prepared for CMIP6 CMIP piControl, Earth System Grid Federation, , doi:https://doi.org/10.22033/ESGF/CMIP6.7380, 2018c.

NASA Goddard Institute for Space Studies (NASA/GISS): NASA-GISS GISS-E2.1H model output prepared for CMIP6 CMIP piControl, Earth System Grid Federation, , doi:https://doi.org/10.22033/ESGF/CMIP6.7381, 2018d.

NASA Goddard Institute for Space Studies (NASA/GISS): NASA-GISS GISS-E2-2-G model output prepared for CMIP6 CMIP abrupt-4xCO2, Earth System Grid Federation, , doi:https://doi.org/10.22033/ESGF/CMIP6.6978, 2019a.

NASA Goddard Institute for Space Studies (NASA/GISS): NASA-GISS GISS-E2.1H model output prepared for CMIP6 CMIP abrupt-4xCO2, Earth System Grid Federation, , doi:https://doi.org/10.22033/ESGF/CMIP6.6977, 2019b.

NASA Goddard Institute for Space Studies (NASA/GISS): NASA-GISS GISS-E2.1H model output prepared for CMIP6 CMIP historical, Earth System Grid Federation, , doi:https://doi.org/10.22033/ESGF/CMIP6.7128, 2019c.

NASA Goddard Institute for Space Studies (NASA/GISS): NASA-GISS GISS-E2.1G model output prepared for CMIP6 ScenarioMIP ssp126, Earth System Grid Federation, , doi:https://doi.org/10.22033/ESGF/CMIP6.7410, 2020a.

NASA Goddard Institute for Space Studies (NASA/GISS): NASA-GISS GISS-E2.1G model output prepared for CMIP6 ScenarioMIP ssp245, Earth System Grid Federation, , doi:https://doi.org/10.22033/ESGF/CMIP6.7415, 2020b.

NASA Goddard Institute for Space Studies (NASA/GISS): NASA-GISS GISS-E2.1G model output prepared for CMIP6 ScenarioMIP ssp370, Earth System Grid Federation, , doi:https://doi.org/10.22033/ESGF/CMIP6.7426, 2020c.

NASA Goddard Institute for Space Studies (NASA/GISS): NASA-GISS GISS-E2.1G model output prepared for CMIP6 ScenarioMIP ssp585, Earth System Grid Federation, , doi:https://doi.org/10.22033/ESGF/CMIP6.7460, 2020d.

Neubauer, D., Ferrachat, S., Siegenthaler-Le Drian, C., Stoll, J., Folini, D. S., Tegen, I., Wieners, K.-H., Mauritsen, T., Stemmler, I., Barthel, S., Bey, I., Daskalakis, M., Heinold, B., Kokkola, H., Partridge, D., Rast, S., Schmidt, H., Schutgens, N., Stanelle, T., Stier, P., Watson-Parrs, D. and Lohmann, U.: HAMMOZ-Consortium MPI-ESM1.2-HAM model output prepared for CMIP6 CMIP6 historical, Earth System Grid Federation, , doi:https://doi.org/10.22033/ESGF/CMIP6.5016, 2019.

Nicholls, Z., Meinshausen, M., Lewis, J., Corradi, M. R., Dorheim, K., Gasser, T., Gieseke, R., Hope, A. P., Leach, N. J., McBride, L. A., Quilcaille, Y., Rogelj, J., Salawitch, R. J., Samset, B. H., Sandstad, M., Shiklomanov, A., Skeie, R. B., Smith, C. J., Smith, S. J., Su, X., Tsutsui, J., Vega-Westhoff, B. and Woodward, D.: Reduced Complexity Model Intercomparison Project Phase 2 : Synthesising Earth system knowledge for probabilistic climate projections, Earth's Futur., doi:https://doi.org/10.1002/essoar.10504793.1, 2020.

Park, S. and Shin, J.: SNU SAM0-UNICON model output prepared for CMIP6 CMIP abrupt-4xCO2, Earth System Grid Federation, , doi:https://doi.org/10.22033/ESGF/CMIP6.7783, 2019a.

Park, S. and Shin, J.: SNU SAM0-UNICON model output prepared for CMIP6 CMIP historical, Earth System Grid Federation, , doi:https://doi.org/10.22033/ESGF/CMIP6.7789, 2019b.

Park, S. and Shin, J.: SNU SAM0-UNICON model output prepared for CMIP6 CMIP piControl, Earth System Grid Federation, , doi:https://doi.org/10.22033/ESGF/CMIP6.7791, 2019c.

Ridley, J., Menary, M., Kuhlbrodt, T., Andrews, M. and Andrews, T.: MOHC HadGEM3-GC31-LL model output prepared for CMIP6 CMIP piControl, Earth System Grid Federation, , doi:https://doi.org/10.22033/ESGF/CMIP6.6294, 2018.

Ridley, J., Menary, M., Kuhlbrodt, T., Andrews, M. and Andrews, T.: MOHC HadGEM3-GC31-LL model output prepared for CMIP6 CMIP, Earth System Grid Federation, , doi:https://doi.org/10.22033/ESGF/CMIP6.6109, 2019a.

Ridley, J., Menary, M., Kuhlbrodt, T., Andrews, M. and Andrews, T.: MOHC HadGEM3-GC31-LL model output prepared for CMIP6 CMIP abrupt-4xCO2, Earth System Grid Federation, , doi:https://doi.org/10.22033/ESGF/CMIP6.5839, 2019b.

Ridley, J., Menary, M., Kuhlbrodt, T., Andrews, M. and Andrews, T.: MOHC HadGEM3-GC31-MM model output prepared for CMIP6 CMIP historical, Earth System Grid Federation, , doi:https://doi.org/10.22033/ESGF/CMIP6.6112, 2019c.

Rong, X.: CAMS CAMS_CSM1.0 model output preapred for CMIP6 CMIP historical, Earth System Grid Federation, , doi:https://doi.org/10.22033/ESGF/CMIP6.9754, 2019a.

Rong, X.: CAMS CAMS-CSM1.0 model output prepared for CMIP6 ScenarioMIP ssp119, Earth System Grid Federation, , doi:https://doi.org/10.22033/ESGF/CMIP6.11045, 2019b.

Rong, X.: CAMS CAMS-CSM1.0 model output prepared for CMIP6 ScenarioMIP ssp126, Earth System Grid Federation, , doi:https://doi.org/10.22033/ESGF/CMIP6.11046, 2019c.

Rong, X.: CAMS CAMS-CSM1.0 model output prepared for CMIP6 ScenarioMIP ssp245, Earth System Grid Federation, , doi:https://doi.org/10.22033/ESGF/CMIP6.11047, 2019d.

Rong, X.: CAMS CAMS-CSM1.0 model output prepared for CMIP6 ScenarioMIP ssp370, Earth System Grid Federation, , doi:https://doi.org/10.22033/ESGF/CMIP6.11048, 2019e.

Rong, X.: CAMS CAMS-CSM1.0 model output prepared for CMIP6 ScenarioMIP ssp585, Earth System Grid Federation, , doi:https://doi.org/10.22033/ESGF/CMIP6.11052, 2019f.

Schupfner, M., Wieners, K.-H., Wachsmann, F., Steger, C., Bittner, M., Jungclaus, J., Früh, B., Pankatz, K., Giorgetta, M., Reick, C., Legutke, S., Esch, M., Gayler, V., Haak, H., de Vrese, P., Raddatz, T., Mauritsen, T., von Storch, J.-S., Behrens, J., Brovkin, V., Claussen, M., Crueger, T., Fast, I., Fiedler, S., Hagemann, S., Hohenegger, C., Jahns, T., Kloster, S., Kinne, S., Lasslop, G., Kornblueh, L., Marotzke, J., Matei, D., Meraner, K., Mikolajewicz, U., Modali, K., Müller, W., Nabel, J., Notz, D., Peters, K., Pincus, R., Pohlmann, H., Pongratz, J., Rast, S., Schmidt, H., Schnur, R., Schulzweida, U., Six, K., Stevens, B., Voigt, A. and Roeckner, E.: DKRZ MIP-ESM1.2-HR model output prepared for CMIP6 ScenarioMIP ssp126, Earth System Grid Federation, , doi:https://doi.org/10.22033/ESGF/CMIP6.4397, 2019a.

Schupfner, M., Wieners, K.-H., Wachsmann, F., Steger, C., Bittner, M., Jungclaus, J., Früh, B., Pankatz, K., Giorgetta, M., Reick, C., Legutke, S., Esch, M., Gayler, V., Haak, H., de Vrese, P., Raddatz, T., Mauritsen, T., von Storch, J.-S., Behrens, J., Brovkin, V., Claussen, M., Crueger, T., Fast, I., Fiedler, S., Hagemann, S., Hohenegger, C., Jahns, T., Kloster, S., Kinne, S., Lasslop, G., Kornblueh, L., Marotzke, J., Matei, D., Meraner, K., Mikolajewicz, U., Modali, K., Müller, W., Nabel, J., Notz, D., Peters, K., Pincus, R., Pohlmann, H., Pongratz, J., Rast, S., Schmidt, H., Schnur, R., Schulzweida, U., Six, K., Stevens, B., Voigt, A. and Roeckner, E.: DKRZ MPI-ESM1.2-HR model output prepared for CMIP6 ScenarioMIP ssp245, Earth System Grid Federation, , doi:https://doi.org/10.22033/ESGF/CMIP6.4398, 2019b.

Schupfner, M., Wieners, K.-H., Wachsmann, F., Steger, C., Bittner, M., Jungclaus, J., Früh, B., Pankatz, K., Giorgetta, M., Reick, C., Legutke, S., Esch, M., Gayler, V., Haak, H., de Vrese, P., Raddatz, T., Mauritsen, T., von Storch, J.-S., Behrens, J., Brovkin, V., Claussen, M., Crueger, T., Fast, I., Fiedler, S., Hagemann, S., Hohenegger, C., Jahns, T., Kloster, S., Kinne, S., Lasslop, G., Kornblueh, L., Marotzke, J., Matei, D., Meraner, K., Mikolajewicz, U., Modali, K., Müller, W., Nabel, J., Notz, D., Peters, K., Pincus, R., Pohlmann, H., Pongratz, J., Rast, S., Schmidt, H., Schnur, R., Schulzweida, U., Six, K., Stevens, B., Voigt, A. and Roeckner, E.: DKRZ MPI-ESM1.2-HR model output prepared for CMIP6 ScenarioMIP ssp370, Earth System Grid Federation, , doi:https://doi.org/10.22033/ESGF/CMIP6.4399, 2019c.

Schupfner, M., Wieners, K.-H., Wachsmann, F., Steger, C., Bittner, M., Jungclaus, J., Früh, B., Pankatz, K., Giorgetta, M., Reick, C., Legutke, S., Esch, M., Gayler, V., Haak, H., de Vrese, P., Raddatz, T., Mauritsen, T., von Storch, J.-S., Behrens, J., Brovkin, V., Claussen, M., Crueger, T., Fast, I., Fiedler, S., Hagemann, S., Hohenegger, C., Jahns, T., Kloster, S., Kinne, S., Lasslop, G., Kornblueh, L., Marotzke, J., Matei, D., Meraner, K., Mikolajewicz, U., Modali, K., Müller, W., Nabel, J., Notz, D., Peters, K., Pincus, R., Pohlmann, H., Pongratz, J., Rast, S., Schmidt, H., Schnur, R., Schulzweida, U., Six, K., Stevens, B., Voigt, A. and Roeckner, E.: DKRZ MPI-ESM1.2-HR model output prepared for CMIP6 ScenarioMIP ssp585, Earth System Grid Federation, , doi:https://doi.org/10.22033/ESGF/CMIP6.4403, 2019d.

Schwartz, S. E.: Determination of Earth's Transient and Equilibrium Climate Sensitivities from Observations Over the Twentieth Century: Strong Dependence on Assumed Forcing, Surv. Geophys., 33(3–4), 745–777, doi:10.1007/s10712-012-9180-4, 2012.

Seferian, R.: CNRM-CERFACS CNRM-ESM2-1 model output prepared for CMIP6 CMIP historical, Earth System Grid Federation, , doi:https://doi.org/10.22033/ESGF/CMIP6.4068, 2018.

Seland, Ø., Bentsen, M., Oliviè, D. J. L., Toniazzo, T., Gjermundsen, A., Graff, L. S., Debernard, J. B., Gupta, A. K., He, Y., Kirkevåg, A., Schwinger, J., Tjiputra, J., Aas, K. S., Bethke, I., Fan, Y., Griesfeller, J., Grini, A., Guo, C., Ilicak, M., Karset, I. H. H., Landgren, O. A., Liakka, J., Moseid, K. O., Nummelin, A., Spensberger, C., Tang, H., Zhang, Z., Heinze, C., Iversen, T. and Schulz, M.: NCC NorESM2-LM model output prepared for CMIP6 CMIP abrupt-4xCO2, Earth System Grid Federation, , doi:https://doi.org/10.22033/ESGF/CMIP6.7836, 2019a.

Seland, Ø., Bentsen, M., Oliviè, D. J. L., Toniazzo, T., Gjermundsen, A., Graff, L. S., Debernard, J. B., Gupta, A. K., He, Y., Kirkevåg, A., Schwinger, J., Tjiputra, J., Aas, K. S., Bethke, I., Fan, Y., Griesfeller, J., Grini, A., Guo, C., Ilicak, M., Karset, I. H. H., Landgren, O. A., Liakka, J., Moseid, K. O., Nummelin, A., Spensberger, C., Tang, H., Zhang, Z., Heinze, C., Iversen, T. and Schulz, M.: NCC NorESM2-LM model output prepared for CMIP6 CMIP piControl, Earth System Grid Federation, , doi:https://doi.org/10.22033/ESGF/CMIP6.8217, 2019b.

Seland, Ø., Bentsen, M., Oliviè, D. J. L., Toniazzo, T., Gjermundsen, A., Graff, L. S., Debernard, J. B., Gupta, A. K., He, Y., Kirkevåg, A., Schwinger, J., Tjiputra, J., Aas, K. S., Bethke, I., Fan, Y., Griesfeller, J., Grini, A., Guo, C., Ilicak, M., Karset, I. H. H., Landgren, O. A., Liakka, J., Moseid, K. O., Nummelin, A., Spensberger, C., Tang, H., Zhang, Z., Heinze, C., Iversen, T. and Schulz, M.: NCC NorESM2-LM model output prepared for CMIP6 ScenarioMIP ssp126, Earth System Grid Federation, , doi:https://doi.org/10.22033/ESGF/CMIP6.8248, 2019c.

Seland, Ø., Bentsen, M., Oliviè, D. J. L., Toniazzo, T., Gjermundsen, A., Graff, L. S., Debernard, J. B., Gupta, A. K., He, Y., Kirkevåg, A., Schwinger, J., Tjiputra, J., Aas, K. S., Bethke, I., Fan, Y., Griesfeller, J., Grini, A., Guo, C., Ilicak, M., Karset, I. H. H., Landgren, O. A., Liakka, J., Moseid, K. O., Nummelin, A., Spensberger, C., Tang, H., Zhang, Z., Heinze, C., Iversen, T. and Schulz, M.: NCC NorESM2-LM model output prepared for CMIP6 ScenarioMIP ssp245, Earth System Grid Federation, , doi:https://doi.org/10.22033/ESGF/CMIP6.8253, 2019d.

Seland, Ø., Bentsen, M., Oliviè, D. J. L., Toniazzo, T., Gjermundsen, A., Graff, L. S., Debernard, J. B., Gupta, A. K., He, Y., Kirkevåg, A., Schwinger, J., Tjiputra, J., Aas, K. S., Bethke, I., Fan, Y., Griesfeller, J., Grini, A., Guo, C., Ilicak, M., Karset, I. H. H., Landgren, O. A., Liakka, J., Moseid, K. O., Nummelin, A., Spensberger, C., Tang, H., Zhang, Z., Heinze, C., Iversen, T. and Schulz, M.: NCC NorESM2-LM model output prepared for CMIP6 ScenarioMIP ssp370, Earth System Grid Federation, , doi:https://doi.org/10.22033/ESGF/CMIP6.8268, 2019e.

Seland, Ø., Bentsen, M., Oliviè, D. J. L., Toniazzo, T., Gjermundsen, A., Graff, L. S., Debernard, J. B., Gupta, A. K., He, Y., Kirkevåg, A., Schwinger, J., Tjiputra, J., Aas, K. S., Bethke, I., Fan, Y., Griesfeller, J., Grini, A., Guo, C., Ilicak, M., Karset, I. H. H., Landgren, O. A., Liakka, J., Moseid, K. O., Nummelin, A., Spensberger, C., Tang, H., Zhang, Z., Heinze, C., Iversen, T. and Schulz, M.: NCC NorESM2-LM model output prepared for CMIP6 ScenarioMIP ssp585, Earth System Grid Federation, , doi:https://doi.org/10.22033/ESGF/CMIP6.8319, 2019f.

Seland, Ø., Bentsen, M., Oliviè, D. J. L., Toniazzo, T., Gjermundsen, A., Graff, L. S., Debernard, J. B., Gupta, A. K., He, Y., Kirkevåg, A., Schwinger, J., Tjiputra, J., Aas, K. S., Bethke, I., Fan, Y., Griesfeller, J., Grini, A., Guo, C., Ilicak, M., Karset, I. H. H., Landgren, O. A., Liakka, J., Moseid, K. O., Nummelin, A., Spensberger, C., Tang, H., Zhang, Z., Heinze, C., Iversen, T. and Schulz, M.: NCC NorESM2-LM output prepared for CMIP6 CMIP historical, Earth System Grid Federation, , doi:https://doi.org/10.22033/ESGF/CMIP6.8036, 2019g.

Semmler, T., Danilov, S., Rackow, T., Sidorenko, D., Barbi, D., Hegewald, J., Sein, D., Wang, Q. and Jung, T.: AWI AWI-CM1.1MR model output prepared for CMIP6 CMIP historical, Earth System Grid Federation, , doi:https://doi.org/10.22033/ESGF/CMIP6.2686, 2018a.

Semmler, T., Danilov, S., Rackow, T., Sidorenko, D., Barbi, D., Hegewald, J., Pradhan, H. K., Sein, D., Wang, Q. and Jung, T.: AWI AWI-CM1.1MR model output prepared for CMIP6 ScenarioMIP ssp126, Earth System Grid Federation, , doi:https://doi.org/10.22033/ESGF/CMIP6.2796, 2018b.

Semmler, T., Danilov, S., Rackow, T., Sidorenko, D., Barbi, D., Hegewald, J., Pradhan, H. K., Sein, D., Wang, Q. and Jung, T.: AWI AWI-CM1.1MR model output prepared for CMIP6 ScenarioMIP ssp246, Earth System Grid Federation, , doi:https://doi.org/10.22033/ESGF/CMIP6.2800, 2018c.

Semmler, T., Danilov, S., Rackow, T., Sidorenko, D., Barbi, D., Hegewald, J., Pradhan, H. K., Sein, D., Wang, Q. and Jung, T.: AWI AWI-CM1.1MR model output prepared for CMIP6 ScenarioMIP ssp370, Earth System Grid Federation, , doi:https://doi.org/10.22033/ESGF/CMIP6.2803, 2019a.

Semmler, T., Danilov, S., Rackow, T., Sidorenko, D., Barbi, D., Hegewald, J., Pradhan, H. K., Sein, D., Wang, Q. and Jung, T.: AWI AWI-CM1.1MR model output prepared for CMIP6 ScenarioMIP ssp585, Earth System Grid Federation, , doi:https://doi.org/10.22033/ESGF/CMIP6.2817, 2019b.

Sherwood, A. S., Webb, M. J., Annan, J. D., Armour, K. C., Forster, P. M., Hargreaves, J. C., Hegerl, G., Klein, S. A., Marvel, K. D., Rohling, E. J., Watanabe, M., Andrews, T., Braconnot, P., Bretherton, C. S., Foster, G. L., Hausfather, Z., von der Heydt, A. S., Knutti, R., Mauritsen, T., Norris, J. R., Proistosescu, C., Rugenstein, M., Schmidt, G. A. and Tokarska, K. B., Zelinka, M. D.: An assessment of Earth ’ s climate sensitivity using multiple lines of evidence, Rev. Geophys., 1–166, 2020.

Shiogama, H., Abe, M. and Tatebe, H.: MIROC MIROC6 model output prepared for CMIP6 ScenarioMIP ssp119, Earth System Grid Federation, , doi:https://doi.org/10.22033/ESGF/CMIP6.5741, 2019a.

Shiogama, H., Abe, M. and Tatebe, H.: MIROC MIROC6 model output prepared for CMIP6 ScenarioMIP ssp126, Earth System Grid Federation, , doi:https://doi.org/10.22033/ESGF/CMIP6.5743, 2019b.

Shiogama, H., Abe, M. and Tatebe, H.: MIROC MIROC6 model output prepared for CMIP6 ScenarioMIP ssp245, Earth System Grid Federation, , doi:https://doi.org/10.22033/ESGF/CMIP6.5746, 2019c.

Shiogama, H., Abe, M. and Tatebe, H.: MIROC MIROC6 model output prepared for CMIP6 ScenarioMIP ssp370, Earth System Grid Federation, , doi:https://doi.org/10.22033/ESGF/CMIP6.5752, 2019d.

Shiogama, H., Abe, M. and Tatebe, H.: MIROC MIROC6 model output prepared for CMIP6 ScenarioMIP ssp434, Earth System Grid Federation, , doi:https://doi.org/10.22033/ESGF/CMIP6.5764, 2019e.

Shiogama, H., Abe, M. and Tatebe, H.: MIROC MIROC6 model output prepared for CMIP6 ScenarioMIP ssp460, Earth System Grid Federation, , doi:https://doi.org/10.22033/ESGF/CMIP6.5766, 2019f.

Shiogama, H., Abe, M. and Tatebe, H.: MIROC MIROC6 model output prepared for CMIP6 ScenarioMIP ssp585, Earth System Grid Federation, , doi:https://doi.org/10.22033/ESGF/CMIP6.5771, 2019g.

Song, Z., Qiao, F., Bao, Y., Shu, Q., Song, Y. and Yang, X.: FIO-QLNM FIO-ESM2.0 model output prepared for CMIP6 CMIP historical, Earth System Grid Federation, , doi:https://doi.org/10.22033/ESGF/CMIP6.9199, 2019a.

Song, Z., Qiao, F., Bao, Y., Shu, Q., Song, Y. and Yang, X.: FIO-QLNM FIO-ESM2.0 model output prepared for CMIP6 ScenarioMIP ssp126, Earth System Grid Federation, , doi:https://doi.org/10.22033/ESGF/CMIP6.9208, 2019b.

Song, Z., Qiao, F., Bao, Y., Shu, Q., Song, Y. and Yang, X.: FIO-QLNM FIO-ESM2.0 model output prepared for CMIP6 ScenarioMIP ssp245, Earth System Grid Federation, , doi:https://doi.org/10.22033/ESGF/CMIP6.9209, 2019c.

Song, Z., Qiao, F., Bao, Y., Shu, Q., Song, Y. and Yang, X.: FIO-QLNM FIO-ESM2.0 model output prepared for CMIP6 ScenarioMIP ssp585, Earth System Grid Federation, , doi:https://doi.org/10.22033/ESGF/CMIP6.9214, 2019d.

Steger, C., Schupfner, M., Wieners, K.-H., Wachsmann, F., Bittner, M., Jungclaus, J., Früh, B., Pankatz, K., Giorgetta, M., Reick, C., Legutke, S., Esch, M., Gayler, V., Haak, H., de Vrese, P., Raddatz, T., Mauritsen, T., von Storch, J.-S., Behrens, J., Brovkin, V., Claussen, M., Crueger, T., Fast, I., Fiedler, S., Hagemann, S., Hohenegger, C., Jahns, T., Kloster, S., Kinne, S., Lasslop, G., Kornblueh, L., Marotzke, J., Matei, D., Meraner, K., Mikolajewicz, U., Modali, K., Müller, W., Nabel, J., Notz, D., Peters, K., Pincus, R., Pohlmann, H., Pongratz, J., Rast, S., Schmidt, H., Schnur, R., Schulzweida, U., Ix, K., Stevens, B., Voigt, A. and Roeckner, E.: DWD MPI-ESM1.2-HR model output prepared for CMIP6 ScenarioMIP ssp585, Earth System Grid Federation, , doi:https://doi.org/10.22033/ESGF/CMIP6.4479, 2019.

Stouffer, R. J.: UA MCM-UA-1-0 model output prepared for CMIP6 CMIP abrupt-4xCO2, Earth System Grid Federation, , doi:https://doi.org/10.22033/ESGF/CMIP6.8882, 2019a.

Stouffer, R. J.: UA MCM-UA-1-0 model output prepared for CMIP6 CMIP historical, Earth System Grid Federation, , doi:https://doi.org/10.22033/ESGF/CMIP6.8888, 2019b.

Stouffer, R. J.: UA MCM-UA-1-0 model output prepared for CMIP6 CMIP piControl, Earth System Grid Federation, , doi:https://doi.org/10.22033/ESGF/CMIP6.8890, 2019c.

Stouffer, R. J.: UA MCM-UA-1-0 model output prepared for CMIP6 ScenarioMIP ssp245, Earth System Grid Federation, , doi:https://doi.org/10.22033/ESGF/CMIP6.13896, 2019d.

Stouffer, R. J.: UA MCM-UA-1-0 model output prepared for CMIP6 ScenarioMIP ssp370, Earth System Grid Federation, , doi:https://doi.org/10.22033/ESGF/CMIP6.13897, 2019e.

Stouffer, R. J.: UA MCM-UA-1-0 model output prepared for CMIP6 ScenarioMIP ssp585, Earth System Grid Federation, , doi:https://doi.org/10.22033/ESGF/CMIP6.13901, 2019f.

Stouffer, R. J.: UA MCM-UA-1.0 model output prepared for CMIP6 ScenarioMIP ssp126, Earth System Grid Federation, , doi:https://doi.org/10.22033/ESGF/CMIP6.13895, 2019g.

Swart, N. C., Jason, N. ., Kharin, V. V., Lazare, M., Scinocca, J. F., Gillett, N. P., Anstey, J., Arora, V. K., Christian, J. R., Jiao, Y., Lee, W. G., Majaess, F., Saenko, O. A., Seiler, C., Seinen, C., Shao, A., Solheim, L., von Salzen, K., Yang, D., Winter, B. and Sigmond, M.: CCCma CanESM5-CanOE model output prepared for CMIP6 CMIP, Earth System Grid Federation, , doi:https://doi.org/10.22033/ESGF/CMIP6.10260, 2019a.

Swart, N. C., Cole, J. N. S., Kharin, V. V., Lazare, M., Scinocca, J. F., Gillett, N. P., Anstey, J., Arora, V. K., Christian, J. R., Jiao, Y., Lee, W. G., Majaess, F., Saenko, O. A., Seiler, C., Seinen, C., Shao, A., Solheim, L., von Salzen, K., Yang, D., Winter, B. and Sigmond, M.: CCCma CaneSM5-CanOE model output prepared for CMIP6 ScenarioMIP ssp126, Earth System Grid Federation, , doi:https://doi.org/10.22033/ESGF/CMIP6.10269, 2019b.

Swart, N. C., Cole, J. N. S., Kharin, V. V., Lazare, M., Scinocca, J. F., Gillett, N. P., Anstey, J., Arora, V., Christian, J. R., Jiao, Y., Lee, W. G., Majaess, F., Saenko, O. A., Seiler, C., Seinen, C., Shao, A., Solheim, L., von Salzen, K., Yang, D., Winter, B. and Sigmond, M.: CCCma CanESM5-CanOE model output prepared for CMIP6 ScenarioMIP ssp245, Earth System Grid Federation, , doi:https://doi.org/10.22033/ESGF/CMIP6.10270, 2019c.

Swart, N. C., Cole, J. N. S., Kharin, V. V., Lazare, M., Scinocca, J. F., Gillett, N. P., Anstey, J., Arora, V., Christian, J. R., Jiao, Y., Lee, W. G., Majaess, F., Saenko, O. A., Seiler, C., Seinen, C., Shao, A., Solheim, L., von Salzen, K., Yang, D., Winter, B. and Sigmond, M.: CCCma CanESM5-CanOE model output prepared for CMIP6 ScenarioMIP ssp370, Earth System Grid Federation, , doi:https://doi.org/10.22033/ESGF/CMIP6.10271, 2019d.

Swart, N. C., Cole, J. N. S., Kharin, V. V., Lazare, M., Scinocca, J. F., Gillett, N. P., Anstey, J., Arora, V., Christian, J. R., Jiao, Y., Lee, W. G., Majaess, F., Saenko, O. A., Seiler, C., Seinen, C., Shao, A., Solheim, L., von Salzen, K., Yang, D., Winter, B. and Sigmond, M.: CCCma CanESM5-CanOE model output prepared for CMIP6 ScenarioMIP ssp585, Earth System Grid Federation, , doi:https://doi.org/10.22033/ESGF/CMIP6.10276, 2019e.

Swart, N. C., Cole, J. N. S., Kharin, V. V., Lazare, M., Scinocca, J. F., Gillett, N. P., Anstey, J., Arora, V., Christian, J. R., Jiao, Y., Lee, W. G., Majaess, F., Saenko, O. A., Seiler, C., Seinen, C., Shao, A., Solheim, L., von Salzen, K., Yang, D., Winter, B. and Sigmond, M.: CCCma CanESM5 model output prepared for CMIP6 CMIP abrupt-4xCO2, Earth System Grid Federation, , doi:https://doi.org/10.22033/ESGF/CMIP6.3532, 2019f.

Swart, N. C., Cole, J. N. S., Kharin, V. V., Lazare, M., Scinocca, J. F., Gillett, N. P., Anstey, J., Arora, V. K., Christian, J. R., Jiao, Y., Lee, W. G., Majaess, F., Saenko, O. A., Seiler, C., Seinen, C., Shao, A., Solheim, L., von Salzen, K., Yang, D., Winter, B. and Sigmond, M.: CCCma CanESM5 model output prepared for CMIP6 CMIP historical, Earth System Grid Federation, , doi:https://doi.org/10.22033/ESGF/CMIP6.3610, 2019g.

Swart, N. C., Cole, J. N. S., Kharin, V. V., Lazare, M., Scinocca, J. F., Gillett, N. P., Anstey, J., Arora, V., Christian, J. R., Jiao, Y., Lee, W. G., Majaess, F., Saenko, O. A., Seiler, C., Seinen, C., Shao, A., Solheim, L., von Salzen, K., Yang, D., Winter, B. and Sigmond, M.: CCCma CanESM5 model output prepared for CMIP6 CMIP piControl, Earth System Grid Federation, , doi:https://doi.org/10.22033/ESGF/CMIP6.3673, 2019h.

Swart, N. C., Cole, J. N. S., Kharin, V. V., Lazare, M., Scinocca, J. F., Gillett, N. P., Anstey, J., Arora, V. K., Christian, J. R., Jiao, Y., Lee, W. G., Majaess, F., Saenko, O. A., Seiler, C., Seinen, C., Shao, A., Solheim, L., von Salzen, K., Yang, D., Winter, B. and Sigmond, M.: CCCma CanESM5 model output prepared for CMIP6 ScenarioMIP ssp119, Earth System Grid Federation, , doi:https://doi.org/10.22033/ESGF/CMIP6.3682, 2019i.

Swart, N. C., Cole, J. N. S., Jason, N. ., Kharin, V. V., Lazare, M., Scinocca, J. F., Gillett, N. P., Anstey, J., Arora, V. K., Christian, J. R., Jiao, Y., Lee, W. G., Majaess, F., Saenko, O. A., Seiler, C., Seinen, C., Shao, A., Solheim, L., von Salzen, K., Yang, D., Winter, B. and Sigmond, M.: CCCma CanESM5 model output prepared for CMIP6 ScenarioMIP ssp126, Earth System Grid Federation, , doi:https://doi.org/10.22033/ESGF/CMIP6.3683, 2019j.

Swart, N. C., Cole, J. N. S., Kharin, V. V., Lazare, M., Scinocca, J. F., Gillett, N. P., Anstey, J., Arora, V., Christian, J. R., Jiao, Y., Lee, W. G., Majaess, F., Saenko, O. A., Seiler, C., Seinen, C., Shao, A., Solheim, L., von Salzen, K., Yang, D., Winter, B. and Sigmond, M.: CCCma CanESM5 model output prepared for CMIP6 ScenarioMIP ssp245, Earth System Grid Federation, , doi:https://doi.org/10.22033/ESGF/CMIP6.3685, 2019k.

Swart, N. C., Cole, J. N. S., Kharin, V. V., Lazare, M., Scinocca, J. F., Gillett, N. P., Anstey, J., Arora, V., Christian, J. R., Jiao, Y., Lee, W. G., Majaess, F., Saenko, O. A., Seiler, C., Seinen, C., Shao, A., Solheim, L., von Salzen, K., Yang, D., Winter, B. and Sigmond, M.: CCCma CanESM5 model output prepared for CMIP6 ScenarioMIP ssp370, Earth System Grid Federation, , doi:https://doi.org/10.22033/ESGF/CMIP6.3690, 2019l.

Swart, N. C., Cole, J. N. S., Kharin, V. V., Lazare, M., Scinocca, J. F., Gillett, N. P., Anstey, J., Arora, V., Christian, J. R., Jiao, Y., Lee, W. G., Majaess, F., Saenko, O. A., Seiler, C., Seinen, C., Shao, A., Solheim, L., von

Salzen, K., Yang, D., Winter, B. and Sigmond, M.: CCCma CanESM5 model output prepared for CMIP6 ScenarioMIP ssp434, Earth System Grid Federation, , doi:https://doi.org/10.22033/ESGF/CMIP6.3692, 2019m.

Swart, N. C., Cole, J. N. S., Kharin, V. V., Lazare, M., Scinocca, J. F., Gillett, N. P., Anstey, J., Arora, V., Christian, J. R., Jiao, Y., Lee, W. G., Majaess, F., Saenko, O. A., Seiler, C., Seinen, C., Shao, A., Solheim, L., von Salzen, K., Yang, D., Winter, B. and Sigmond, M.: CCCma CanESM5 model output prepared for CMIP6 ScenarioMIP ssp460, Earth System Grid Federation, , doi:https://doi.org/10.22033/ESGF/CMIP6.3693, 2019n.

Swart, N. C., Cole, J. N. S., Kharin, V. V., Lazare, M., Scinocca, J. F., Gillett, N. P., Anstey, J., Arora, V., Christian, J. R., Jiao, Y., Lee, W. G., Majaess, F., Saenko, O. A., Seiler, C., Seinen, C., Shao, A., Solheim, L., von Salzen, K., Yang, D., Winter, B. and Sigmond, M.: CCCma CanESM5 model output prepared for CMIP6 ScenarioMIP ssp585, Earth System Grid Federation, , doi:https://doi.org/10.22033/ESGF/CMIP6.3696, 2019o.

Tachiiri, K., Abe, M., Hajima, T., Arakawa, O., Suzuki, T., Komuro, Y., Ogochi, K., Watanabe, M., Yamamoto, A., Tatebe, H., Noguchi, M. A., Ohgaito, R., Ito, A., Yamazaki, D., Ito, A., Takata, K., Watanabe, S. and Kawamiya, M.: MIROC MIROC-ES2L model output prepared for CMIP6 ScenarioMIP ssp119, Earth System Grid Federation, , doi:https://doi.org/10.22033/ESGF/CMIP6.5740, 2019a.

Tachiiri, K., Abe, M., Hajima, T., Arakawa, O., Suzuki, T., Komuro, Y., Ogochi, K., Watanabe, M., Yamamoto, A., Tatebe, H., Noguchi, M. A., Ohgaito, R., Ito, A., Yamazaki, D., Ito, A., Takata, K., Watanabe, S. and Kawamiya, M.: MIROC MIROC-ES2L model output prepared for CMIP6 ScenarioMIP ssp126, , doi:https://doi.org/10.22033/ESGF/CMIP6.5742, 2019b.

Tachiiri, K., Abe, M., Hajima, T., Arakawa, O., Suzuki, T., Komuro, Y., Ogochi, K., Watanabe, M., Yamamoto, A., Tatebe, H., Noguchi, M. A., Ohgaito, R., Ito, A., Yamazaki, D., Ito, A., Takata, K., Watanabe, S. and Kawamiya, M.: MIROC MIROC-ES2L model output prepared for CMIP6 ScenarioMIP ssp245, Earth System Grid Federation, , doi:https://doi.org/10.22033/ESGF/CMIP6.5745, 2019c.

Tachiiri, K., Abe, M., Hajima, T., Arakawa, O., Suzuki, T., Komuro, Y., Ogochi, K., Watanabe, M., Yamamoto, A., Tatebe, H., Noguchi, M. A., Ohgaito, R., Ito, A., Yamazaki, D., Ito, A., Takata, K., Watanabe, S. and Kawamiya, M.: MIROC MIROC-ES2L model output prepared for CMIP6 ScenarioMIP ssp370, Earth System Grid Federation, , doi:https://doi.org/10.22033/ESGF/CMIP6.5751, 2019d.

Tachiiri, K., Abe, M., Hajima, T., Arakawa, O., Suzuki, T., Komuro, Y., Ogochi, K., Watanabe, M., Yamamoto, A., Tatebe, H., Noguchi, M. A., Ohgaito, R., Ito, A., Yamazaki, D., Ito, A., Takata, K., Watanabe, S. and Kawamiya, M.: MIROC MIROC-ES2L model output prepared for CMIP6 ScenarioMIP ssp585, Earth System Grid Federation, , doi:https://doi.org/10.22033/ESGF/CMIP6.5770, 2019e.

Tang, Y., Rumbold, S., Ellis, R., Kelley, D., Mulcahy, J., Sellar, A., Walton, J. and Jones, C.: MOHC UKESM1.0-LL model output prepared for CMIP6 CMIP abrupt-4xCO2, Earth System Grid Federation, , doi:https://doi.org/10.22033/ESGF/CMIP6.5843, 2019a.

Tang, Y., Rumbold, S., Ellis, R., Kelley, D., Mulcahy, J., Sellar, A., Walton, J. and Jones, C.: MOHC UKESM1.0-LL model output prepared for CMIP6 CMIP piControl, Earth System Grid Federation, , doi:https://doi.org/10.22033/ESGF/CMIP6.6298, 2019b.

Tang, Y., Rumbold, S., Ellis, R., Kelley, D., Mulcahy, J., Sellar, A., Walton, J. and Jones, C.: MOHC UKESM1.0LL model output prepared for CMIP6 CMIP historical, Earth System Grid Federation, , doi:https://doi.org/10.22033/ESGF/CMIP6.6113, 2019c.

Tatebe, H. and Watanabe, M.: MIROC MIROC6 model output prepared for CMIP6 CMIP abrupt-4xCO2, Earth System Grid Federation, , doi:https://doi.org/10.22033/ESGF/CMIP6.5411, 2018a.

Tatebe, H. and Watanabe, M.: MIROC MIROC6 model output prepared for CMIP6 CMIP historical, Earth System Grid Federation, , doi:https://doi.org/10.22033/ESGF/CMIP6.5603, 2018b.

Tatebe, H. and Watanabe, M.: MIROC MIROC6 model output prepared for CMIP6 CMIP piControl, Earth System Grid Federation, , doi:https://doi.org/10.22033/ESGF/CMIP6.5711, 2018c.

Thompson, D. W. J., Wallace, J. M., Jones, P. D. and Kennedy, J. J.: Identifying signatures of natural climate variability in time series of global-mean surface temperature: Methodology and insights, J. Clim., 22(22), 6120–6141, doi:10.1175/2009JCLI3089.1, 2009.

Tokarska, K. B., Hegerl, G. C., Schurer, A. P., Forster, P. M. and Marvel, K.: Observational constraints on the effective climate sensitivity from the historical period, IOP Publishing, Environ. Res. Lett., 15(3), doi:10.1088/1748-9326/ab738f, 2020a.

Tokarska, K. B., Stolpe, M. B., Sippel, S., Fischer, E. M., Smith, C. J., Lehner, F. and Knutti, R.: Past warming trend constrains future warming in CMIP6 models, Sci. Adv., 6(12), 1–13, doi:10.1126/sciadv.aaz9549, 2020b.

Voldoire, A.: CMIP6 simulations of the CNRM-CERFACS based on CNRM-CM6-1 model for CMIP experiment historical, Earth System Grid Federation, , doi:https://doi.org/10.22033/ESGF/CMIP6.4066, 2018.

Voldoire, A.: CNRM-CERFACS CNRM-CM6-1-HR model output prepared for CMIP6 ScenarioMIP ssp245, Earth System Grid Federation, , doi:https://doi.org/10.22033/ESGF/CMIP6.4190, 2019a.

Voldoire, A.: CNRM-CERFACS CNRM-CM6-1-HR model output prepared for CMIP6 ScenarioMIP ssp585, Earth System Grid Federation, , doi:https://doi.org/10.22033/ESGF/CMIP6.4225, 2019b.

Voldoire, A.: CNRM-CERFACS CNRM-CM6-1 model output prepared for CMIP6 ScenarioMIP for ssp245, Earth System Grid Federation, , doi:https://doi.org/10.22033/ESGF/CMIP6.4189, 2019c.

Voldoire, A.: CNRM-CERFACS CNRM-CM6-1 model output prepared for CMIP6 ScenarioMIP ssp126, Earth System Grid Federation, , doi:https://doi.org/10.22033/ESGF/CMIP6.4184, 2019d.

Voldoire, A.: CNRM-CERFACS CNRM-CM6-1 model output prepared for CMIP6 ScenarioMIP ssp370, Earth System Grid Federation, , doi:https://doi.org/10.22033/ESGF/CMIP6.4197, 2019e.

Voldoire, A.: CNRM-CERFACS CNRM-CM6-1 model output prepared for CMIP6 ScenarioMIP ssp585, Earth System Grid Federation, , doi:https://doi.org/10.22033/ESGF/CMIP6.4224, 2019f.

Voldoire, A.: CNRM-CERFACS CNRM-ESM2-1 model output prepared for CMIP6 ScenarioMIP ssp119, Earth System Grid Federation, , doi:https://doi.org/10.22033/ESGF/CMIP6.4182, 2019g.

Voldoire, A.: CNRM-CERFACS CNRM-ESM2-1 model output prepared for CMIP6 ScenarioMIP ssp126, Earth System Grid Federation, , doi:https://doi.org/10.22033/ESGF/CMIP6.4186, 2019h.

Voldoire, A.: CNRM-CERFACS CNRM-ESM2-1 model output prepared for CMIP6 ScenarioMIP ssp245, Earth System Grid Federation, , doi:https://doi.org/10.22033/ESGF/CMIP6.4191, 2019i.

Voldoire, A.: CNRM-CERFACS CNRM-ESM2-1 model output prepared for CMIP6 ScenarioMIP ssp370, Earth System Grid Federation, , doi:https://doi.org/10.22033/ESGF/CMIP6.4199, 2019j.

Voldoire, A.: CNRM-CERFACS CNRM-ESM2-1 model output prepared for CMIP6 ScenarioMIP ssp434, Earth System Grid Federation, , doi:https://doi.org/10.22033/ESGF/CMIP6.4213, 2019k.

Voldoire, A.: CNRM-CERFACS CNRM-ESM2-1 model output prepared for CMIP6 ScenarioMIP ssp460, Earth System Grid Federation, , doi:https://doi.org/10.22033/ESGF/CMIP6.4217, 2019l.

Voldoire, A.: CNRM-CERFACS CNRM-CM6-1-HR model output prepared for CMIP6 ScenarioMIP ssp126, Earth System Grid Federation, , doi:https://doi.org/10.22033/ESGF/CMIP6.4185, 2020a.

Voldoire, A.: CNRM-CERFACS CNRM-CM6-1-HR model output prepared for CMIP6 ScenarioMIP ssp370, Earth System Grid Federation, , doi:https://doi.org/10.22033/ESGF/CMIP6.4198, 2020b.

Volodin, E., Mortikov, E., Gritsun, A., Lykossov, V., Galin, V., Diansky, N., Gusev, A., Kostrykin, S., Iakovlev, N., Shestakova, A. and Emelina, S.: INM INM-CM4-8 model output prepared for CMIP6 CMIP abrupt-4xCO2, Earth System Grid Federation, , doi:https://doi.org/10.22033/ESGF/CMIP6.4931, 2019a.

Volodin, E., Mortikov, E., Gritsun, A., Lykossov, V., Galin, V., Diansky, N., Gusev, A., Kostrykin, S., Iakovlev, N., Shestakova, A. and Emelina, S.: INM INM-CM4-8 model output prepared for CMIP6 CMIP historical, Earth System Grid Federation, , doi:https://doi.org/10.22033/ESGF/CMIP6.5069, 2019b.

Volodin, E., Mortikov, E., Gritsun, A., Lykossov, V., Galin, V., Diansky, N., Gusev, A., Kostrykin, S., Iakovlev, N., Shestakova, A. and Emelina, S.: INM INM-CM4-8 model output prepared for CMIP6 CMIP piControl, Earth System Grid Federation, , doi:https://doi.org/10.22033/ESGF/CMIP6.5080, 2019c.

Volodin, E., Mortikov, E., Gritsun, A., Lykossov, V., Galin, V., Diansky, N., Gusev, A., Kostrykin, S., Iakovlev, N., Shestakova, A. and Emelina, S.: INM INM-CM4-8 model output prepared for CMIP6 ScenarioMIP ssp126, Earth System Grid Federation, , doi:https://doi.org/10.22033/ESGF/CMIP6.12325, 2019d.

Volodin, E., Mortikov, E., Gritsun, A., Lykossov, V., Galin, V., Diansky, N., Gusev, A., Kostrykin, S., Iakovlev, N., Shestakova, A. and Emelina, S.: INM INM-CM4-8 model output prepared for CMIP6 ScenarioMIP ssp245, Earth System Grid Federation, , doi:https://doi.org/10.22033/ESGF/CMIP6.12327, 2019e.

Volodin, E., Mortikov, E., Gritsun, A., Lykossov, V., Galin, V., Diansky, N., Gusev, A., Kostrykin, S., Iakovlev, N., Shestakova, A. and Emelina, S.: INM INM-CM4-8 model output prepared for CMIP6 ScenarioMIP ssp370, Earth System Grid Federation, , doi:https://doi.org/10.22033/ESGF/CMIP6.12329, 2019f.

Volodin, E., Mortikov, E., Gritsun, A., Lykossov, V., Galin, V., Diansky, N., Gusev, A., Kostrykin, S., Iakovlev, N., Shestakova, A. and Emelina, S.: INM INM-CM4-8 model output prepared for CMIP6 ScenarioMIP ssp585, Earth System Grid Federation, , doi:https://doi.org/10.22033/ESGF/CMIP6.12337, 2019g.

Volodin, E., Mortikov, E., Gritsun, A., Lykossov, V., Galin, V., Diansky, N., Gusev, A., Kostrykin, S., Iakovlev, N., Shestakova, A. and Emelina, S.: INM INM-CM5-0 model output prepared for CMIP6 CMIP historical, Earth System Grid Federation, , doi:https://doi.org/10.22033/ESGF/CMIP6.5070, 2019h.

Volodin, E., Mortikov, E., Gritsun, A., Lykossov, V., Galin, V., Diansky, N., Gusev, A., Kostrykin, S., Iakovlev, N., Shestakova, A. and Emelina, S.: INM INM-CM5-0 model output prepared for CMIP6 ScenarioMIP ssp126, Earth System Grid Federation, , doi:https://doi.org/10.22033/ESGF/CMIP6.12326, 2019i.

Volodin, E., Mortikov, E., Gritsun, A., Lykossov, V., Galin, V., Diansky, N., Gusev, A., Kostrykin, S., Iakovlev, N., Shestakova, A. and Emelina, S.: INM INM-CM5-0 model output prepared for CMIP6 ScenarioMIP ssp245, Earth System Grid Federation, , doi:https://doi.org/10.22033/ESGF/CMIP6.12328, 2019j.

Volodin, E., Mortikov, E., Gritsun, A., Lykossov, V., Galin, V., Diansky, N., Gusev, A., Kostrykin, S., Iakovlev, N., Shestakova, A. and Emelina, S.: INM INM-CM5-0 model output prepared for CMIP6 ScenarioMIP ssp370, Earth System Grid Federation, , doi:https://doi.org/10.22033/ESGF/CMIP6.12330, 2019k.

Volodin, E., Mortikov, E., Gritsun, A., Lykossov, V., Galin, V., Diansky, N., Gusev, A., Kostrykin, S., Iakovlev, N., Shestakova, A. and Emelina, S.: INM INM-CM5-0 model output prepared for CMIP6 ScenarioMIP ssp585, Earth System Grid Federation, , doi:https://doi.org/10.22033/ESGF/CMIP6.12338, 2019l.

Volodin, E., Mortikov, E., Gritsun, A., Lykossov, V., Galin, V., Diansky, N., Gusev, A., Kostrykin, S., Iakovlev, N., Shestakova, A. and Emelina, S.: NM INM-CM5-0 model output prepared for CMIP6 CMIP abrupt-4xCO2, Earth System Grid Federation, , doi:https://doi.org/10.22033/ESGF/CMIP6.4932, 2019m.

Volodin, E., Mortikov, E., Gritsun, A., Lykossov, V., Galin, V., Diansky, N., Gusev, A., Kostrykin, S., Iakovlev, N., Shestakova, A. and Emelina, S.: NM INM-CM5-0 model output prepared for CMIP6 CMIP piControl, Earth System Grid Federation, , doi:https://doi.org/10.22033/ESGF/CMIP6.5081, 2019n.

Wieners, K.-H., Giorgetta, M., Jungclaus, J. H., Reick, C., Esch, M., Bittner, M., Legutke, S., Schupfner, M., Wachsmann, F., Gayler, V., Haak, H., de Vrese, P., Raddatz, T., Mauritsen, T., von Storch, J.-S., Behrens, J., Brovkin, V., Claussen, M., Crueger, T., Fast, I., Fiedler, S., Hagemann, S., Hohenegger, C., Jahns, T., Kloster, S., Kinne, S., Lasslop, G., Kornblueh, L., Marotzke, J., Matei, D., Meraner, K., Mikolajewicz, U., Modali, K., Muller, W., Nabel, J. E. M. S., Notz, D., Peters, K., Pincus, R., Pohlmann, H., Pongratz, J., Rast, S., Schmidt, H., Schnur, R., Schulzweida, U., Six, K., Stevens, B., Voigt, A. and Roeckner, E.: MPI-M MPI-ESM1.2-LR model output prepared for CMIP6 CMIP historical, Earth System Grid Federation, , doi:https://doi.org/10.22033/ESGF/CMIP6.6595, 2019a.

Wieners, K.-H., Giorgetta, M., Jungclaus, J., Reick, C., Esch, M., Bittner, M., Gayler, V., Haak, H., de Vrese, P., Raddatz, T., Mauritsen, T., von Storch, J.-S., Behrens, J., Brovkin, V., Claussen, M., Crueger, T., Fast, I., Fiedler, S., Hagemann, S., Hohenegger, C., Jahns, T., Kloster, S., Kinne, S., Lasslop, G., Kornblueh, L., Marotzke, J., Matei, D., Meraner, K., Mikolajewicz, U., Modali, K., Müller, W., Nabel, J., Notz, D., Peters, K., Pincus, R., Pohlmann, H., Pongratz, J., Rast, S., Schmidt, H., Schnur, R., Schulzweida, U., Six, K., Stevens, B., Voigt, A. and Roeckner, E.: MPI-M MPI-ESM1.2-LR model output prepared for CMIP6 ScenarioMIP ssp126, Earth System Grid Federation, , doi:https://doi.org/10.22033/ESGF/CMIP6.6690, 2019b.

Wieners, K.-H., Giorgetta, M., Jungclaus, J., Reick, C., Esch, M., Bittner, M., Gayler, V., Haak, H., de Vrese, P., Raddatz, T., Mauritsen, T., von Storch, J.-S., Behrens, J., Brovkin, V., Claussen, M., Crueger, T., Fast, I., Fiedler, S., Hagemann, S., Hohenegger, C., Jahns, T., Kloster, S., Kinne, S., Lasslop, G., Kornblueh, L., Marotzke, J., Matei, D., Meraner, K., Mikolajewicz, U., Modali, K., Müller, W., Nabel, J., Notz, D., Peters, K., Pincus, R., Pohlmann, H., Pongratz, J., Rast, S., Schmidt, H., Schnur, R., Schulzweida, U., Six, K., Stevens, B., Voigt, A. and Roeckner, E.: MPI-M MPI-ESM1.2-LR model output prepared for CMIP6 ScenarioMIP ssp245, Earth System Grid Federation, , doi:https://doi.org/10.22033/ESGF/CMIP6.6693, 2019c.

Wieners, K.-H., Giorgetta, M., Jungclaus, J., Reick, C., Esch, M., Bittner, M., Gayler, V., Haak, H., de Vrese, P., Raddatz, T., Mauritsen, T., von Storch, J.-S., Behrens, J., Brovkin, V., Claussen, M., Crueger, T., Fast, I., Fiedler, S., Hagemann, S., Hohenegger, C., Jahns, T., Kloster, S., Kinne, S., Lasslop, G., Kornblueh, L., Marotzke, J., Matei, D., Meraner, K., Mikolajewicz, U., Modali, K., Müller, W., Nabel, J., Notz, D., Peters, K., Pincus, R., Pohlmann, H., Pongratz, J., Rast, S., Schmidt, H., Schnur, R., Schulzweida, U., Six, K., Stevens, B., Voigt, A. and Roeckner, E.: MPI-M MPI-ESM1.2-LR model output prepared for CMIP6 ScenarioMIP ssp370, Earth System Grid Federation, , doi:https://doi.org/10.22033/ESGF/CMIP6.6695, 2019d.

Wieners, K.-H., Giorgetta, M., Jungclaus, J., Reick, C., Esch, M., Bittner, M., Gayler, V., Haak, H., de Vrese, P., Raddatz, T., Mauritsen, T., von Storch, J.-S., Behrens, J., Brovkin, V., Claussen, M., Crueger, T., Fast, I., Fiedler, S., Hagemann, S., Hohenegger, C., Jahns, T., Kloster, S., Kinne, S., Lasslop, G., Kornblueh, L., Marotzke, J., Matei, D., Meraner, K., Mikolajewicz, U., Modali, K., Müller, W., Nabel, J., Notz, D., Peters, K., Pincus, R., Pohlmann, H., Pongratz, J., Rast, S., Schmidt, H., Schnur, R., Schulzweida, U., Six, K., Stevens, B., Voigt, A. and Roeckner, E.: MPI-M MPI-ESM1.2-LR model output prepared for CMIP6 ScenarioMIP ssp585, Earth System Grid Federation, , doi:https://doi.org/10.22033/ESGF/CMIP6.6705, 2019e.

Wu, T., Chu, M., Dong, M., Fang, Y., Jie, W., Li, J., Li, W., Liu, Q., Shi, X., Xin, X., Yan, J., Zhang, F., Zhang, J., Zhang, L. and Zhang, Y.: BCC BCC-CSM2MR model output prepared for CMIP6 CMIP abrupt-4xCO2, Earth System Grid Federation, , doi:https://doi.org/10.22033/ESGF/CMIP6.2845, 2018a.

Wu, T., Chu, M., Dong, M., Fang, Y., Jie, W., Li, J., Li, W., Liu, Q., Shi, X., Xin, X., Yan, J., Zhang, F., Zhang, J., Zhang, L. and Zhang, Y.: BCC BCC-CSM2MR model output prepared for CMIP6 CMIP historical, Earth System Grid Federation, , doi:https://doi.org/10.22033/ESGF/CMIP6.2948, 2018b.

Wu, T., Chu, M., Dong, M., Fang, Y., Jie, W., Li, J., Li, W., Liu, Q., Shi, X., Xin, X., Yan, J., Zhang, F., Zhang, J., Zhang, L. and Zhang, Y.: BCC BCC-CSM2MR model output prepared for CMIP6 CMIP piControl, Earth System Grid Federation, , doi:https://doi.org/10.22033/ESGF/CMIP6.3016, 2018c.

Xin, X., Wu, T., Shi, X., Zhang, F., Li, J., Chu, M., Liu, Q., Yan, J., Ma, Q. and Wei, M.: BCC BCC-CSM2MR model output prepared for CMIP6 ScenarioMIP ssp126, Earth System Grid Federation, , doi:https://doi.org/10.22033/ESGF/CMIP6.3028, 2019a.

Xin, X., Wu, T., Shi, X., Zhang, F., Li, J., Chu, M., Liu, Q., Yan, J., Ma, Q. and Wei, M.: BCC BCC-CSM2MR model output prepared for CMIP6 ScenarioMIP ssp245, Earth System Grid Federation, , doi:https://doi.org/10.22033/ESGF/CMIP6.3030, 2019b.

Xin, X., Wu, T., Shi, X., Zhang, F., Li, J., Chu, M., Liu, Q., Yan, J., Ma, Q. and Wei, M.: BCC BCC-CSM2MR model output prepared for CMIP6 ScenarioMIP ssp370, Earth System Grid Federation, , doi:https://doi.org/10.22033/ESGF/CMIP6.3035, 2019c.

Xin, X., Wu, T., Shi, X., Zhang, F., Li, J., Chu, M., Liu, Q., Yan, J., Ma, Q. and Wei, M.: BCC BCC-CSM2MR model output prepared for CMIP6 ScenarioMIP ssp585, Earth System Grid Federation, , doi:https://doi.org/10.22033/ESGF/CMIP6.3050, 2019d.

YU, Y.: CAS FGOALS-f3-L model output prepared for CMIP6 CMIP historical, Earth System Grid Federation, , doi:https://doi.org/10.22033/ESGF/CMIP6.3355, 2019a.

YU, Y.: CAS FGOALS-f3-L model output prepared for CMIP6 ScenarioMIP ssp126, Earth System Grid Federation, , doi:https://doi.org/10.22033/ESGF/CMIP6.3464, 2019b.

YU, Y.: CAS FGOALS-f3-L model output prepared for CMIP6 ScenarioMIP ssp245, Earth System Grid Federation, , doi:https://doi.org/10.22033/ESGF/CMIP6.3468, 2019c.

YU, Y.: CAS FGOALS-f3-L model output prepared for CMIP6 ScenarioMIP ssp370, Earth System Grid Federation, , doi:https://doi.org/10.22033/ESGF/CMIP6.3479, 2019d.

YU, Y.: CAS FGOALS-f3-L model output prepared for CMIP6 ScenarioMIP ssp585, Earth System Grid Federation, , doi:https://doi.org/10.22033/ESGF/CMIP6.3502, 2019e.

Yukimoto, S., Koshiro, T., Kawai, H., Oshima, N., Yoshida, K., Urakawa, S., Tsujino, H., Deushi, M., Tanaka, T., Hosaka, M., Yoshimura, H., Shindo, E., Mizuta, R., Ishii, M., Obata, A. and Adachi, Y.: MRI MRI-ESM2.0 model output prepared for CMIP6 CMIP historical, Earth System Grid Federation, , doi:https://doi.org/10.22033/ESGF/CMIP6.6842, 2019a.

Yukimoto, S., Koshiro, T., Kawai, H., Oshima, N., Yoshida, K., Urakawa, S., Tsujino, H., Deushi, M., Tanaka, T., Hosaka, M., Yoshimura, H., Shindo, E., Mizuta, R., Ishii, M., Obata, A. and Adachi, Y.: MRI MRI-ESM2.0 model output prepared for CMIP6 ScenarioMIP ssp119, Earth System Grid Federation, , doi:https://doi.org/10.22033/ESGF/CMIP6.6908, 2019b.

Yukimoto, S., Koshiro, T., Kawai, H., Oshima, N., Yoshida, K., Urakawa, S., Tsujino, H., Deushi, M., Tanaka, T., Hosaka, M., Yoshimura, H., Shindo, E., Mizuta, R., Ishii, M., Obata, A. and Adachi, Y.: MRI MRI-ESM2.0 model output prepared for CMIP6 ScenarioMIP ssp126, Earth System Grid Federation, , doi:https://doi.org/10.22033/ESGF/CMIP6.6909, 2019c.

Yukimoto, S., Koshiro, T., Kawai, H., Oshima, N., Yoshida, K., Urakawa, S., Tsujino, H., Deushi, M., Tanaka, T., Hosaka, M., Yoshimura, H., Shindo, E., Mizuta, R., Ishii, M., Obata, A. and Adachi, Y.: MRI MRI-ESM2.0 model output prepared for CMIP6 ScenarioMIP ssp245, Earth System Grid Federation, , doi:https://doi.org/10.22033/ESGF/CMIP6.6910, 2019d.

Yukimoto, S., Koshiro, T., Kawai, H., Oshima, N., Yoshida, K., Urakawa, S., Tsujino, H., Deushi, M., Tanaka, T., Hosaka, M., Yoshimura, H., Shindo, E., Mizuta, R., Ishii, M., Obata, A. and Adachi, Y.: MRI MRI-ESM2.0 model output prepared for CMIP6 ScenarioMIP ssp370, Earth System Grid Federation, , doi:https://doi.org/10.22033/ESGF/CMIP6.6915, 2019e.

Yukimoto, S., Koshiro, T., Kawai, H., Oshima, N., Yoshida, K., Urakawa, S., Tsujino, H., Deushi, M., Tanaka, T., Hosaka, M., Yoshimura, H., Shindo, E., Mizuta, R., Ishii, M., Obata, A. and Adachi, Y.: MRI MRI-ESM2.0 model output prepared for CMIP6 ScenarioMIP ssp434, Earth System Grid Federation, , doi:https://doi.org/10.22033/ESGF/CMIP6.6925, 2019f.

Yukimoto, S., Koshiro, T., Kawai, H., Oshima, N., Yoshida, K., Urakawa, S., Tsujino, H., Deushi, M., Tanaka, T., Hosaka, M., Yoshimura, H., Shindo, E., Mizuta, R., Ishii, M., Obata, A. and Adachi, Y.: MRI MRI-ESM2.0 model output prepared for CMIP6 ScenarioMIP ssp460, Earth System Grid Federation, , doi:https://doi.org/10.22033/ESGF/CMIP6.6926, 2019g.

Yukimoto, S., Koshiro, T., Kawai, H., Oshima, N., Yoshida, K., Urakawa, S., Tsujino, H., Deushi, M., Tanaka, T., Hosaka, M., Yoshimura, H., Shindo, E., Mizuta, R., Ishii, M., Obata, A. and Adachi, Y.: MRI MRI-ESM2.0 model output prepared for CMIP6 ScenarioMIP ssp585, Earth System Grid Federation, , doi:https://doi.org/10.22033/ESGF/CMIP6.6929, 2019h.

Zelinka, M. D., Myers, T. A., McCoy, D. T., Po-Chedley, S., Caldwell, P. M., Ceppi, P., Klein, S. A. and Taylor, K. E.: Causes of Higher Climate Sensitivity in CMIP6 Models, Geophys. Res. Lett., 47(1), doi:10.1029/2019GL085782, 2020.

Zhang, J., Wu, T., Shi, X., Zhang, F., Li, J., Chu, M., Liu, Q., Yan, J., Ma, Q. and Wei, M.: BCC BCC-ESM1 model output prepared for CMIP6 CMIP historical, Earth System Grid Federation, , doi:https://doi.org/10.22033/ESGF/CMIP6.2949, 2018a.

Zhang, J., Wu, T., Shi, X., Zhang, F., Li, J., Chu, M., Liu, Q., Yan, J., Ma, Q. and Wei, M.: BCC BCC-ESM1 model output prepared for CMIP6 CMIP piControl, Earth System Grid Federation, , doi:https://doi.org/10.22033/ESGF/CMIP6.3017, 2018b.

Zhang, J., Wu, T., Shi, X., Zhang, F., Li, J., Chu, M., Liu, Q., Yan, J., Ma, Q. and Wei, M.: BCC BCC-ESM1 model output prepared for CMIP6 CMIP abrupt-4xCO2, Earth System Grid Federation, , doi:https://doi.org/10.22033/ESGF/CMIP6.2846, 2019.

Ziehn, T., Chamberlain, M., Lenton, A., Law, R., Bodman, R., Dix, M., Wang, Y., Dobrohotoff, P., Srbinovsky, J., Stevens, L., Vohralik, P., Mackallah, C., Sullivan, A., O'Farrell, S. and Druken, K.: CSIRO ACCESS-ESM1.5 model output prepared for CMIP6 CMIP abrupt-4xCO2, Earth System Grid Federation, , doi:https://doi.org/10.22033/ESGF/CMIP6.4238, 2019a.

Ziehn, T., Chamberlain, M., Lenton, A., Law, R., Bodman, R., Dix, M., Wang, Y., Dobrohotoff, P., Srbinovsky, J., Stevens, L., Vohralik, P., Mackallah, C., Sullivan, A., O'Farrell, S. and Druken, K.: CSIRO ACCESS-ESM1.5 model output prepared for CMIP6 CMIP historical, Earth System Grid Federation, , doi:https://doi.org/10.22033/ESGF/CMIP6.4272, 2019b.

Ziehn, T., Chamberlain, M., Lenton, A., Law, R., Bodman, R., Dix, M., Wang, Y., Dobrohotoff, P., Srbinovsky, J., Stevens, L., Vohralik, P., Mackallah, C., Sullivan, A., O'Farrell, S. and Druken, K.: CSIRO ACCESS-ESM1.5 model output prepared for CMIP6 CMIP piControl, Earth System Grid Federation, , doi:https://doi.org/10.22033/ESGF/CMIP6.4312, 2019c.

Ziehn, T., Chamberlain, M., Lenton, A., Law, R., Bodman, R., Dix, M., Wang, Y., Dobrohotoff, P., Srbinovsky, J., Stevens, L., Vohralik, P., Mackallah, C., Sullivan, A., O'Farrell, S. and Druken, K.: CSIRO ACCESS-ESM1.5 model output prepared for CMIP6 ScenarioMIP ssp126, Earth System Grid Federation, , doi:https://doi.org/10.22033/ESGF/CMIP6.4320, 2019d.

Ziehn, T., Chamberlain, M., Lenton, A., Law, R., Bodman, R., Dix, M., Wang, Y., Dobrohotoff, P., Srbinovsky, J., Stevens, L., Vohralik, P., Mackallah, C., Sullivan, A., O'Farrell, S. and Druken, K.: CSIRO ACCESS-ESM1.5 model output prepared for CMIP6 ScenarioMIP ssp245, Earth System Grid Federation, , doi:https://doi.org/10.22033/ESGF/CMIP6.4322, 2019e.

Ziehn, T., Chamberlain, M., Lenton, A., Law, R., Bodman, R., Dix, M., Wang, Y., Dobrohotoff, P., Srbinovsky, J., Stevens, L., Vohralik, P., Mackallah, C., Sullivan, A., O'Farrell, S. and Druken, K.: CSIRO ACCESS-ESM1.5 model output prepared for CMIP6 ScenarioMIP ssp370, Earth System Grid Federation, , doi:https://doi.org/10.22033/ESGF/CMIP6.4324, 2019f.

Ziehn, T., Chamberlain, M., Lenton, A., Law, R., Bodman, R., Dix, M., Wang, Y., Dobrohotoff, P., Srbinovsky, J., Stevens, L., Vohralik, P., Mackallah, C., Sullivan, A., O'Farrell, S. and Druken, K.: CSIRO ACCESS-ESM1.5 model output prepared for CMIP6 ScenarioMIP ssp585, Earth System Grid Federation, , doi:https://doi.org/10.22033/ESGF/CMIP6.4333, 2019g.